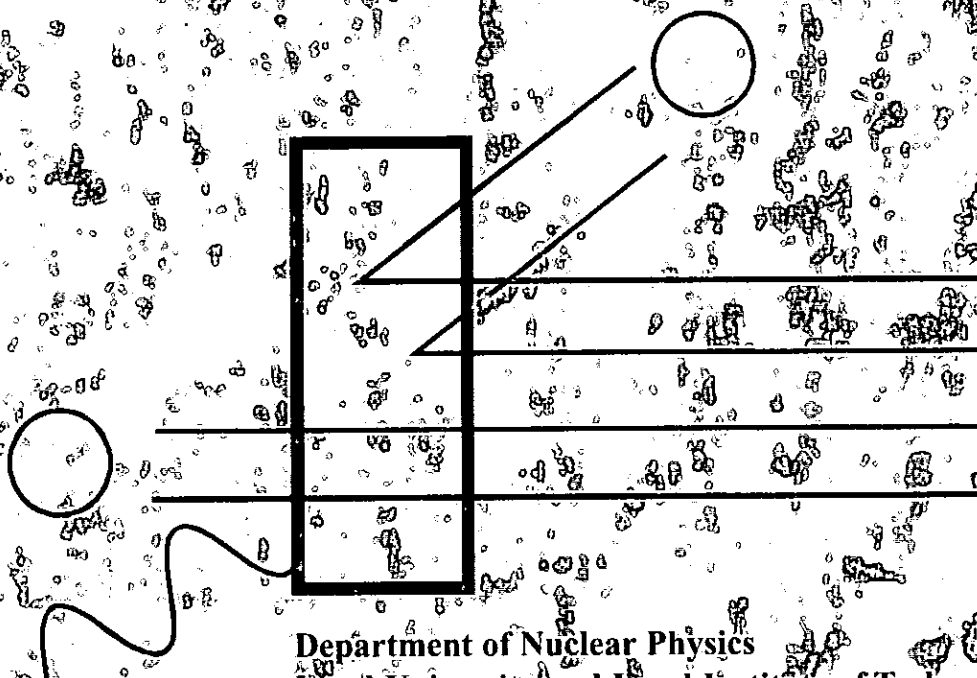


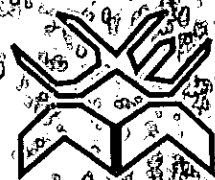
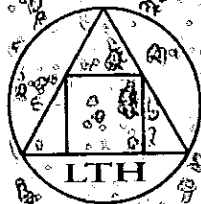
SCP-07

Rogério Utui
Doctoral Thesis

Assembling of a low energy ion beam analysis
facility and use of Nuclear Microprobe
techniques in geological studies



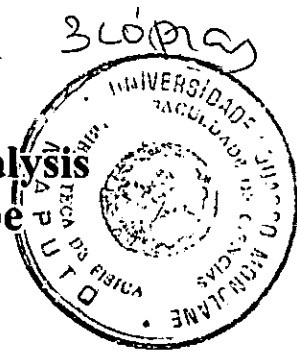
Department of Nuclear Physics
Lund University and Lund Institute of Technology
Lund, Sweden, 1996



Rogério Utui

Doctoral Thesis

**Assembling of a low energy ion beam analysis
facility and use of Nuclear Microprobe
techniques in geological studies.**



av

Rogério José Utui

Handwritten signatures and notes:
- A large signature, possibly "R. Utui", with a flourish above it.
- The word "Bibliografia" written vertically on the left.
- The word "Física" written vertically in the middle.
- The word "Física" written vertically on the right.
- A signature "Whi" on the right side.

Akademisk avhandling för avläggande av teknisk doktorsexamen vid tekniska fakulteten vid Lunds Tekniska Högskola, kommer att offentligas försvaras i fysiska institutionens föreläsningssal B, fredagen den 29 november 1996, kl. 10.15.

Organization LUND UNIVERSITY Department of Nuclear Physics Box 118, S - 221 00 LUND, SWEDEN	Document name DOCTORAL DISSERTATION	
	Date of issue November 1 st , 1996	
	CODEN: LUTFD2/(TFKF-1020)/144/(1996)	
Author(s) Rogério José Utui	Sponsoring organization SAREC - SIDA	
Title and subtitle Assembling of a low energy ion beam analysis facility and use of Nuclear Microprobe techniques in geological studies.		
Abstract <p>In about four decades, ion beam analysis (IBA) techniques have evolved to become well established analytical techniques for routine analysis in archaeological, bio-medical, geological and environmental sciences. They basically make use of the different interactions of a high energy ion beam (of few MeV/amu) with the specimen matter so they presuppose the use of a particle accelerator. In laboratories where an accelerator is available, setting up an IBA facility can be for many reasons, a good choice.</p> <p>In conditions when neither enough analytical facilities nor skilled personnel are available, the possibility of creating a research facility which is accessible to multidisciplinary users allowing at the same time a manpower build up can be regarded as a worthwhile investment. At the present work, special emphasis was put in these two issues in developing a low energy IBA facility at the Eduardo Mondlane University in Maputo, Mozambique.</p> <p>By using an ion beam focused down to micrometer scale and some scanning mechanism with synchronised detection of the spectra of each pixel, digital elemental maps of the analysed specimen can be generated. This feature confers microscopic ability to the IBA techniques which are then known as Nuclear Microprobe (NMP) techniques. In this work, both particle induced X-ray emission (PIXE) and ion beam induced luminescence, or just ionoluminescence (IL) were used for geochemical studies. The possibility of rapid absolute quantification of elements in the ppm level by PIXE combined with the yet higher sensitivity of IL method to transition metals and REE activators, in the absence of quenching phenomena, allow for a synergic use of the two methods in geological applications with enhanced sensitivity.</p> <p>IL and PIXE were combined for studying Rare Earth Elements (REE) distribution in apatite minerals and ion beam induced damage in inorganic material in general with emphasis to synthetically grown zircon crystals doped with REE. Due to the sensitivity of IL to changes in chemical bonding in the material, beam damage effects can be studied even at low integrated doses, through wavelength shift or fading of the induced light.</p> <p>Micro PIXE technique was used for studying line profile concentrations of trace elements in pyrite grains and of elements used as geothermometers. Geothermometry allowed to assess the cooling rates in iron meteorites and the mineralisation conditions in metamorphic rocks, attempting to describe the tectonic history of the terranes, with application in petrologic studies and geological prospecting.</p>		
Key words Ion Beam Analysis, Low energy IBA, Nuclear Microprobe, μ PIXE, geological application, Ionoluminescence (IL), zonation, geothermometry.		
Classification system and/or index terms (if any)		
Supplementary bibliographical information		Language English
ISSN and key title		ISBN 91-628-2272-1
Recipient's notes	Number of pages 144	Price
	Security classification	

Distribution by Department of Nuclear Physics, Lund University and Lund Institute of Technology
 Box 118, S - 221 00, Lund, Sweden.

I, the undersigned, being the copyright owner of the abstract of the above-mentioned dissertation, hereby grant to all reference sources permission to publish and disseminate the abstract of the above-mentioned dissertation.

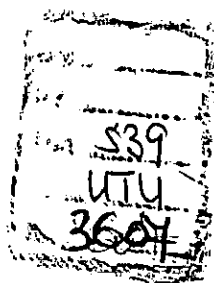
Signature Rogério José Utui

Date October 22nd 1996

**Assembling of a low energy ion beam analysis
facility and use of Nuclear Microprobe
techniques in geological studies.**

by

Rogério José Utui



**Thesis for the degree of Doctor of Philosophy in Engineering (PhD Eng.)
by the Department of Nuclear Physics
Lund University and Lund Institute of Technology
Lund, Sweden - 1996**

ISBN 91-628-2272-1

**Assembling of a low energy ion beam analysis facility and use of Nuclear
Microprobe techniques in geological studies.**

Rogério Utui

**Lund University and Lund Institute of Technology
Department of Nuclear Physics
Lund, Sweden, 1996**

Printed in Sweden, KFS AB, Lund 1996

ISBN 91-628-2272-1

Acknowledgements

First of all, I would like to express my gratitude to my supervisor, Prof. Klas Malmqvist, for all of the contributions he gave for starting the research project on Ion Beam Analysis at the Eduardo Mondlane University, Maputo, for the confidence that he inspires to the graduate students and for keeping a healthy working atmosphere at the Department.

I am indebted to my friends and close work comrades Dr. Changyi Yang for willingly sharing with me his knowledge on μ PIXE and IL and Mike Elfman for support and interesting discussions.

A very special mention to my friend and former colleague Dr. Pelle Homman who participated directly in setting up the lab in Maputo and, with his wife Kristina, helped to create a family environment around me in Lund.

Special thanks to

- Docent Jan Pallon for helping me to get acquainted with the (now old) data acquisition system and for proof-reading my manuscripts;

- Britt-Marie for patiently taking care of all administrative and organisational aspects of my stays in Lund;

- Anders Sjöland for coming up with new ideas about low energy IBA applications;

- Christer Nielsson for keeping the accelerator running and Kjell Håkansson for helping in designing mechanical parts for the Lab in Maputo;

- the whole staff at the Department of Nuclear Physics for a nice environment.

Special thanks to Rikard Anehus from the Department of Mineralogy who helped in sample preparation for geothermometric studies.

I'd like to thank the couple Bill Jarema & Lida Gifford from New Jersey, for checking my biased English and exposing me to "cinemania".

The financial support granted since 1991 by the Swedish Authority for Research Cooperation with Developing Countries (SAREC), which enabled the creation of the research lab in Maputo and my studies here in Lund, is specially acknowledged. I should mention here the valuable contributions of Drs. Malur Baghavan and Berit Olsson, who showed a great understanding of the conditions and priorities for building up research capacity in Third World Countries.

At the Eduardo Mondlane University, I'd like to express my gratitude to Mrs. Célia Diniz and Mr. Alfredo Macamo for administrating the project and to the folks at the Faculty of Science that were in some way involved in setting up things...

Last, but not least special thanks to my family: my mother and my siblings for all the moral support through all these years and my beloved wife Irene and our daughters Nádia, Erika and Yara (Ngurutinhas) for missing me during my half year stints to Lund, on scientific pilgrimage.

My *KHANIMAMBO** to all.

**khanimambo* /kaneemam:boo/ n - *thank you* in some southern african languages.

To

Celeste - the mother;
Nádia, Erika & Yara - the daughters; and
Jrene - the holy spirit...

Contents

1. General Introduction.	7
2. Assembling of a low energy Ion Beam Analysis facility at the Eduardo Mondlane University, Maputo.	10
2.1 - Background.....	10
2.2 - Accelerator Based IBA techniques:.....	11
2.2.1 - Particle-induced X-ray emission (PIXE)..	11
2.2.2 - Rutherford Backscattering (RBS).....	20
2.2.3 - Recoil Spectroscopy.....	25
2.2.4 - Nuclear Reaction Analysis (NRA)..	26
2.2.5 - Other techniques.....	28
2.3 - Characteristics of low energy IBA techniques.....	30
2.4 - The installed laboratory.....	32
2.5 - Further development.....	33
3. Microprobe Techniques in geological studies.	36
3.1 - Why geological studies?	36
3.2 - Microprobe techniques for geological studies:.....	40
3.2.1 - Optical Microscopy.....	41
3.2.2 - X-ray Microscopy (XRF, TRXRF, SRXRF).....	42
3.2.3 - Electron Microscopy (SEM, TEM, EMPA).....	45
3.2.4 - Ion Microscopy (static and dynamic SIMS).....	49
3.2.5 - Laser Microscopy (LAMMA, Laser ablation techniques)..	52
3.2.6 - Nuclear Microscopy :	52
3.2.6.1 - Micro PIXE.....	53
3.2.6.2 - Ionoluminescence (IL).....	54
3.2.6.2.1 - The phenomenon.....	54
3.2.6.2.2 - Causes of luminescence.....	55
3.2.6.2.3 - Methods of detection of IL.....	61
3.2.6.2.4 - Quantification and sensitivity.....	62
3.2.6.2.5 - Application of IL in geological studies.....	63
3.2.6.3 - Other techniques.....	64
3.3 - The Lund Nuclear Microprobe.....	65
3.4 - Specifics of geological studies with Nuclear Microprobe Techniques.....	67
4. Results of geological studies using Nuclear Microprobe Techniques.	75
4.1 - A procedure for beam line alignment.....	75
4.2 - Characterisation of inorganic material using IL method.....	77
4.3 - Study of mineral apatites by combined IL/ μ PIXE methods...	81

4.4 - Study of mineral zonation by IL/ μ PIXE methods.....	82
4.5 - μ PIXE studies of pyrites.....	85
4.6 - Geothermometry using μ PIXE.	88
5. Conclusions.	90
6. Bibliography.	91
7. Thesis.	99
I. <i>A new low energy Ion Beam Analysis facility at the Eduardo Mondlane University, Maputo.....</i>	101
II. <i>Nuclear Microprobe analysis of Evate (Mozambique) apatites..</i>	109
III. <i>Ionoluminescence combined with PIXE in the Nuclear Microprobe for the study of inorganic material.....</i>	115
IV. <i>Corrosion phenomena in electron, proton and synchrotron X-ray microprobe analysis of Roman glass from Qumran, Jordan.....</i>	127
V. <i>Application of Nuclear Microprobe in the study of granulite facies rocks from the Namama Thrust Belt.....</i>	133

1. General Introduction

1.1 Ion Beam Analysis facility

The subject of elemental analysis has always been of paramount importance. In the realm of natural sciences and modern technology, the main task remains related to the determination of different elements and compounds present in the specimens at different concentration ranges. A myriad of analytical methods are presently available and more continue to come to light and find appropriate application in different fields.

The exhaustive investigation of atom and nucleus during the late 19th century enabled the discovery of radioactivity and other atomic and nuclear phenomena like, for example, the X-ray emission by electron excitation. These facts galvanised the scientists, who targeted their attention to the atom and nucleus as object of analysis and, since then, many different spectroscopic techniques based on nuclear properties or phenomena were developed. The first experiments using ions as probes, as a subset of these nuclear methods, were designed early this century and normally in all of them, alpha particles were used which were readily available from natural radioactive sources. It wasn't, however, until the 1930's, with the advent of particle accelerators, that copious fluxes of high energy ions could be produced and used with analytical capability. The second most important technological breakthrough was the development of solid state particle detectors in the late 1960's which enabled the rapid evolution of the instrumental, Ion Beam Analysis (IBA) techniques.

IBA techniques are based on the different kinds of interactions of a high energy ion beam (several MeV/amu) with matter. The detection of the products of such interactions (X-rays, gamma rays, light, charged particles or nuclei) can provide a wealth of information regarding elemental distribution and concentration as well as the chemical state of the analysed specimen. Several qualities of the IBA techniques, such as the high sensitivity, the possibility of combined use of different techniques during the same measurement, the non - destructiveness allied with the possibility of absolute quantification in some of them, have attracted the attention of multidisciplinary teams of researchers. This allowed their rapid development during the two decades, since the early 1970's, to become well established analytical techniques finding applications mainly in bio-medical, archaeological, geological and environmental studies.

However, the need for a small accelerator with commissioning prices in the several hundreds of thousands USD range, hampers a wider spreading of these techniques. Eventually some laboratories can have inherited from early nuclear physicists, small Van de Graaff accelerators

which are suitable for use in IBA. In these cases accelerator based IBA techniques can be installed at no expense.

One of the goals of this work was setting up an IBA facility at the existing low energy (500 keV) Van de Graaff particle accelerator at the Department of Physics of the Eduardo Mondlane University (EMU). The accelerator was commissioned in the late 1960's and, as in many laboratories, had been used for early nuclear physics experiments. Following some shift in the profile of the department towards atomic physics in the early 1970's, no more development of the peripherals was made. The mid 1970's brought up a new rather unstable political environment that ended in the migration of all the staff and the research installations were deemed to abandon. This is basically the starting point in the late 1980's when the first generation of mozambican physicists just came out of the bench and brought about some ideas on how to make use of the available scientific infrastructures. This fact constitutes the main motivation for installing an IBA facility at the Department of Physics of the Eduardo Mondlane University (EMU), Maputo.

This work can be, therefore, seen in the framework of a long term research capacity building including training of skilled personnel and building up of analytical facilities for multi-disciplinary users.

1.2 Application of Nuclear Microprobe Techniques in geological studies

The natural abundance of elements on the crust of the Earth is very uneven. Only eight elements make up 98,6% of the earth's crust, which means that the remaining 84 are present in very tiny amounts. These minor and trace elements, present at sub-percent to parts per million (ppm) levels, are good indicators of different geological conditions during mineralisation, since their distribution pattern can vary in a very wide range and, therefore, are the main object of study in Earth Sciences. Some IBA techniques, like particle-induced X-ray emission (PIXE), ionoluminescence (IL) and nuclear reaction analysis (NRA) are suitable for analysis of geological samples due to their sensitivity (tens ppm readily achievable with PIXE in a ten-minute run, for elements heavier than Na), possibility of combined use in the same run, non-destructiveness and possibility of absolute quantification.

Different analytical techniques, for instance, atomic absorption spectroscopy (AAS) and X-ray fluorescence spectroscopy (XRF), have been used in geological studies of bulk samples for long time now, with inherent advantages and disadvantages, which are presented in detail below. However, on the possibility of studying micrometer sized distribution patterns without destroying the samples, in a reasonable

measuring time and yet with detection limits going down to the ppm level for the majority of the elements, lies the powerfulness of the IBA techniques in microscopic mode known by the generic name of nuclear microprobe (NMP) techniques.

In a nuclear microprobe, the ion beam (normally protons) passes through a micrometer-sized probe forming slit and this object is further demagnified by a magnetic lens to form the microprobe. The proton microprobe can then be scanned through the surface of the sample and the spectra collected at each point are used to generate digital maps with colour or height coded values of the elemental concentrations.

Different microprobe (microscopic) techniques have been applied in geological studies: the classical optical microscope (known as petrographic microscope) and scanning electron microscope (SEM) don't have analytical techniques associated to them. In electron microprobe analysis (EMPA), the sensitivity to trace elements is normally two orders lower than in its ion equivalent PIXE, because of the much higher **bremstrahlung** radiation of the electrons in the matter, when compared with protons. Synchrotron radiation X - ray fluorescence (SRXRF), which can also be utilised in the microprobe mode, has limited use because of the inaccessibility of storage rings in many laboratories. The newly developed ion probe (static and dynamic SIMS - secondary ion mass spectroscopy) has much higher spatial resolution and sensitivity than NMP techniques, but its use as analytical technique is fraught with difficulties. This is due to interference of different molecular clusters and to the lack of consistent theoretical models that describe the phenomenon of sputtering.

The NMP techniques are, hence, the most suitable for geological studies in general, provided that the necessary trade-off is made between costs and sensitivity.

The newly-developed method of ionoluminescence (IL), which consists in detecting the light generated during electron de-excitation in activator's levels, has proved to be very sensitive (few ppm down to ppb level) in cases where the role of quenchers is negligible. Similar to its electron sibling, cathodoluminescence (CL), IL is well suited to imaging growth zonation patterns in crystals, and changes of chemical environment (caused, for example, by beam damage). When used in a NMP, it allows rapid diagnostics of the sample permitting identification of minerals and, sometimes, of trace elements present, as well as providing additional information to other analytical techniques.

In this work, IL and μ PIXE were used in combination or separately, for characterisation of geological samples in a nuclear microprobe.

2. Assembling of a low energy ion beam analysis facility at the Eduardo Mondlane University, Maputo

2.1 Background

When a mega-electron-volt ion beam impinges onto a target, different atomic and nuclear reactions can occur. A schematic of the ion beam induced reactions which are commonly used for analytical purposes is illustrated in Figure 2.1. Depending on which product of the

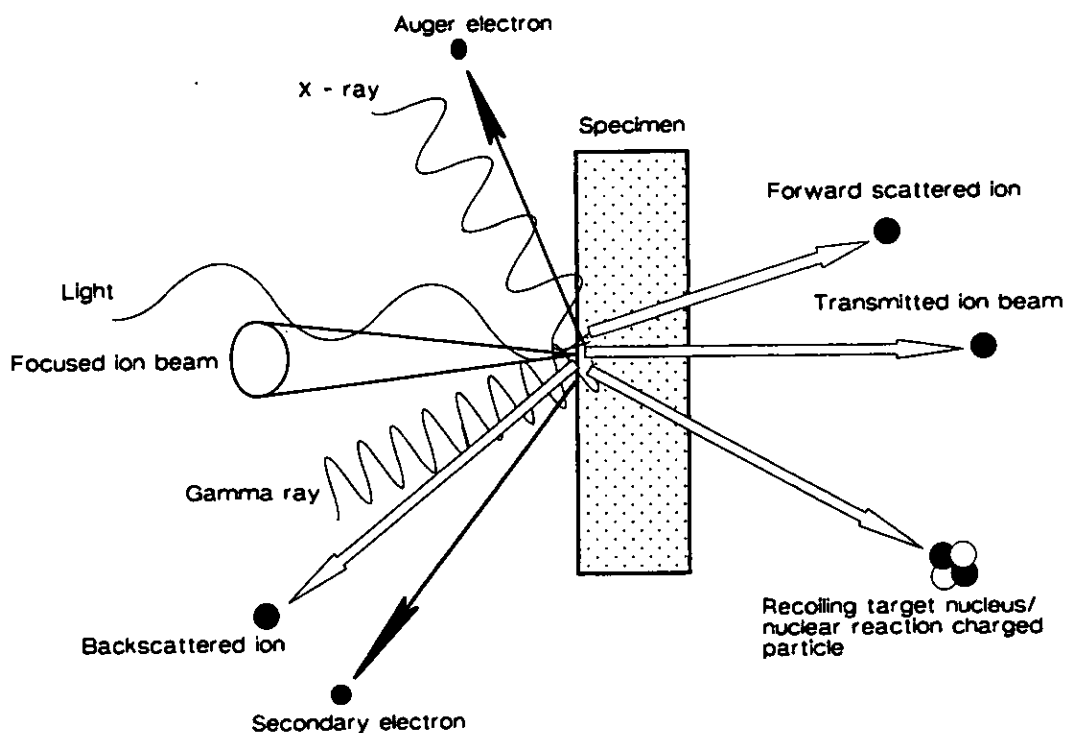


Figure 2.1. Schematic illustration of the induced radiation processes following the impact of a high-energy ion into a solid specimen. (Adapted from [Tap-91]).

interaction is detected, different methods can be regarded that are sensitive to specific properties of the material on the specimen.

The special features of these techniques, which are normally grouped under the generic name of ion beam analysis techniques, include their speed, sensitivity and versatility. Often, two or more of the IBA techniques can be used simultaneously to fully characterise the analysed specimen in a single short irradiation. Moreover, IBA techniques require little sample preparation and often can be applied non-destructively.

Despite the advantages of the information that can be inferred from IBA measurements, they have been regarded as suitable to large laboratories, which could afford the costs of small accelerators. However, small Van de Graaff accelerators suitable for IBA research are eventually available in many laboratories from nuclear physics groups. Besides that, the technological advance made the price of these accelerators comparable with that of other large analytical instrumentation, like inductively coupled plasma - mass spectrometers (ICP-MS), nuclear magnetic resonance spectrometers (NMR), secondary ion mass spectrometers (SIMS) or atomic absorption spectrometers (AAS).

During the last couple of decades, the IBA techniques have evolved so quickly that they moved out from the habitual nuclear physics laboratory into the habitat's of scientists of different areas like museums, hospitals and material science research centres and industry. This attests to the widespread applications of these techniques and their establishment as methods for routine analysis.

2.2 Accelerator based Ion Beam Analysis techniques

2.2.1 Particle induced X - ray emission (PIXE)

Since its invention in the early 1970's in Lund, PIXE rapidly became the most ubiquitous of the IBA techniques and, in a way, has set the pace of their development. The physical principles involved, though, have been known since 1912 [Joh-95]: charged particles bombarding some material can ionise the atoms by creating inner shell vacancies. Outer shells' electrons fill these vacancies, releasing the extra energy in the form of X-ray quanta or pulling an Auger electron out of orbit. The schematic of this process is illustrated in figure 2.2.

By detecting the emitted characteristic X - rays, one can infer about the elements present in the sample at ppm concentration levels. The use of a MeV ion beam as an excitation source offers several advantages over other X-ray techniques like higher rate of spectrum accumulation across the entire periodic table (in fact for elements heavier than Na), and better overall sensitivities. The better sensitivity, if compared to the electron excitation, is due to the much reduced **bremstrahlung** background of the bombarding particles in the material, while in the case of XRF, to the lack of a background continuum across the entire spectrum. In the newly developed total reflection X-ray fluorescence method (TXRF), however [Aig-74] this continuum is very low since the primary X-rays are reflected out of the "sight" of the detector by using a suitable geometry. A

considerable drawback is that only very thin samples can be analysed (μl solutions or few μg of sample), which puts a constraint in the sample size and type.

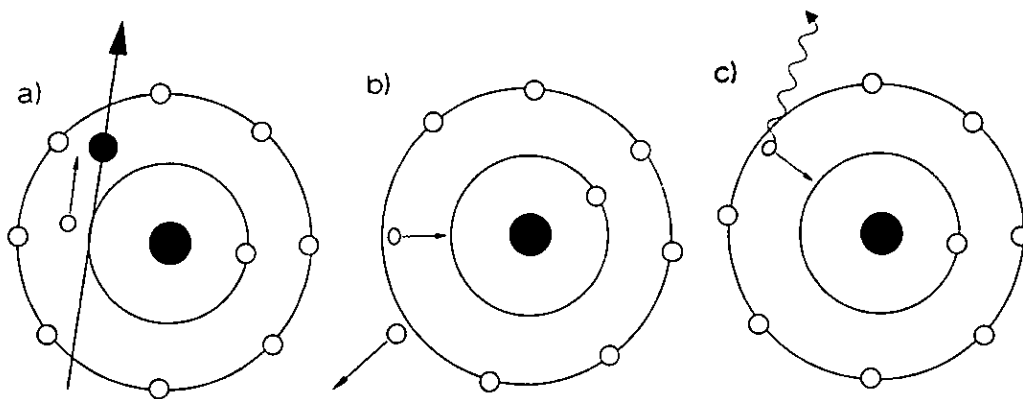


Figure 2.2. Schematic of a) inner shell vacancy creation by an incoming charged particle, with subsequent release of b) an Auger electron, or c) X - ray emission. (Adapted from [Joh.-95]).

The X-rays are normally detected by a Si(Li) energy dispersive semiconductor detector, with resolution in the range of 160 eV for the Mn K_{α} peak (at 5,9 keV). A typical PIXE spectrum is shown in figure 2.3. The multi-elemental capability of the method is displayed for the case of a rain water sample.

In PIXE analysis, the samples can be classified into one of the three categories: thin, intermediate, and thick targets. For thin samples (area density of 1 mg/cm^2 or less), the degradation of proton beam energy in the sample, as well as self absorption of the X-rays, is negligible and the system can be calibrated using thin film standards [Joh-81]. At the other extreme, the thick samples are those that are thick enough to stop the proton beam. In analysing such samples, non-linear effects like proton stopping and, hence, change on X-ray production cross-section with depth, self-absorption of X-rays in the matrix, as well as secondary fluorescence induced by X-rays coming from elements in deeper layers on the material, must be considered in the quantification.

Unlike some traditional analytical methods like AAS, absolute quantification is straightforward in PIXE. For thick targets, the yield of

specific X-rays (K_α or L_α X-rays, for example) of an element with atomic number Z and mass A_Z under proton bombardment is given by:

$$Y(Z) = \frac{N_{AV} \omega_z b_z t_z \varepsilon_z^i \left(\frac{\Omega}{4\pi}\right)}{A_Z} N_p C_Z \int_{E_0}^{E_f} \frac{\sigma_Z(E) T_Z(E)}{S_M(E)} dE \quad (2.1)$$

where: N_{AV} - Avogadro's number;
 ω_z - fluorescence yield;
 b_z - branching ratio of the specific line;
 t_z - transmission of the X-ray through any absorber in the path to the detector;
 ε_z^i - intrinsic detector efficiency;
 $\frac{\Omega}{4\pi}$ - fractional solid angle covered by the detector;
 N_p - number of protons;
 C_Z - concentration of the Z -element;
 E_0, E_f - initial and final energy of the protons;
 $\sigma_Z(E)$ - ionisation cross-section of the specific shell.

$$\text{The transmission factor } T_Z = \exp \left[- \left(\frac{\mu}{\rho} \right)_{z,M} \frac{\cos \alpha}{\sin \Theta} \int_{E_0}^{E_f} \frac{dE}{S_M(E)} \right] \quad (2.2)$$

of the X-rays through the matrix elements is a function of their weighted mass attenuation coefficient μ/ρ , and takes into account the degradation of the energy of the proton beam from E_0 to E_f at the end of the path. In this notation, α and Θ are the beam incidence and X-rays take off angles respectively, and the matrix stopping power S_M is given by:

$$S_M = \frac{1}{\rho} \frac{dE}{dx} \quad (2.3)$$

where ρ is the matrix density.

For the case of thin sample, the expression (2.1) becomes simpler

$$Y(Z) = \frac{N_p m_a(Z) N_{AV} \sigma_Z(E_0) \omega_z b_z t_z \varepsilon_z^i \left(\frac{\Omega}{4\pi}\right)}{A_Z \cos \alpha} \quad (2.4)$$

since no more slowing down of the protons or absorption of X-rays is regarded. Here, $m_a(Z)$ is the mass per unit area of element Z . All of these

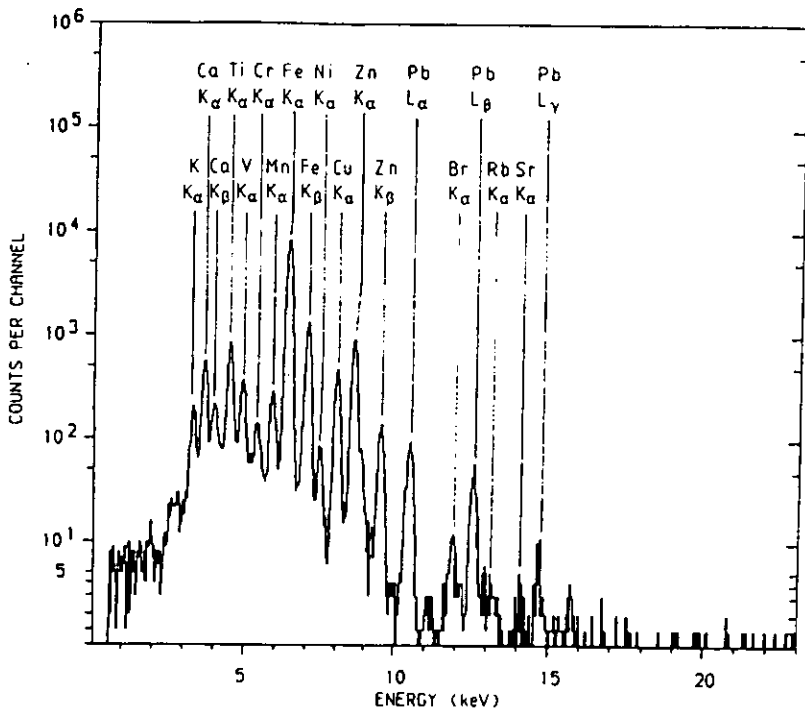


Figure 2.3. PLXE spectrum of a rain water sample (From [Joh-88]).

effects are taken into account when designing computer codes for spectrum handling. A spectrum generated by the computer is made to fit to the measured one using some regression criteria, like the least-square method. The heights of the different peaks correspond then to the X-ray

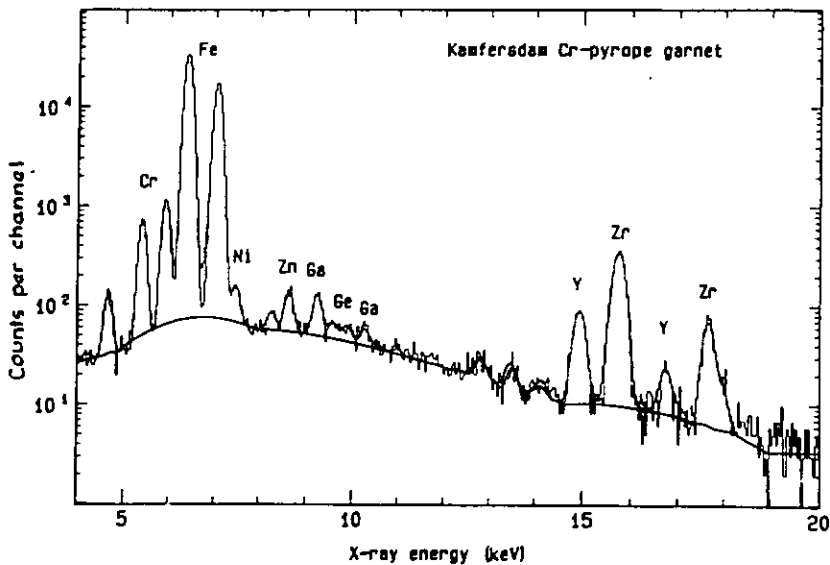


Figure 2.4. Spectrum of a Cr - pyrope garnet sample fitted using GEOPIXE package [Rya-90].

yield $Y(Z)$ and the concentrations of the different elements are determined by (2.1) or (2.4), provided that all the remaining variables are known:

ω - fluorescence yield

As shown in Figure 2.2, following the creation of an inner shell vacancy, two competing processes can occur on de-excitation: the emission of either an X-ray or an Auger electron. K- or L-shell fluorescence yield is the probability of the emission of a K- or L- X-ray line and is a function of the atomic number Z . As a rule of thumb it is valid that for $Z < 18$, the Auger process is dominant and, conversely, the X-ray de-excitation is more probable for heavier atoms.

X-rays fluorescence yields are calculated using the Dirac-Hartree-Slater treatment [Che-80] for the K - shell. For higher shells the Coster-Kronig transfer probabilities (transfer of an initial vacancy to other subshells) must be taken into account.

ϵ_z - detector intrinsic efficiency

The typical hat-shaped efficiency curve of the commonly used Si(Li) detectors is displayed in Figure 2.5. Actually, the intrinsic efficiency of such a detector is a function of different parameters, like its active volume, the thickness and material of the window, and the energy of the incoming X-rays. An overall efficiency just below 100% is attainable for X-ray energies in the range 5 - 25 keV, which is the "region of interest" (ROI) in many cases (Figure 2.6).

Normally, in PIXE analysis, the sensitivity of the method to trace elements is at a premium and absolute efficiency must be maximised. This implies choosing a better geometry in order to increase the solid angle subtended by the detector, $\Omega/4\pi$.

N_p - number of protons (integrated charge)

Measuring charge is performed easily when thin specimens are concerned. The beam, which is assumed to pass through the specimen without losses, can be dumped into a Faraday cup and the current flowing from it to the ground is integrated in a big capacitor. Normally, current digitisers and counters are used in almost all of the PIXE set-ups. When dealing with thick samples, attempts to integrate the current flow, for example through the sample holder, can be fraught with difficulties leading to big errors. Some precautions must be undertaken in order to avoid the escaping of secondary electrons from the surface of the sample.

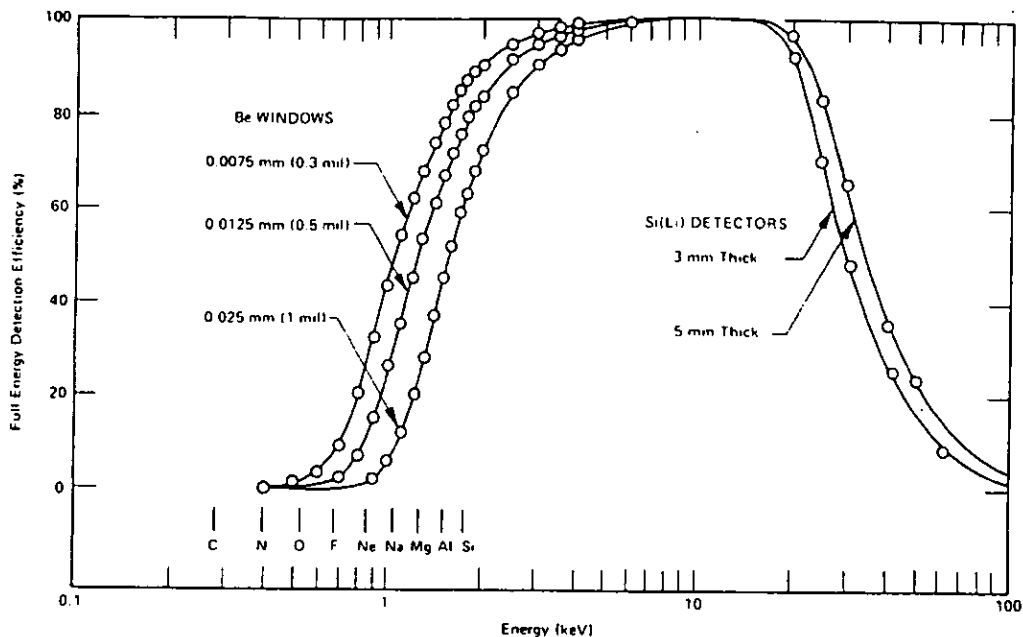


Figure 2.5. Measured efficiency curve for 3- and 5-mm-thick Si(Li) detectors of area 30 mm^2 . (From [Jen-81]).

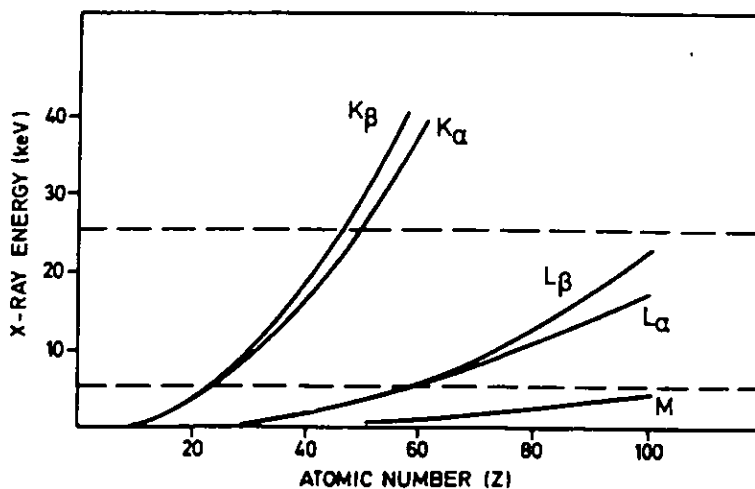


Figure 2.6. Energy of X-rays as function of the atomic number. The dashed lines limit the region with 100% detector efficiency. (From [Joh-88]).

Better results, however, are achieved when a thin foil or a rotating vane are interposed on the beam path in the front of the sample, transmitting the beam in the first case, or just stopping it at a defined rate

in the second case. The backscattered protons can then be counted to give a current value against some pre-calibrated yields.

$\sigma_Z(E)$ - ionisation cross-section.

Ionisation cross-section is the probability of creating an inner shell vacancy at a particle impact. It has its maximum value when the projectile velocity matches that of the ejected electron, which occurs at projectile energies of $E_p = (M/m)U(Z)$ where m and M are the mass of the electron and the projectile, respectively, and U is the binding energy of the electron at the given shell.

Different theoretical models exist to compute the ionisation cross-sections for different shells and projectile energies. In the Binary Encounter Approximation model (BEA), the bound electrons are assumed as "free" ones when interacting with the incoming particle. The differential cross-section for a typical Coulomb scattering can be written and integrated over the whole range of energy exchanges between the electron with binding energy U and the incoming projectile with energy E_p . From this model, the scaling law can be deduced,

$$\sigma_{Z_p, A_p}(E_p, Z) = Z_p^2 \sigma_{1,1}\left(\frac{E_p}{A_p}, Z\right) \quad (2.5)$$

which gives the cross-section σ for any projectile with charge Z_p and nucleon number A_p in terms of that for a proton of the same velocity.

In the Semiclassical Approximation (SCA) and Plane Wave Born Approximation (PWBA), the Coulomb interaction between the inner shell electron and the projectile is used as a perturbation. In the later model, the incoming projectile is described in terms of a plan wave. Higher order perturbation effects like the projectile energy impairment due to its movement in repulsive Coulomb field and the relativistic movement of the electrons are accounted for in the ECPSSR model (Perturbed Stationary State model corrected for Coulomb deflections and Energy loss as well as Relativistic effects). Figure 2.7 gives an illustration of different ionisation cross-sections for different elements and shells, as a function of projectile energy.

Detection limits

The most crucial parameter of any trace analytical method is its ability to detect small amounts of elements present in the specimen. This depends chiefly on the following experimental conditions: the absolute efficiency of the detecting system, the resolution of the spectral apparatus

used, the duration of the measurement to ensure better statistics, and the underlying background noise.

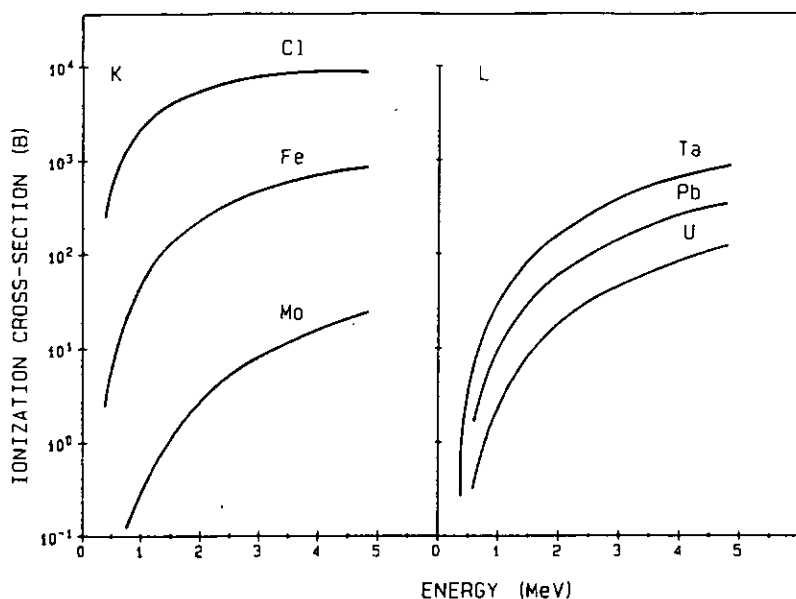


Figure 2.7. Ionisation cross-sections for different elements as function of proton energies. (From [Joh-88]).

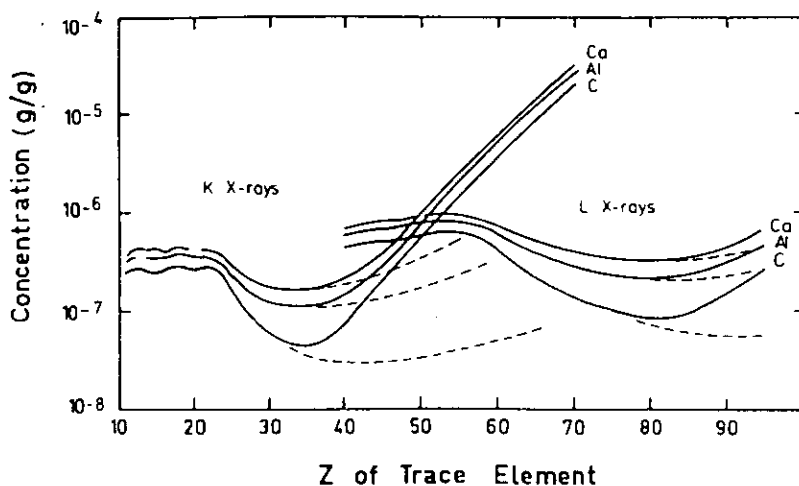


Figure 2.8. Detection limits for 100 μC of accumulated charge of 3 MeV protons on 1 mg/cm^2 targets of carbon, aluminium and calcium. (From [Joh-88]).

In the case of PIXE for thin samples, the following relationship is valid:

$$MDL \propto \frac{\sqrt{\sigma_B}}{\sigma_Z} \sqrt{\frac{FWHM}{Q\Omega}}, \quad (2.6)$$

where σ_B and σ_Z are the cross-sections for background and X-ray production respectively, Q is the accumulated charge and Ω - the absolute detector solid angle. Here the confidence level of 99.9% recommended by IUPAC was applied. FWHM specifies the energy interval at which the background is determined (one, two or three FWHM - full width at half maximum). It follows that several measures have to be undertaken in order to capitalise on the high intrinsic sensitivity of the PIXE method which is, for a range of elements, in the units of ppm level. These include increasing the fractional detector solid angle as much as possible by keeping the Si(Li) detector close to the sample, making longer measurement (increasing the accumulated charge), using detectors with improved resolution and reducing the background.

The commonly used Si(Li) detector has a typical resolution of 160eV at the 5.9 keV peak of Mn. Wavelength dispersive X-ray spectroscopy, which makes use of the diffraction phenomenon in crystals to resolve the different X-ray energies, can easily achieve 10 eV resolution at the price of detecting one element each time. In some applications, the use of this detection technique can be favourable.

The major component of the background in PIXE spectra is originated by electrons of the sample: a) quasi-free electron **bremsstrahlung** (QFEB) due to the scattering of the target electrons in the Coulomb field of the projectile; b) secondary electron **bremsstrahlung** (SEB), due to the scattering of secondary electrons ejected by the projectile in the nuclear Coulomb field, and c) atomic **bremsstrahlung** due to the de-excitation of target atoms. The relative contributions of each of these backgrounds is plotted in Figure 2.9. Background due to electrons is anisotropic and can be reduced by placing the detector at backwards angles.

For the wide energy range of interest in PIXE measurements the projectile **bremsstrahlung** component is negligible if compared with the electron one. Gamma-ray background, however, can reach several tens of counts throughout the PIXE spectrum and is a factor for major concern. It is normally originated when the projectiles excite nuclear reaction in light elements present in the target, producing prompt γ -radiation which can then be Compton-scattered in the detector material. Attempts to reduce the

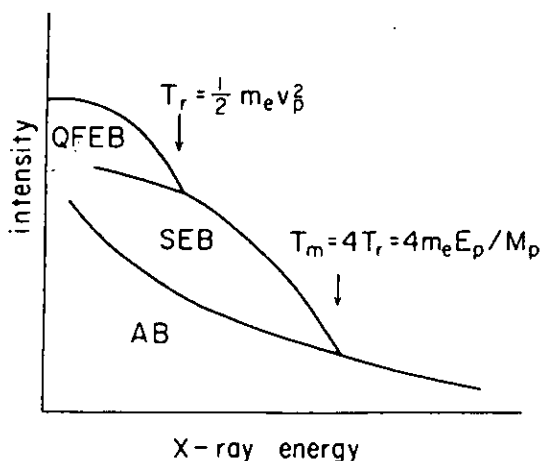


Figure 2.9. Relative contributions of QFEB, SEB, and AB to the electron bremsstrahlung background. The formulae represent the "end-point" of the respective spectra, where m_e , M_p , E_p , and v_p are the mass of the electron, mass, energy and velocity of the projectile respectively. (From [Gri-92]).

weight of this component have been made by a number of researchers (for example [Elf-95]) and rely on the painstaking use of an "anti-coincidence" shield to produce a veto signal whenever a gamma-ray is detected simultaneously at the Si(Li) and some high efficiency scintillating detector like BGO. This can prove to be suitable for use with geological samples where gamma rays are produced in the matrix of low Z elements, causing the Compton background at the region of the X-rays of heavier trace elements.

Moreover, when analysing insulating materials, electrical charging-up can eventually occur which produces spurious events in the 20-30 keV region. Carbon coating the sample is usually enough to eliminate this problem.

2.2.2 Rutherford backscattering Spectroscopy (RBS)

In Rutherford backscattering spectroscopy, the projectile ions scattered at angles greater than 90° are detected. This method was first used by Rutherford and co-workers when trying to prove Rutherford's planetary model of the atom. In these experiments, they used a beam of alpha particles from a radioactive source to bombard a thin gold foil.

The physical processes of interest, in this case, are rather simple to figure out: the projectile beam can undergo small angles forward

scattering and pass through with degraded energy, if the foil is thin enough, or stop completely at some depth if the foil is thick. Eventually, some particles can come close enough to the scattering centres so that elastic interactions become possible. These particles will be deflected at backwards angles and constitute the object of study in RBS (Figure 2.10).

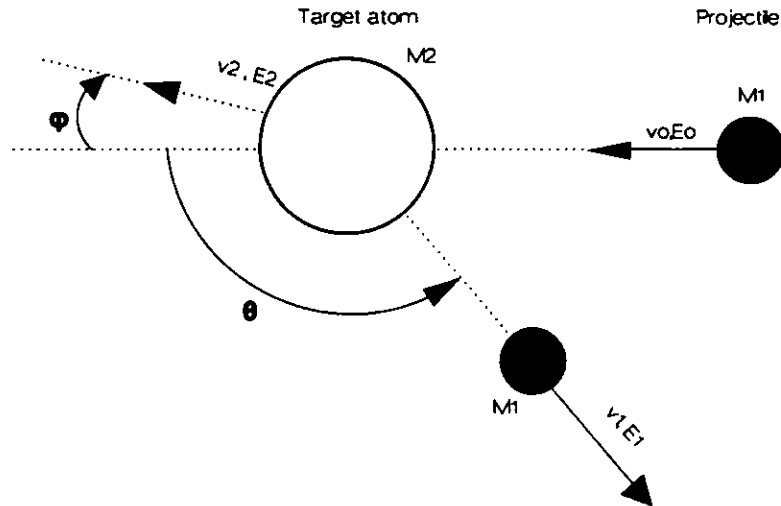


Figure 2.10. Schematic representation of an elastic collision between a projectile of mass M_1 , velocity v_0 , and energy E_0 and a target mass M_2 which is initially at rest. (Adapted from [Chu-78]).

The four basic physical principles involved in backscattering spectroscopy are [Chu-78]: i) energy transfer from the projectile to a target nucleus. This can be treated classically as a two body elastic collision and the ratio of energy loss of the projectile is determined by the **kinematic factor**, which enables the mass resolution of RBS; ii) probability of the occurrence of such a collision, characterised by the **scattering cross section**, which leads to the capability for quantification; iii) average energy loss of a particle moving inside some medium. This property is characterised by the stopping cross section and enables for depth resolution, and, finally, iv) **energy straggling**, which sets a limit on the mass and depth resolution of backscattering spectroscopy.

k - kinematic factor

For a two body elastic collision in the laboratory frame (Figure 2.10) between a projectile of mass M_1 , velocity v_0 , and energy E_0 and a target nucleus of mass M_2 initially at rest, the final velocities v_1 , v_2 and energies E_1 , E_2 , can be derived classic-mechanically by making the assumption of energy and momentum conservation. The ratio of energy loss by the projectile $k = E_1/E_2$, denominated kinematic factor is a function of the target nucleus mass and experiment geometry and, in the laboratory frame, is given by:

$$K_{M_2} = \left\{ \frac{[1 - (M_1 / M_2)^2 \sin^2 \theta]^{1/2} + (M_1 / M_2) \cos \theta}{1 + (M_1 / M_2)} \right\}^2. \quad (2.7)$$

For angles close to 180° , this formula can be approximated by:

$$K \approx 1 - (4 - \delta^2) \frac{M_1}{M_2}, \quad \text{with } \delta = \pi - \theta. \quad (2.8)$$

Normally in RBS measurements, the backscattered particles are counted at angles close to 180° using semiconductor surface barrier detectors (SBD). The ultimate mass resolution that can be attained is derived from:

$$\Delta E_1 = E_0(4 - \delta^2) \Delta M_2 \frac{M_1}{M_2^2}, \quad (2.9)$$

where it was assumed that $M_2 \gg M_1$. Therefore, higher mass resolutions are achievable at higher projectile energies E_0 , and masses M_2 , as well as by detecting the particles at angles with small δ - values (close to 180°). The constraint on energy is imposed by the threshold for nuclear reactions excitation in the sample, while projectile mass M_1 must be chosen, taking into account that targets with mass $M_2 < M_1$ cannot deflect back the projectile particles.

dσ/dΩ - differential scattering cross section.

The probability of a beam of Q particles being scattered at some angle θ relative to its incidence by Nt atoms per unit area (areal density) of the target and being detected at a detector subtending a solid angle $d\Omega$ is given by:

$$\frac{d\sigma}{d\Omega} = \frac{1}{Nt} \frac{dQ}{Qd\Omega}. \quad (2.10)$$

For the case of RBS, assuming a scattering at a Coulomb potential, of projectile particles with mass M_1 and charge Z_1 , on target atoms with mass M_2 and atomic number Z_2 this formula has the following explicit aspect:

$$\frac{d\sigma}{d\Omega} = \left(\frac{Z_1 Z_2 e^2}{4E} \right)^2 \frac{4}{\sin^4 \theta} \frac{\left\{ \left[1 - \left(\frac{M_1}{M_2} \right) \sin^2 \theta \right]^{1/2} + \cos \theta \right\}^2}{\left[1 - \left(\frac{M_1}{M_2} \right) \sin^2 \theta \right]^{1/2}}, \quad (2.11)$$

where e is the elementary charge of the electron. It can be seen that the cross section and, hence, the yield of scattered particles, is proportional to Z_1^2 . So, for a given target atom, alpha particles give four times larger signal than protons.

The formula (2.11) is derived assuming spinless projectile and scattering nucleus. Protons (spin $\frac{1}{2}$), therefore, can only be approximated to Rutherford cross sections at the energies commonly used in IBA.

ϵ - stopping cross section

When bombarding a material with high energy particles, energy loss and subsequent slowing down of the projectiles is by far the most prolific event, if compared to large angle scattering or forward recoils' ejection. The average energy loss per unit path in the material is called **stopping power** dE/dx . Stopping power depends not only on the material, but also on the energy of the particles, since different phenomena concur for the slowing down process of the particles in matter. In higher energies, the behaviour of this magnitude is governed by electronic interactions, while at the lower energy end the nuclear processes take over (Figure 2.14).

For practical uses, however, in RBS, the stopping cross section is often used instead and is defined as:

$$\epsilon = \frac{1}{N} \frac{dE}{dx}, \quad (2.12)$$

where N is the atomic density. For a target composed of different kinds of atoms, the stopping cross sections can be added, with weights pointing for the abundance of each atomic species. This is **Bragg's rule** and accounts

for the sensitivity of the method to the stoichiometry of the sample. For a compound A_mB_n , the stopping cross section is given by:

$$\epsilon^{A,B} = m\epsilon^A + n\epsilon^B. \quad (2.13)$$

Applications

In RBS, the energy of the backscattered particle is related to that of the incoming one by the kinematic factor. This is valid for particles scattered on the surface. For particles scattered at a certain depth x , the energy decrease of the particle in the path to and from the scattering centre must be taken into account. This means that one can distinguish particles scattered at different depths in the RBS spectrum. This property determined the main field of application for the RBS technique: depth profiling atoms, surface analysis (very important in material science), accurate thickness measurement and analytical characterisation in thin film technology.

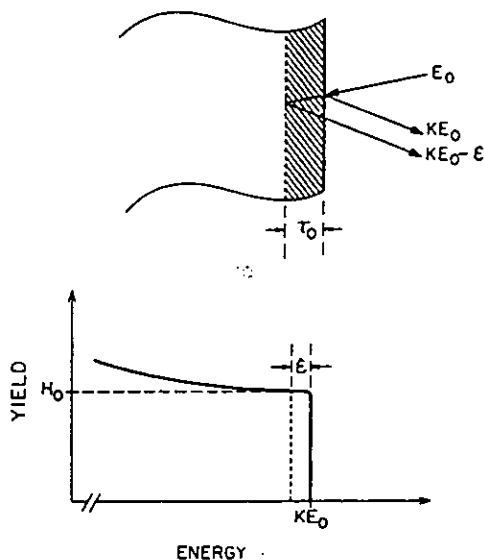


Figure 2.11. Schematic of the RBS process showing the basic principle by which depth profiling is done. The energy width $\epsilon = [\epsilon_0]N\tau_0$, where ϵ_0 is the stopping cross section and N , the density per unit area of scattering centres. (Adapted from [Chu-78]).

Absolute detection limits going down to 10^{-9} g for heavy elements in a low-Z matrix are achievable. The method is normally used as a complement to other surface analysis methods (like SIMS or Auger spectroscopy) to probe several thousands of atom layers with a spatial resolution of hundreds of Ångstroms. The main limitation of RBS is its poor mass resolution at heavy masses. Normally, isotopes up to mass 40 can be successfully resolved.

A variant of RBS technique, RBS-channelling adds another dimension in solid state materials studies, enabling the localisation of atom impurities in oriented crystal samples.

2.2.3 Recoil Spectroscopy

In RBS, the detection of very light elements is troublesome, due to their very small kinematic factor. However, the quantification with this method is rather straightforward and the cross sections very high. These advantages can be used in Recoil Spectroscopy, where the forward recoiling light nucleus under bombardment of heavier projectile ion is detected. The schematic illustration of this process is shown in Figure 2.12.

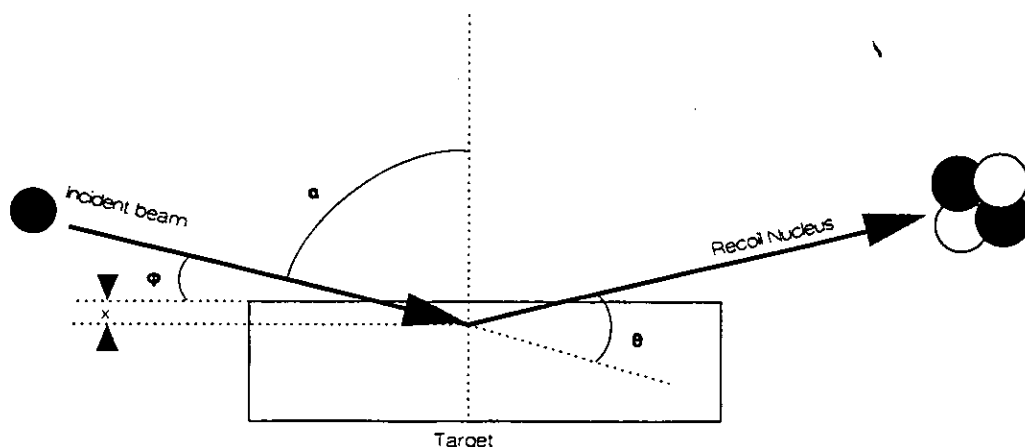


Figure 2.12. Schematic illustration of the principles of recoil spectroscopy.

In much the same way as in RBS, the kinematic factor of the recoil nucleus can be derived to give:

$$k = \frac{E_2}{E_0} = \frac{4M_1M_2 \cos^2 \theta}{(M_1 + M_2)^2} \quad (2.14)$$

Here E_0 and E_2 are the energy of the incoming projectile ion and the recoil target nucleus respectively. The kinematics of the process shown in Figure 2.12 allows, for a heavy incident projectile M_1 , a multitude of nuclei and particles to recoil forwards so the detection system in this case must be able to discriminate not only the energy, as in RBS, but also the nature of ion by its mass M_2 , for example, or velocity v_2 (notations in Figure 2.10).

Looking solely at the elastic processes (Elastic Recoil Detection Analysis - ERDA), one can choose mono- or multi-dispersive methods of detection. In the mono-dispersive method, only the energy of the particle is detected. Particle selection is usually made by placing a simple foil of suitable thickness in front of the SBD, in order to stop other recoils or forward scattered particles. This method is employed normally with alpha particles as projectiles, to depth profile hydrogen [Doy-79].

When aiming at simultaneous detection and depth profiling of different elements, multi-dispersive methods are used. These can be the $\Delta E - E$ or the time of flight (ToF) methods, in which mass and energy or mass and velocity of the recoils are measured [Whi-90].

Different varieties of Recoil Spectroscopy found large application in material science where depth profiling of different elements after material treatment (e.g., implantation, annealing, deposition) is very important for studying their physical properties.

2.2.4 Nuclear reaction analysis (NRA)

As was stated above in IBA, whenever the projectile energy is high enough to overcome the Coulomb barrier of the target nucleus, inelastic scattering can occur. The nucleus can then be excited and different products will be emitted during the de-excitation process are emitted. The emission of such products can be more of an asset than a drawback since its detection brings up more information about the elemental composition of the sample. One then talks about nuclear reaction analysis (NRA). Since at proton energies normally used in IBA only nuclei with $Z \leq 15$ can be excited, NRA is commonly used to detect low- Z elements as a complementary technique to PIXE.

The geometry of the experiment is essentially the same as for the other IBA techniques, but now the products of nuclear reactions are detected. These can be β - or γ -rays, alpha-particles, protons, different ions or any

combination of them. Table 2.1 displays some reactions used in the energy interval of IBA techniques.

Table 2.1. Some nuclear reactions commonly used for detection of light elements. (From [Fel-77]).

Nuclear reactions with release of a particle	Ion energy (MeV)	Emitted energy (MeV)	Q-value (MeV)
${}^2\text{H}(d, p){}^3\text{H}$	1.0	2.3	4.03
${}^3\text{He}(d, p){}^4\text{He}$	0.45	13.6	18.35
${}^7\text{Li}(p, \alpha){}^4\text{He}$	1.5	7.7	17.35
${}^9\text{Be}(d, \alpha){}^7\text{Li}$	0.6	4.1	7.15
${}^{11}\text{B}(p, \alpha){}^8\text{Be}$	0.65	5.6	8.59
${}^{12}\text{C}(d, p){}^{13}\text{C}$	1.2	3.1	2.72
${}^{15}\text{N}(p, \alpha){}^{12}\text{C}$	0.8	3.9	4.96
${}^{16}\text{O}(d, p){}^{17}\text{O}$	0.9	2.4	1.92
${}^{19}\text{F}(p, \alpha){}^{16}\text{O}$	1.3	6.9	8.11
${}^{23}\text{Na}(p, \alpha){}^{20}\text{Ne}$	0.6	2.2	2.38
${}^{31}\text{P}(p, \alpha){}^{28}\text{Si}$	1.5	2.7	1.92
Nuclear reactions with release of γ -rays	ion energy (MeV)	γ (MeV)	Resonance width (keV)
${}^7\text{Li}(p, \gamma){}^8\text{Be}$	0.44	17.65	12
${}^9\text{Be}(p, \gamma){}^{10}\text{Be}$	0.33	6.15	160
${}^{11}\text{B}(p, \gamma){}^{12}\text{C}$	0.16	16.11	7
${}^{13}\text{C}(p, \gamma){}^{14}\text{N}$	0.55	8.06	32.5
${}^{15}\text{N}(p, \alpha\gamma){}^{16}\text{O}$	0.36	12.43	94
${}^{19}\text{F}(p, \alpha\gamma){}^{16}\text{O}$	0.22	7.12	1

The detection of γ -rays, known as particle induced gamma-ray emission (PIGE), can normally be performed using scintillator detectors in order to capitalise on their higher efficiency since the resolution is not at premium. Detecting particles, however, requires much more accuracy since their emission process is not isotropic. The geometric conditions of the experiment are determined by the concepts of momentum conservation, taking into account the Q-value of the particles.

In the cases when more than one product is emitted (e.g., pp' , $p\gamma$, $\alpha\gamma$, etc. reactions), coincidence techniques can be used. In the photon-tagged NRA (pNRA) variant [Kri-90], the γ -photon is used to "tag" the real proton or alpha particle from a $(p, p'\gamma)$ or $(p, \alpha\gamma)$ reaction. The charged particle is simultaneously energy analysed. This method allows higher detection efficiency, thereby improving the detection limits attainable.

As a complementary technique in IBA set-ups, NRA is normally used to, simultaneously with some other methods, detect trace amounts of low-Z elements. Common applications include bio-medical, environmental and geological studies.

Resonance and threshold nuclear reactions, with enhanced cross sections at certain energy values of the projectile ion, can be used to depth profile light elements, with special applications in material sciences. A good example for this is the "inverse" reaction ${}^1\text{H}({}^{15}\text{N}, \alpha\gamma){}^{12}\text{C}$ normally used to depth profile hydrogen. The off-resonance cross section values are more than four orders of magnitude lower than the values at the resonance energy.

2.2.5 Other techniques

It is clear from Figure 2.1 that the detection of any of the enumerated products of the interaction of an ion beam with matter can lead to another IBA technique that proves itself to be suitable for specific applications and rather awkward to others. The different techniques that are eventually brought to light envisage the solution of a peculiar analytical problem.

The detection of electrons, for example, (Auger or secondary electrons) is very much a surface analysis technique. Secondary electrons are produced copiously at ion bombardment and the ones coming from a very shallow depth of the sample can escape from the surface without absorption and are commonly used for quick imaging (since good statistics are readily achievable) in microprobe facilities, as an auxiliary method. Moreover, Auger electrons convey information about the chemical bonding at the surface, as well as the chemical neighbourhood of the atoms, so Auger electron spectroscopy (AES) is an ubiquitous technique in solid state physics laboratories. Since the technique is sensitive to monolayer quantities, a much cleaner vacuum than that commonly used in IBA facilities ($\sim 10^{-6}$ Torr) is required and so, very seldom Auger spectrometers are coupled alongside with other IBA methods. Energetic analysis of these electrons is normally performed using magnetic or electrostatic spectrometers.

Light induced in the sample by ion excitation of the atoms can also be detected. This is the relatively newly developed ionoluminescence phenomenon, which is treated later in more detail.

In special cases, the complement to PIXE used for light elements detection is particle elastic scattering analysis (PESA). Normally, the cross sections for elastic scattering of the protons are one order higher than the

those for inelastic scattering (nuclear reactions). So, in the specific case of thin targets, like environmental samples on Filter backing, detecting the forward elastic scattered protons is much more productive than hunting for the less probable nuclear reaction events. PESA has been successfully used for detection of carbon, nitrogen and oxygen in samples of up to 1 mg/cm^2 thickness [Nel-77]. Thicker samples provide less mass resolution due to higher proton energy loss in the material. The PESA technique can be enhanced by the coincidence detection of the recoiling hydrogen nucleus and scattered proton in a convenient geometry to become a powerful method for hydrogen analysis. Provided that careful time discrimination is made in order to get rid of the interfering inelastic events ${}^9\text{Be}(p, p'){}^9\text{Be}$ and ${}^7\text{Li}(p, p'){}^7\text{Li}$, detection limits in the range of 8 pg/cm^2 can be achieved in thin samples [Mar-93].

An overwhelming illustration of the complementarity, degree of automation, versatility and powerfulness of the IBA techniques is given by the ion beam thermography (IBT). In this method, the fact that during ion impact light elements are sputtered away and volatile compounds are evaporated under the heat developed in a small area is used to study the stoichiometry of thin aerosol samples collected on a conductive substrate [Mar-88b]. A computer-controlled heating system is used to raise the temperature of the sample in fixed steps while simultaneous PIXE, PESA, cPESA and pNRA spectra are collected. The proton beam is brought outside the vacuum into a helium atmosphere to avoid the evaporation of volatile elements in the sample, due to their high saturation vapour pressure. A schematic of the experiment geometry is shown in Figure 2.13. This technique, as described by Mentès et al., [Men-96], allows the detection of all elements from H through Pb, as well as the identification

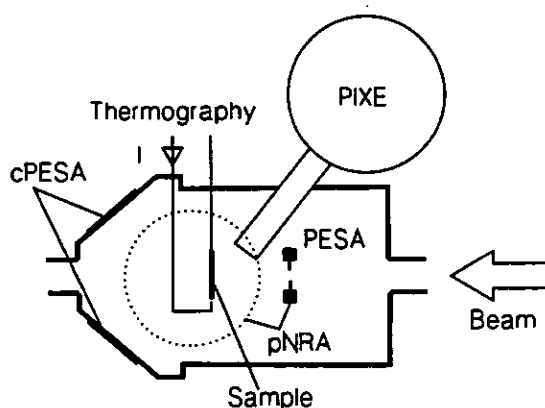


Figure 2.13. Schematic of the geometry used for the IBT experiment. The dotted circle indicates two large plastic scintillators. (From [Men-96]).

of ammonium nitrate (NH_4NO_3) and ammonium sulphate ($(\text{NH}_4)_2\text{SO}_4$), by analysing the fall of the concentration curve of the elements H, N, O, and S versus the temperature of the sample.

2.3 Characteristics of low energy IBA techniques

The above described IBA techniques are commonly used with projectile energies of 2 - 3 MeV. The choice of energy is done by making a trade-off among ionisation cross sections for different elements, cross section for background production, range of the particles in the target material and the best resolution achievable. It is expected, therefore, that a particular IBA method can be optimised to give better sensitivity for the interesting elements in a particular experiment, disregarding the less interesting regions. This fact explains the use of IBA techniques at low energies (sub-MeV), which prove to outstrip the conventional ones at specific applications.

For sub-MeV PIXE, one must bear in mind that:

- i) the detection limit for K X-rays is very poor for elements with $Z > 30$, due to the much lower excitation cross sections;
- ii) the lower part of the MDL curve is shifted towards $Z=15$ (phosphorus), which can be detected at units of ppm levels due to the lower continuous background. In general, PIXE at a proton energy of 350 keV displays lower detection limits for elements between $Z = 12$ (Mg) and $Z = 26$ (Fe) than the commonly used energy of 3 MeV. This sensitivity to low Z elements is even more pronounced in high Z matrixes. This analytical regime can be extended to elements like Na, F, O, N and C, provided that windowless or ultra-thin window Si(Li) detectors are used. The ultra-thin window is made of a light polymer material that enables the detection of elements down to boron. The windowless mode, however, is more difficult to operate, since hazardous condensing of residual vapours on the crystal can damage the detector. Ultrahigh vacuum is normally recommended [Wil-91];
- iii) the range of sub-MeV protons in materials is about one order of magnitude lower than that of protons with 3 MeV energy (Figure 2.14). This means that in low energy PIXE all the samples are considered thick. Absorption of X-rays in the material, however, can be neglected, due to the very shallow depth of excitation considered;

iv) in low energies, dE/dx is near the maximum in the electronic stopping power (Figure 2.14), hence the higher values of this magnitude allow depth profiling using sub-MeV PIXE .

Several applications of low energy PIXE can be found in literature. Almost all of them point to analysis of low - Z impurities in a high - Z

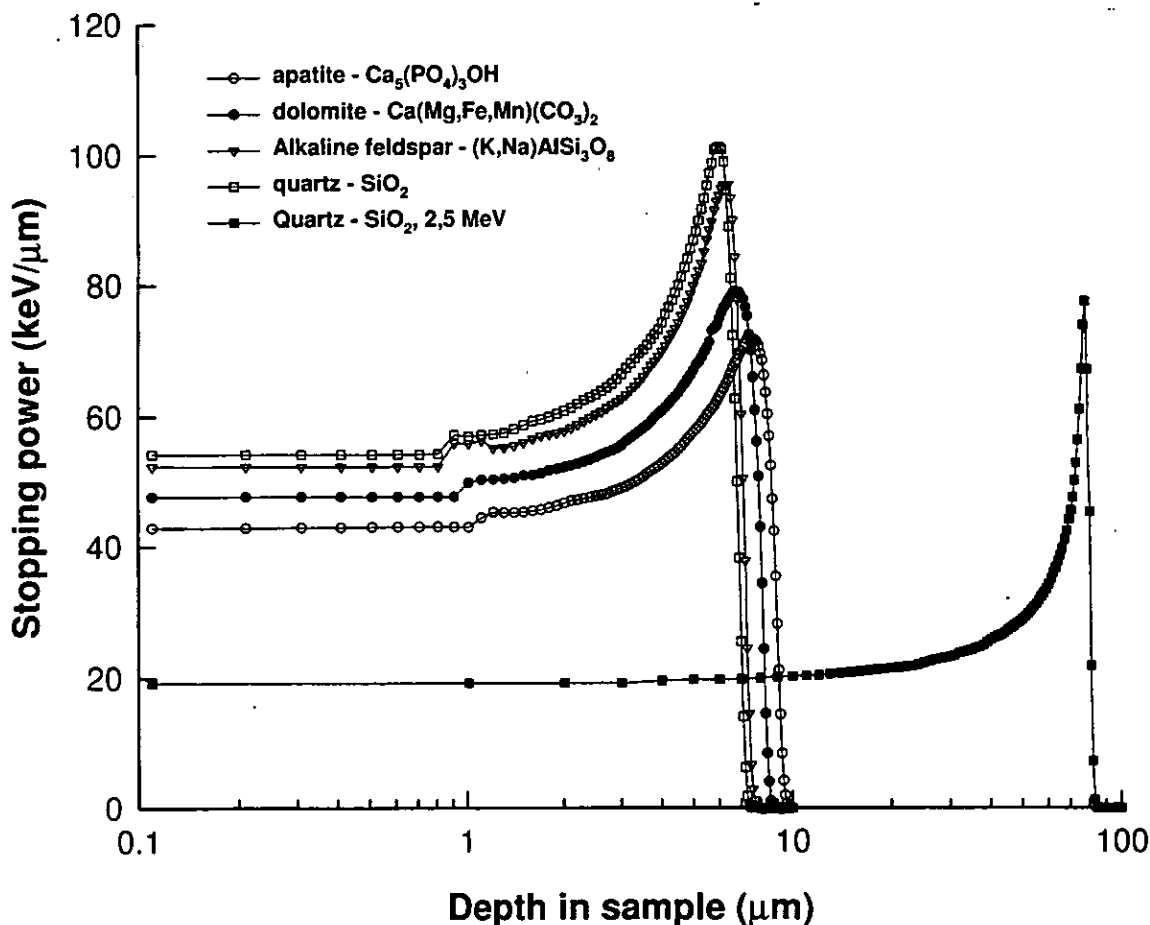


Figure 2.14. Stopping power of protons in common minerals. The beam energy is 500 keV for all the curves except the long one (to the right), which corresponds to an energy of 2,5 MeV. The calculations were done using the code TRIM-95 [Zie-95]

matrixes, impurity depth profiling near the surface, analysis of surface layers and thin films in solid state samples.

Low energy RBS has been used by a number of researchers, specially in material science studies. This technique is usually available at

no expense in the same facilities used for other material treatment like implantation. At these energies, however, RBS has poor elemental separability, so high resolution SBDs must be used. PIXE and RBS can be used in combination to characterise solid state samples.

The use of the microprobe variant of RBS at low energies allows precision three-dimensional characterisation of semiconductor devices [Tak-95]. Further improvements of this method, such as the use of liquid metal ion sources, make it possible to achieve lateral resolutions about 100 nm, which is very important in nanometer technology for three-dimensional studies of integral circuits features like single event upset - SEU ([Kis-95] and [Tak-95]).

Other IBA techniques like ERDA and NRA have been used chiefly for depth profiling hydrogen, fluorine, oxygen and nitrogen. As already stated, the separability of elastic scattering processes for low-Z elements at low projectile energies is very poor, so magnetic spectrometers are used to enhance the resolution of the method [Ros-84]. In the NRA method, resonance reactions are used with detection of γ rays. Some commonly used resonance reactions in the sub-MeV energy range are displayed in Table 2.1.

2.4 The installed laboratory

A low energy IBA facility was assembled at the Eduardo Mondlane University, Maputo. Setting up such a modern facility in local conditions proved to be a challenging exercise. It cannot be overstated that both materially and psychologically the institution was not prepared to run scientific research projects at some complicated levels. Precautions had to be undertaken in order to ensure some degree of self-standingness that would guarantee medium- and long-term running of the project. For this purpose all the details related to equipment and auxiliary services to the IBA facility had to be regarded in minute detail.

The main installation work included:

- Repair of an available small liquid nitrogen plant;
- design and construction of two closed-circuit water cooling systems for both the accelerator laboratory and the liquid nitrogen plant;
- refurbishing of the accelerator laboratory;
- repair and reconditioning the accelerator;
- complete installation and testing of the IBA beam line.

The beam line is mounted at the end of a 500 keV Van de Graaff proton accelerator. This machine was initially designed as a convertible multi-purpose electron/proton accelerator and features some key parameters, which make it possible to be used both as an analytical tool (for producing X-rays, protons, electrons or neutrons) and as an ion implanter. Energy stability $\Delta E/E$ is better than 5×10^{-4} and beam currents as high as 150 μA are attainable.

The schematic drawing of the assembled IBA line is presented in Figure 2.15. An electrostatic lens at the exit tube of the accelerator, with a small aperture (1 cm in diameter) is used to define the beam size. The beam is analysed by a suitable magnet and switched to one of the three arms available (0° , $\pm 21^\circ$). The beam line was built on the $+21^\circ$ arm. Downstream, a magnetic quadrupole doublet is used to focus the beam into the reaction chamber. The specimen chamber was described elsewhere [Mal-82]. It allows the placement of different detectors at different geometries, X-ray absorbers in the front of the detector and a Faraday cup for current measurements when working with thin samples.

For data acquisition, two PC based multi-channel analyser (MCA) slot cards are used, allowing for simultaneous detection of two experimental parameters.

The system was tested and some beam diagnostic experiments were performed. Further tune-up is under way in order to ensure more reliability and stability in the long term.

2.5 Further development

As stated previously, setting up this system was regarded as a means of providing the natural sciences branch of the EMU with a multi-disciplinary analytical tool. Having the system running in a sustainable way, however, poses new questions to be addressed carefully. The most important of these is the training of researchers at different levels and fields to become the day-to-day users of the facility.

This is a medium- to long-term task that we have been working on for several years. The complete package of measures undertaken included: i) redesigning the undergraduate course in Physics offered at the department, putting the main focus on experimental and application profile; ii) starting to form a research team to work with IBA techniques; and iii) focusing on institutional cooperation envisaging rapid crystallisation of the research ideas and applications.

All of these aspects can be regarded as a determinant part in building research capacity in developing countries. The described IBA facility is an example of a multi-disciplinary analytical tool that is starting to be used at the Eduardo Mondlane University.

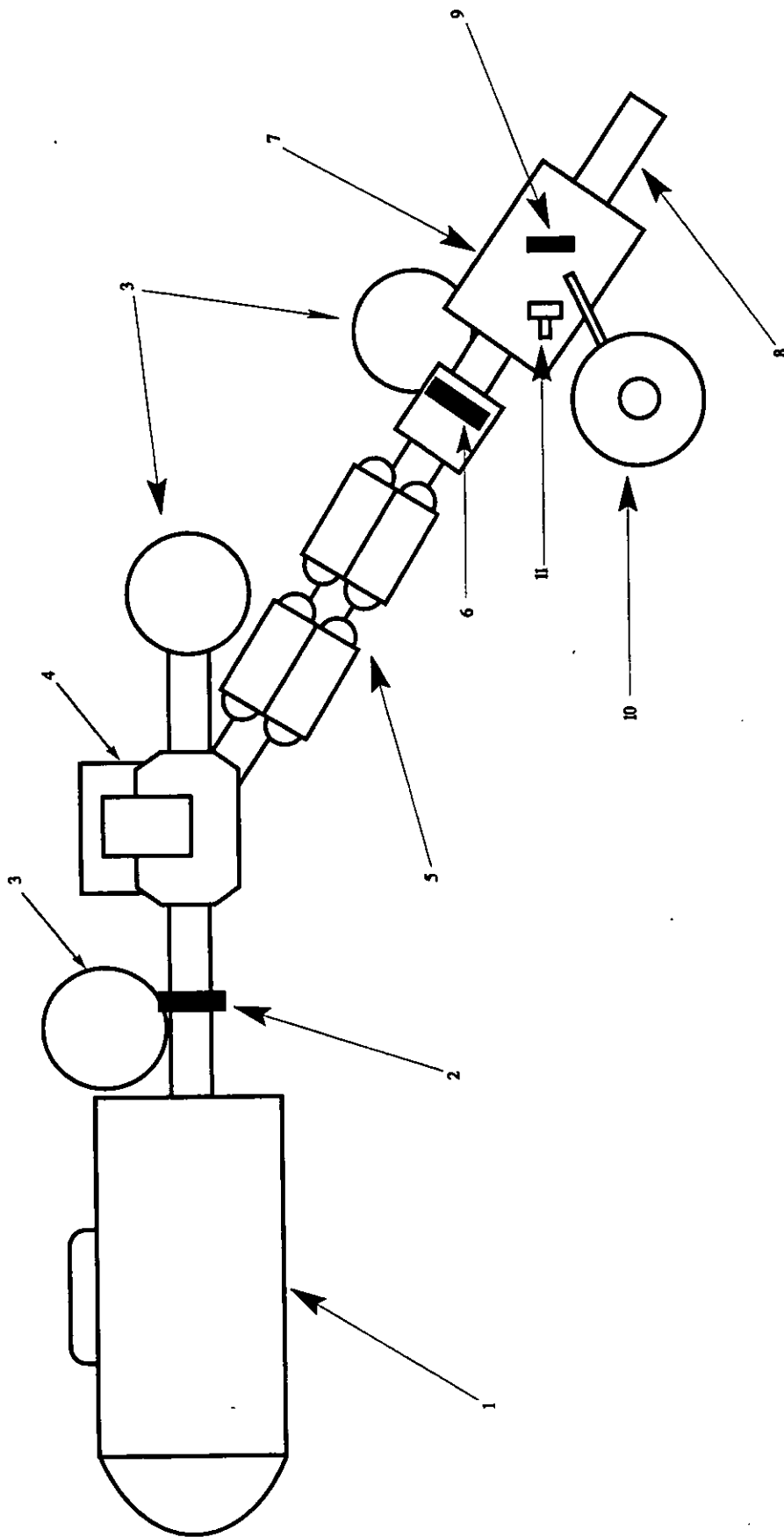


Figure 2.15. Schematic drawing of the assembled beam line (not to scale). 1 - 500 keV Van de Graaff accelerator; 2 - exit slit/ electrostatic lens; 3 - diffusion pumps; 4 - analysing and switching magnet; 5 - magnetic quadrupole doublet; 6 - beam viewer; 7 - reaction chamber; 8 - Faraday cup; 9 - sample position; 10 - Si(Li) X-ray detector; 11 - Surface barrier detector.

3. Microprobe Techniques in geological studies

3.1 Why geological studies...?

Contemporary knowledge about the Earth is built on centuries of patient observations and careful insights. Geology is the earth sciences' branch dealing with the nature of minerals, the meaning and history of mineral associations, as well as their properties and use.

Minerals have been used as tools, decorations or means of exchange since the earliest stages of human life. Records of the use of metals extend 4000 years into the past indicating that Humankind has had to learn, where to find and how to refine iron, gold, silver and copper systematically.

Many references to minerals and ores are found in ancient Greek writings of the philosophers. The first attempts to describe the matter in general were made by Lucretius (99 - 55 B.C.), who established the theory according to which all matter was formed by atoms of the four components of the Universe: earth, water, fire and air. Although minerals were used rather extensively for millennia, the first document that attempted to establish a systematic study of minerals came to light only in 1556. It was the *De Re Metallica*, published by the German physician Agricola. The work presented practical aspects of mining and metallurgy and is often regarded as the cornerstone of the establishment of Mineralogy as a science.

Since then, and during the Renaissance-to-Modern period, several breakthroughs marked the evolution of mineralogy and hence, of the geological sciences: the invention of the goniometer for measuring interfacial crystal angles (Carangeot in 1780); establishment of the Freiberg, Germany, school of mines by A.G. Werner (1750 - 1817) and the development of the mathematical crystallography (R.J. Haüy in 1801).

A great contribution to the understanding of mineral chemistry was supplied by the Swedish scientist J.J. Berzelius (1779 - 1848) who devised the chemical classification of the minerals that is still in use today. Some remarkable breakthroughs in the Modern era include the invention of the polarising microscope by Nicol, 1828, and the demonstration of the diffraction of X-rays in crystals (von Laue, 1912). Then, W.H. Bragg and his son, W.L. Bragg, determined the structure of several crystals using X-ray diffraction. The internal structure of minerals was being studied for the first time!

The most recent developments of analytical tools applied in mineralogy, and geology in general, allowed to get a close insight into

the matter structure at atomic level and its relation to the minerals' properties. Scanning electron microscopy (SEM) enabled the observation of mineral grains amplified up to one million times; transmission electron microscopy (TEM) permits studying the internal structure of the minerals (Section 3.2.3). Electron Microprobe Analysis, Nuclear Microprobe and Ion Microprobe are relatively new variants of electron or ion focused beams analytical techniques with microscopic capability and their extensive use added a new dimension in geological studies.

In studying Earth sciences, a threefold aim is pursued:

- i) to achieve a better understanding of the processes involved in mineral genesis for better prospecting and more effective use of natural resources;
- ii) to assess the common threads in the history of the planets and the Universe in general (comparative planetology), for better understanding the Earth and, eventually, searching for life conditions and useful goods on other planets, and
- iii) to try to understand how and to what extent the human activity is changing the Earth on a more global scale. This is a newly raised concern and springs from the uncomfortable feeling that seemingly irreversible changes have been taking place since the surge on industrialisation and establishment of consumer societies in rich countries.

...and why microprobe?

The atoms form 104 chemical elements, and 88 of these occur naturally on the Earth. However, the 12 most abundant elements make up 99,2% of the Earth's crust, which means that the remaining elements occur at minor or trace levels. The dynamic range of concentration change of these minor and trace elements is much wider and depends heavily on the conditions at which the minerals crystallised. Studying trace elements, therefore, provides more information and, in geological studies, techniques sensitive to low concentration levels are the most adequate.

Normally, the minor and trace elements are used as indicators of a particular feature to be studied; the most important subjects of analysis are individual mineral phases [Rya-93]. These mineral phases are typically a few μm in dimensions and so small are the patterns normally studied like, for example, zonation [Sie-89]. Techniques with microscopic capability are very convenient in this case. The following subjects are addressed in microscopic studies of geological samples:

i) **rock textures:** a magnified view of a thin section sample of a rock enables, to an experienced operator, its rapid identification through recognition of the mineral assemblages present as well as a tentative quantification of the same minerals [Bla-88]. This is generally the first step in any kind of analysis. For this purpose, petrographic microscopy with light polarising attachments or cathodoluminescence [Kea-88] are used;

ii) **mineral exploration:** the distribution of trace elements in a single grain can give clues about the physicochemical environment that governed the process of crystallisation (ore genesis), which, by its turn, can improve targeting during mineral prospecting activities [Sie-89]. Normally the occurrence of a certain mineral of interest is associated with the presence in certain amounts of a set of other more common minerals, which are then established as indicators [Gri-89], [Rya-96]. Techniques like μ PIXE, EMPA, SIMS or SRXRF can be used for this purpose;

iii) **zonation:** when different minerals coexist in cooling magma, the crystallisation will occur in steps so that minerals with higher melting point will crystallise first. This phenomenon (fractional crystallisation) is normally accompanied by processes like exsolution of elements dissolved in excess in the liquid phase of a certain mineral [Ski-87]. It follows, hence, that the cooling magma will change its chemical composition as more minerals solidify. The study of elemental distribution along these zones can help to increase the understanding of the processes involved in ore genesis, with applications in petrologic and tectonic studies [Rei-93], [Smi-91]. Cathodoluminescence very beautifully helps in identification of zonation in minerals [Mar-88a]. Any other analytical technique (from point ii) can be used in quantification;

iv) **fluid inclusions:** crystal imperfections can range from minute defects at atomic scale to gross macroscopic structures. Fluid inclusions represent perhaps the most valuable of the crystal imperfections: they are formed by small amounts of liquids, solids and vapours, trapped inside the minerals as they grow. These inclusions are unique samples of the ore forming material that have interacted with the earth's crust and the upper mantle [She-85]. The main information that can be extracted from fluid inclusion studies include: understanding fluid flow paths at the time of ore formation [Rya-95a] and, through the

determination of PT state of the fluids, inferring whether ore deposition could occur at these conditions, which has applications in geological prospecting. Using fluid inclusions as tracers can help to identify the provenance of minerals, which aids in finding migration pathways and possible reservoir rocks.

Methods commonly used for fluid inclusion studies are: optical microscopy with a heating/cooling attachment; laser ablation - inductively coupled plasma atomic spectrometry (LA-ICP-AS), synchrotron radiation X-ray fluorescence (SRXRF), SIMS and μ PIXE [Rya-93a].

v) ***geobarometry and geothermometry***: The partition of certain elements in two or more coexisting mineral phases during crystallisation is a function of many variables, amongst them the pressure and temperature at which solidification occur. The concentration of these elements can vary, in certain cases, over a large range for different temperature values, permitting them to be used as indicators of the temperature, or geothermometers [Gri-89a]. The same assumptions are valid for geobarometry. These two "instruments" are normally used in studying ore genesis in metamorphic petrology and tectonics.

During large-scale metamorphic events processes like burial, heating of rocks by some new heat source (e.g., an intruding igneous rock), or compression due to continental collisions, take place. Hence metamorphic rocks keep a record of the intermediate steps through which the igneous and sedimentary rocks are transformed. Using geothermometers and geobarometers the history of rock transformation can be followed by constructing the so-called pressure-temperature-time (PTt) paths [Eng-84], [Eng-84a]. The microprobe methods used for these analysis must be sensitive enough to detect units of ppm levels [Gri-89a], so SIMS, μ PIXE, LA-ICP-AS and SRXRF are commonly employed.

vi) ***geochronology or geological datation***: Geological age is normally determined using radioactive tracers, which have been present in the minerals since their formation, and have decayed or are in decay to stable daughter-isotopes. The commonly used radiometric clocks are: $^{40}\text{K}/^{40}\text{Ar}$, $^{87}\text{Rb}/^{87}\text{Sr}$, $^{235}\text{U}/^{207}\text{Pb}$ and $^{238}\text{U}/^{206}\text{Pb}$. The daughter elements are retained in the host mineral in substituting positions (for the solid metals) or trapped in sub-microscopic fractures in the minerals. Performing geological dating is a microscopic task that involves choosing the right accessory mineral or material that can be dated and

performing microanalysis with isotope separation and detection limits in the units of ppm level. This can be performed successfully using μ PIXE combined with IL [Yan-94], SIMS, SRXRF or LA-ICP-AS.

3.2 Microprobe techniques for geological studies

The aim of any microprobe (microscopic) technique is to provide a magnified image of a solid object, allowing the observation of features beyond the resolution of the human eye, which is about 100 μ m. The image can be produced by some conventional lens system in which all the parts are formed simultaneously, or by a scanning mechanism in which each point, or **pixel**, of the picture appears serially. The possibility of subdividing the picture into small elements permits their encoding for digital storing in computers for *a posteriori* processing.

In microscopic techniques, a probe signal is sent to the object and some response signals coming from it are collected. These response signals must have the ability of providing the **contrast**, the property that makes possible to distinguish the pixels.

Analysed objects are tri-dimensional so the microprobe techniques, in tandem with **magnification** or **lateral resolution**, can have some ability to represent the depth (**depth resolution**). The topological contrast in light microscopy, for example, is provided by shadowing in reflection and in SEM, by the fact that the efficiency for generating secondary electrons (the response signal) from the top tens of monolayers of the material, depends on the angle at which the probe beam strikes the surface.

Moreover, optical systems, like lenses, are prone to aberrations. The easiest lenses to make are spherical and the sphericity *per se* gives rise to two kind of aberrations: **chromatic** and **achromatic**. Chromatic aberrations arise from the fact that different wavelengths (or particles with different energies in electron or ion optics) are focused at different points. The non-monochromaticity of the probe signal is, hence, the source of this type of aberration. This error can be corrected for by using electrons or ions that are energy analysed before forming the probe, or, in light optics, more monochromatic sources.

Achromatic aberrations arise from the difference in path lengths of different light rays or energetic particles from an object point to the corresponding image point. The most simple of these is the **spherical aberration**, which is caused by the fact that light rays (in optical systems) or particles (in electron- or ion-optical systems) have different focal planes depending on their orientation relative to the optical axis of

the lens. The resulting spherical aberration is proportional to the third power of the inclination angle and can be corrected for by keeping the probe beam as parallel as possible to the optical axis. Another spin-off of the spherical aberration is the **astigmatism**, which arises from different focusing strengths in the horizontal and vertical axis. In ion optical systems, this error can be corrected by setting different focusing currents in the horizontal and vertical magnets.

In the case of ion optics, making spherical or cylindrical symmetric magnetic lenses, is fraught with enormous difficulties due to limitations in the maximum attainable focusing strength. Normally, a combination of quadrupole lenses, each focusing into a line, is used. The obvious departure from the cylindrical symmetry in these lenses gives rise to parasitic aberrations like **rotational and translational**, which can be corrected for by careful alignment, and intrinsic **sextupole, octupole** and higher order multipoles, which are due to the contamination of the quadrupole field and are dependent on the construction of the lenses themselves.

Optimising these parameters is very important for a microscopic system to attain the best spatial resolution.

3.2.1 Optical microscopy

In its simplest version, the optical microscope is composed by two sets of lenses: the objective and the ocular. Light is made to pass through the analysed sample towards the magnifying column (transmission light mode) or is reflected on the surface of the former (reflected light mode). The overall magnification of a microscopic system is given by

$$M = \frac{(v_1 - f_1)(v_2 - f_2)}{f_1 f_2}, \quad (3.1)$$

where v_1 is the distance from the objective to the intermediate image, v_2 - the distance from the ocular to the final image, and f_1 and f_2 are the focal distances of the objective and ocular lenses respectively.

For light optical systems, the resolution is theoretically limited by the diffraction phenomenon and is given by:

$$R = \frac{0.61\lambda}{\mu \sin \alpha}, \quad (3.2)$$

where λ is the wavelength of the used radiation, μ - the refractive index of the medium between the object and the objective lens, and α - the half angle subtended by the aperture in the front of the objective lens.

In geological applications, several attachments to the common optical microscope are often used, allowing more information from the sample to be collected. Among these are polarisers and analysers, condenser lenses, xy movable stages, a cathodoluminescence apparatus and a heating/freezing stage for fluid inclusions' studies. Polarisers and analysers are used to identify the different minerals by their different refractive indexes using the phenomenon of birefringence in anisotropic crystals.

Samples to be studied with the petrographic microscope (as it is called, when equipped with such attachments), are usually either finely crushed mineral powders or very thin rock slices (20 to 30 μm thickness), polished and mounted on a slide backing, called **thin sections**.

Aside from some direct measurements of refractive indexes and identification of mineral colours, additional information regarding size and shape of the different mineral facies, exact chemical composition and micrometer features like zonation can be readily obtained.

Optical microscopy is generally the first step in the analysis of any geological sample and, in some cases, it can be the only one, due to the wealth of information that can be gathered. Resolution in the order of units of μm are attainable in good systems.

3.2.2 X-ray microscopy

X-ray fluorescence (XRF)

X-ray fluorescence is a well established analytical technique that has been in use for several decades now. The main advantages are: the easy to use and low cost of the set up, non-destructiveness, multi-elemental capability and high sensitivity for elements from sodium across the periodic table.

The physical principles behind the XRF method are similar to the ones described for PIXE (section 2.2.1), with the difference residing in the excitation mode. In XRF, a flux of primary X-ray photons is used to create the inner shell vacancies in the atoms of the sample.

Instrumental

The microscopic ability of XRF springs from the fact that tiny capillary tubes, tens of μm across, can be made to convey the ionising radiation to the analysed pixel on the sample and the X-ray spectrum of each pixel can be measured. An additional xy scanning stage moves the sample relative to the beam and "image" information of each pixel is recorded successively.

X-ray tubes are normally used as sources of primary X-rays. They consist of an evacuated tube in which electrons are accelerated by a potential difference of several tens of kV to bombard a window material and produce X-rays. This one is chosen so that the emitted X-rays have higher energy than the electron binding energy in the shell. Eventually, some mono-chromatisation of the primary beam is necessary in order to avoid complicated artefacts in the X-ray spectra caused by the different energies of excitation.

For X-ray detection, both wavelength dispersive (WDS) or energy dispersive spectrometers (EDS) can be used. In WDS, the phenomenon of diffraction of X-rays in single crystals is used to resolve different X-ray lines. The principle governing this phenomenon is described by Bragg's law:

$$n\lambda = 2d \sin \vartheta , \quad (3.3)$$

which states that a crystal with lattice planes parallel to its surface reflects radiation of specific wavelength λ at certain angles of incidence ϑ , in a direction with the same exit angle. Here n is an integer ($n = 1, 2, 3, \dots$) and d is the lattice plane spacing. The limitation that $\sin\vartheta$ cannot be greater than 1 implies that a single crystal analyser can be used to detect only one part of the spectrum. Commercial crystal spectrometers cover a range of $\vartheta = 15^\circ$ to $\vartheta = 65^\circ$, so several crystals are used with different lattice spacing (at least four) to cover all the range of elements accessible to X-ray analysis.

Such a system can achieve a resolution of about 10 eV, but the analysis are too slow and the intensity of the X-rays is strongly damped by the diffraction/reflection phenomenon. This dictates the use of high power tubes in WDS (up to 3 - 4 kW), while for the most efficient EDS mode, powers less than 100 W are sufficient. EDS systems use a Si(Li) detector with typical resolution of 160 eV at 5.9 keV, which permits the simultaneous recording of the whole spectrum.

The samples used for microprobe analysis can be the same thin sections as in the case of optical microscope. For bulk analysis, samples consist of powders of the crushed rocks that have been pressed into pellets.

Detection limits

Typical detection limits are on the order of a few ppm for a range of elements. Disadvantages of this method related to PIXE, for example, are: i) it is always possible to make combined use of complementary analytical methods in IBA, increasing the sensitivity to virtually all the elements in the periodic table, and ii) a large source of background is introduced by the X-ray excitation radiation itself in XRF. Compton scattering of these primary X-rays in the sample material forms a large continuum over the entire spectrum, which impairs the detection limits of the method. A common way of reducing this parasitic background is to use a secondary target in the path of the X-rays to the detector. The background is then polarised and can be strongly reduced by placing the detector at a suitable geometry.

An important advantage of XRF related to PIXE is the fact that it is a non-vacuum technique and, so, it poses less constraints on the samples.

Total reflection X-ray fluorescence (TRXRF)

In total reflection X-ray fluorescence, a grazing angle incidence (about 1 mrad) of the primary beam is used. A pencil of X-rays illuminates a very small volume of sample and is totally reflected on the backing material. The fluorescence X-rays from the sample are then detected at a normal direction without the "contamination" of the parasitic background.

Very low detection limits can be achieved by this method (down to ppt) due to the following reasons:

- the sample is efficiently excited by both the primary and the reflected beam, thereby doubling the intensity of the fluorescence signal;
- the spectral background due to primary X-rays scattering on the backing material is reduced drastically, since the beam impinges at angles below the critical angle for total X-ray reflection, and

- the detector can be placed very close to the sample, since it doesn't interfere with the incoming and outgoing X-ray beams, allowing the increase of the absolute detection efficiency.

Unfortunately this method can be used only with very thin samples, which imposes serious constraints on such a sensitive technique. The microscopic ability of this method can be attributed to the fact that μl of the samples are normally used in the analysis.

Synchrotron Radiation X-ray Fluorescence (SRXRF)

Albeit all of the advantages of a synchrotron light source over the others X-ray sources, SRXRF is not likely to become a routine analytical method for geological research and the reported work that has been done can only be seen in a pure academic perspective. Synchrotrons are very complicated instruments to operate and are extremely expensive to run. However, the copious fluxes of X-rays radiated in the curvature points of a storage ring feature very suitable properties for analytical purposes, like high brilliance, low divergence, continuous spectrum over a very wide range and high degree of polarisation, just to name a few. The insertion of **undulators** or **wigglers** increase both the intensity and the high energy component of the emitted spectrum.

The X-rays can be made to pass through a pin-hole or special focusing mirrors to form the microprobe, which irradiates a target mounted on a xy scanning stage. Absolute detection limits of 1 pg and relative MDL better than 0.1 ppm in bulk samples are attainable.

Some other, more exotic X-ray sources, like multi-million degree plasma and the X-ray laser (available in the 100 Å region only), can prove to outstrip the presented sources in special applications but I remain rather sceptical about their possible application in geological analysis.

3.2.3 Electron Microscopy

Scanning electron microscopy (SEM)

In scanning electron microscopy, a focused beam of electrons is scanned across the sample. The response signal can be chosen between the copious fluxes of either secondary or backscattered electrons. The electrons are detected by scintillators and the signal, after amplification,

is used to modulate the brightness of the scanning electron beam of a cathode-ray tube (CRT).

SEM is an imaging technique with outstanding lateral resolution and, since its invention in the late 1950's, it has found place virtually in any field of studies.

Instrumentation

A source of electrons, which can be either a tungsten hot cathode or a field emission cathode, delivers a beam of electrons that is preliminarily focused by an electrostatic lens. The beam crossover can be adjusted to fit the opening of the exit anode, which forms the object. The electrons are accelerated by voltages from 2 to 30 kV and the probe is formed by two sets of magnetic lenses. Electrons are very light particles and at the magnetic fields of simple solenoids, probe sizes of about 5 nm can be easily achieved with currents of about 10 pA.

The physical principle behind the method is quite similar to that already analysed in chapter 2 with more detail. Electrons with several tens of keV of energy have the same velocity as the few MeV/amu ions, so the probabilities for almost all the interactions showed in Figure 2.1 have the same order of magnitude.

The signal from secondary or backscattered electrons can eventually be collected sequentially and stored in computers after analogue-to-digital conversion. Further image processing is then possible. SEM microscopes are very compact instruments and easy to use, so they are widely applied in medicine, geology and in the semiconductor industry as imaging accessories.

Contrast

The contrast in SEM is provided by the fact that the yield of secondary electrons is dependent on the angle of inclination of the probe. A small inclination, in the case of flat polished samples, can provide the tri-dimensional visual feature. In "normal" samples, the topographical variations are enough to provide the needed contrast.

Samples

The surface of the samples must be kept conductive in order to avoid charge build up. Gold coating is normally used in insulator and semiconductor samples, since it warrants continuity of higher conductivity of the thin films even at very small thicknesses. However, if

analytical methods like EMPA are to be used, then gold must be avoided since it can give rise to spurious X-rays peaks. Carbon coating is used instead.

In geological applications, SEM can be also the first step before moving to an analytical microscopic technique. The thin samples prepared for the optical microscopy are used and identification of minute crystals or features is made by this method. SEM microphotographs are normally used for finding the region of interest in further analysis, as well as for helping in qualitative evaluation of the data.

Transmission Electron Microscopy (TEM)

Unlike the SEM mode, in which bulk samples are analysed, i.e., samples thick enough to stop the electron beam, in transmission electron microscopy, very thin samples (around 0,1 μm or less in thickness) are illuminated by an electron beam. The electrons are then transmitted through the sample and the object thus formed is amplified in two or more stages by electron-optical lenses. The image is normally projected on a CRT directly and not pixel by pixel as in SEM. This method is very similar to optical microscopy in the transmitted light mode.

The image contrast is generated by the electrons, which undergo large angles scattering in the sample and are, hence, excluded from the beam that forms the image. In the image, regions with less intensity correspond to some scattering centres in the object.

The need for extremely thin samples implies the use of very accurate procedures for sample preparation, which constitutes the Achilles' heel of the method. However, the very fact that only very thin samples are used, warrants a resolution some two orders better than the SEM method because of the much lesser material volume probed. Indeed, the signal from the SEM image formation comes from the typical onion-shaped volume that is excited by electron bombardment (Figure 3.1). In TEM, the values for range and straggling are lower and thus, the resolution higher, extending down to atomic dimensions. Moreover, the transmitted electrons give information about the material structure like crystal defects and grain sizes.

In tandem with the backscattering of electrons, which is used to form the image in TEM, some other processes occur in much the same way as in Figure 2.1, and the emitted signals can be used to add some analytical ability to the TEM microscope. Eventually the beam can be scanned, permitting the combination of TEM and SEM. Then, new analytical methods possessing the advantages of the two imaging

techniques can be used. The instrument is then called STEM (scanning transmission electron microscopy) and methods like electron energy loss spectroscopy (EELS) or electron microprobe analysis can be used. EELS is the electron sibling of STIM (scanning transmission ion microscopy), in which the beam of incident particles is scanned across a thin sample and the energy loss of the particles is analysed downstream. The image contrast is warranted by the difference in mass densities of different pixels.

In geological studies, TEM and related techniques are used to study the structure of the crystals and minerals, so it is rather a mineralogical method.

Electron Microprobe Analysis (EMPA)

The electron microprobe analysis is based on the use of X-ray spectroscopy in a scanning electron microscope. X-ray spectra of each pixel is then recorded, encoded and stored with the corresponding coordinates. Digital maps (images) can be reconstructed on- or off-line where the contrast is given by the difference in point concentration of the different chemical elements.

The physical principles are identical to those for PIXE method. However, if compared to μ PIXE, EMPA suffers from the following disadvantages:

- i) the electron excitation *per se* implies that the signal comes from a very shallow depth of the sample, so "buried" structures like fluid inclusions cannot be directly analysed.
- ii) the very high **bremsstrahlung** of the incident particles yields a prominent broad peak in the low-to-medium energy part of the X-ray spectrum, which leads to detection limits poorer than in PIXE by two orders of magnitude.
- iii) although different analytical techniques can be used simultaneously in a SEM instrument, the Nuclear Microprobe is much more open to the user system, so the implementation of new analytical ideas is only limited by the imagination of the physicist. SEM is a more compact and ready to use system in which fundamentally new approaches imply a new design.

(P. P. 5)

This last disadvantage, however, can also be regarded as a great achievement since the "black-box" approach of an electron microscope enabled its widespread use among almost all research fields and the users require less training. A very big share in geological studies, presently, belongs to SEM and EMPA.

3.2.4 Ion Microscopy

Dynamic secondary ion mass spectroscopy (SIMS)

Secondary ion mass spectroscopic methods make use of a phenomenon known since the 1890's; when solid surfaces are subjected to ion bombardment of high fluency, components of their outer surface are abraded with emission of neutral clusters and secondary ions. These products are mass analysed by a mass spectrometer and depth profiling of elements present at trace levels in areas as small as 10 μm in diameter can be performed. In geological applications, this method is normally used in datation and geothermobarometry. The high resolution that can be achieved by this method (better than 1 μm) coupled to its high sensitivity makes possible "spot" datation, i.e., in a zoned crystal, the age of each growth layer is determined.

Dynamic SIMS is one of the most sensitive analytical techniques, with typical detection limits ranging from ppm to sub-ppb levels, depth resolution better than 2 nm and spatial resolution from 50 nm to 2 μm for elements from hydrogen through uranium. It is typically a monolayer sensitive technique (10^{12} to 10^{12} atoms/cm³).

Absolute quantification, however, is fraught with serious troubles and only relative quantification with standards is commonly used. This puts serious constraints on geological studies, since absolute geological standards are difficult to synthesise due to varying mineral composition from terrain to terrain.

The sputtering process

Ions heavier than oxygen with energies between 1 and 20 keV impinging on a surface can efficiently transfer their energy to the generation of cascades of neutrals or secondary ions moving at different velocities in backwards directions. Eventually the energy of these clusters can be high enough to overcome the surface potential barrier and then the neutrals and secondary ions are sputtered from the surface.

It is accepted that the current of secondary ions collected by the SIMS instrument is given by:

$$i_A^\pm = \eta_A^\pm \gamma_A^\pm C_A S D_p \pi \left(\frac{d}{2} \right)^2, \quad (3.4)$$

where i_A^\pm is the secondary ion current for element A,
 η_A^\pm - the isotope collection efficiency,
 γ_A^\pm - the ratio of ions produced to the total number of particles (neutrals and charged) sputtered of element A,
 C_A - concentration of element A,
 S - the sputter yield (sputtered particles per incident ion),
 D_p - primary ion current density (ions /cm².s), and
 d - diameter of the primary beam.

This formula is only semi-quantitative since strong deviations from it arise depending on the matrix in which the element A is inserted.

Detection limits

The MDL for each element depends on its electron affinity or ionisation potential, the chemical nature of the sample and the type and intensity of the primary ion beam. At the absence of **spectral interference**, the higher the sputtering yield, the lower the MDL. In some cases, methods of increasing the secondary ion beam are used. Then, a second ionising radiation is rastered close to the sputtered surface so that a more efficient ionisation of the particles occur. High intensity laser beams (SALI - surface analysis by laser ionisation) are normally used.

Samples

For better depth resolution it is important to keep the samples very well polished with micrometer finishing. For geological studies, thin sections of minerals or, preferentially, single grains are cut and polished in a glass mount of about 2,5 cm in diameter.

Instrumental

SIMS instruments are mainly distinguished by their primary ion beams and the type of spectrometers they use to analyse the secondary

ions. Beams of oxygen, argon and caesium from duoplasmatron sources or gallium from liquid metal ion sources are used depending on the applications. The use of high brilliant liquid metal ion sources allows to achieve high spatial resolutions.

For the measurement of secondary ions, different types of mass spectrometers can be used: time of flight, magnetic quadrupole and double focusing electrostatic or magnetic sector.

Artefacts

Several artefacts are inherent to SIMS analysis and complicate its application. The most important amongst them is **mass interference**. Nominal mass-to-charge ratio can be equal for several atomic clusters in the sample, interfering with the atomic species of interest. An example of this is the molecular ion $^{29}\text{Si}^{30}\text{Si}^{16}\text{O}^+$, which interferes with the atomic ion $^{75}\text{As}^+$ when studying arsenic depth profile in silicon oxide SiO_2 . This problem is partially solved by using some voltage offset to distinguish atomic from molecular ions. Other artefacts include crater bottom roughening, presence of oxides on the surface and sample charging up.

Static SIMS

By definition, SIMS methods are destructive. The sample surface is eroded as clusters of atoms are sputtered away to the analyser. However, it is possible to keep the sputtering rate very low, improving thereby the sensitivity of the method to surface chemical environment. This operation mode, known as static SIMS, uses very low primary ion beam current densities, normally not exceeding 5 nA/cm^2 (the current density in nuclear microprobes is one million times higher). An atomic monolayer is sputtered in several hours of bombardment so very sensitive detection methods are used. The low currents required make it possible to use electron bombardment for producing the primary beam of ions, which are then accelerated to energies between 0,5 and 4 keV.

Static SIMS is labelled a micro-analytical technique because of the very small volume of material probed. It can be used to perform chemical mapping of surfaces and is never used in depth profiling imaging or measurement of trace elements concentrations.

3.2.5 Laser Microscopy

Laser Microprobe Mass Analysis (LAMMA)

The advent of very powerful lasers emitting short wavelength radiation in pulses as brief as 1 ps provided a new sort of ion source to be used for several analytical methods. In laser microprobe mass analysis, a sharp pencil of laser light (normally Nd-YAG, power density of 10^{10} to 10^{11} W/cm²) is used to probe a small spot (down to 0,5 μ m in diameter). The probed spot is adiabatically transformed into a plasma and the emitted ions are mass analysed. Since this can be done only once in each spot, because the spot is literally evaporated, only dynamic methods like time-of-flight mass spectroscopy can be used.

By mounting a sample on a convenient xy movable stage, mass and elemental distribution on the sample can be mapped. Typical detection limits are in the sub-ppm range.

As in the case of SIMS, the process of ion emission from a hot plasma cannot be easily described analytically. Quantitative results are thus difficult to obtain. Matrix effects, however, are less important than in the SIMS method.

Laser ablation methods

Powerful laser beams can be used to ablate minute samples, functioning as ion sources. In geological applications, the laser ablation method is normally coupled to an inductively coupled plasma - mass spectrometer (ICP - MS) for studying micrometer sized fluid inclusions in minerals.

The strongest advantages of laser ablation is that it is practically adiabatic, virtually causing no influence to the surrounding sample and analysis can be performed very quickly (a few seconds for each cycle).

3.2.6 Nuclear Microscopy

A Nuclear Microprobe is an IBA facility normally using protons or alpha particles as projectiles, and equipped with some means of forming the probe and scanning it across the target. As stated before, a multitude of analytical techniques can be used then, by detecting the different kinds of signals that are emitted from a sample under ion bombardment. The diversity of tasks that can be accomplished at a NMP, and consequent

demand on beam time for both application and development, led some NMP groups to build up dedicated facilities [Mal-93].

The physical processes involved in NMP techniques were reviewed in considerable detail in Chapter 2. In this case, however, imaging capability is added to all the IBA methods. The imaging in NMP is invariably made in the scanning mode and digital elemental maps with different kinds of information are recorded.

The first use of a nuclear microbeam was by Zirkle and Bloom in 1953 to study radiation damage in different parts of animal cells. They used tens micrometers-sized apertures to collimate a beam of alpha particles. A long time passed until the reports on the use of microbeams for analytical purposes appeared. In 1966, Pierce and co-workers described the use of a deuteron beam with 250 μm in diameter in NRA of aluminium using a mechanic scanning stage. Since then and following the invention of semiconductor detectors, different nuclear microprobe techniques have appeared and have demonstrated their advantage over other trace analytical techniques with imaging capability, mainly due to the possibility of the combined use of different techniques in a single run.

Unfortunately, a NMP is a very complicated set up composed of different parts, each of them requiring sharp understanding of the physics behind its operation in order to run it more efficiently. So, to the dismay of the scientific community, the NMP is only associated with nuclear physicists who develop techniques and run application projects. Attempts exist [God-95] of trying to look at a NMP facility as a whole (holistic approach) and simplify the operation procedures to the maximum so that researchers with low training level in nuclear physics could yet use the facility appropriately. In this trend, I see the future of NMP techniques, which have to move out of the nuclear physics institutions, much in the same way electron microscopy quite successfully did in the past, to snick their way through the galaxy of analytical techniques used in the realm of the natural sciences.

3.2.6.1 Micro PIXE

The technique of μPIXE is the microprobe variant of PIXE, which was comprehensively described in Section 2.2.1. The high sensitivity of the method combined with the imaging capability enables quick and accurate analysis of micrometer-sized structures in archaeological, biomedical, environmental and geological samples.

In geological applications, μ PIXE is normally used to detect trace amounts of medium-to-high Z elements in a low-Z mineral matrix, enabling its use for studying virtually all the areas delineated pointed in Section 3.1.

3.2.6.2 Ionoluminescence

3.2.6.2.1 The phenomenon

Ionoluminescence is the process by which infra-red, visible or ultraviolet light is emitted by a sample under ion bombardment. The term luminescence is common to different kinds of excitation mechanisms and has been known since the antiquity. This phenomenon includes both **phosphorescence** and **fluorescence**. The former stands for the processes where the radiation is emitted even after cessation of the excitation, while fluorescence is the prompt (within 10^{-8} s) emission of light under excitation.

The physical principle involved is rather straightforward: electrons in the specimen can absorb energy from some excitation source and jump into excited states. The de-excitation process is accompanied by light emission. In the case of phosphorescence, the electrons are excited to metastable levels with long lifetimes. Eventually, some kind of ionising radiation can excite the electrons onto the metastable states, the decay rate of which is known and very low. Heating the sample at controlled conditions, however, increases the decay rate and a glow curve as a function of temperature can be recorded. This method is applied in geological datation and radiation detection in personal thermo-luminescent dosimeters.

Provided that the radiation quanta from the exciting source have an energy high enough for the electrons to cross the gap between the ground and excited states, no difference in the nature will be shown for luminescence excited by different sources. The only remark remains only for some spin-off's arising from the nature of the excitation radiation like penetration in the material (and hence probed depth) and radiation damage of the specimen.

Depending on the excitation, luminescence phenomena can be grouped in the following categories:

i) **Photoluminescence (PL)**, where the light is induced by optical quanta (UV, VIS and IR);

ii) **Chemiluminescence (ChL)**, induced by chemical reactions;

- iii) **Röntgenoluminescence (RL)**, induced by X-ray bombardment;
- iv) **Cathodoluminescence (CL)**, induced by electron beam bombardment, and
- v) **Ionoluminescence (IL)**, induced by ion bombardment.

Of these excitation processes, only photo- (VIS and IR) and ChL efficiently use the energy to excite the electrons. In the other excitation methods, the energy of the quanta or particles is so high that a great deal of it gets deposited in the specimen crystal, heating it and damaging its structure, thereby reducing the light emission.

In characterisation of geological material, the traditional optical excitation methods [Mor-70] were replaced by CL coupled to SEM instruments. A wealth of information about CL for geological material is available [Mar-88]. Recently, NMP groups have reported the novel use of IL much the same way as CL in electron microscopy [Yan-95]. The difference between the excitation processes by several tens keV electron beam and by a few MeV proton beam is illustrated in Figure 3.1.

The onion shaped excitation volume of the electrons is normally a few micrometers long in typical geological material (1 to 6 μm) while protons penetrate ten times as deep. It follows that the IL light comes from much deeper layers and the opacity of the sample can be regarded as a drawback. IL is, thus, more suitable for studying structures buried "deep" in the material. Moreover, the ionising power of protons is higher and beam damage is more severe in IL studies. Since luminescence is sensitive to chemical changes, the damage induced by the probing beam can be monitored on-line by charring and tarnishing of the sample.

3.2.6.2.2 Causes of luminescence

Luminescence from a mineral can be classified into two categories: *intrinsic* or *impurity-activated*. The first group accounts for the luminescence from very pure natural or synthetic minerals and the second for minerals with minor or trace impurities of different elements.

Activated luminescence - activators

During the process of mineral formation, different types of defects can be introduced in the crystals as they grow. The most important of

them, from the point of view of optical characteristics of the crystal, is the substitution in lattice positions of host atoms by impurities. The energy levels of the substitutional ions will be influenced by the crystal field, which can lead to the creation of *colour centres*.

The crystal field formalism best explains the luminescence phenomena in ionic crystals containing impurities of ions with unpaired electrons. These electrons originate either from the transition metals (elements from Sc through Ni), which have a partially filled *d* shell, or from rare earth elements (REE), with a partially filled *f* shell.

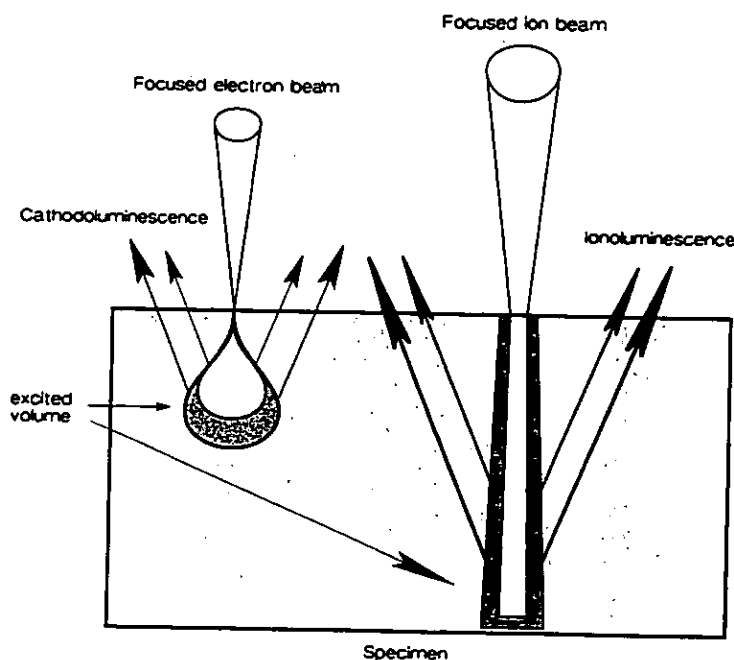
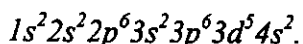


Figure 3.1. Difference in electron (left) and proton (right) luminescence excitation range and volume (not to scale).

Out of all these elements, iron is the most prevalent in the earth's crust (about 5%), so iron ions will contribute greatly in the formation of colour centres in minerals. In Figure 3.2, the effect of a crystal field of some strength, Dq , on the energy levels of the Mn^{2+} ion is represented.

Because of its relatively higher abundance (0,1 %) and its similarity to Ca^{2+} and Mg^{2+} in terms of radius, it substitutes for these ions in different minerals. The electronic structure of a neutral Mn atom is



To form the ion, this atom gets stripped of its 4s electrons. The energy levels of a free Mn^{2+} ion are represented in the left side of Figure 3.2. The first two excited states are termed ^4G and ^4P .

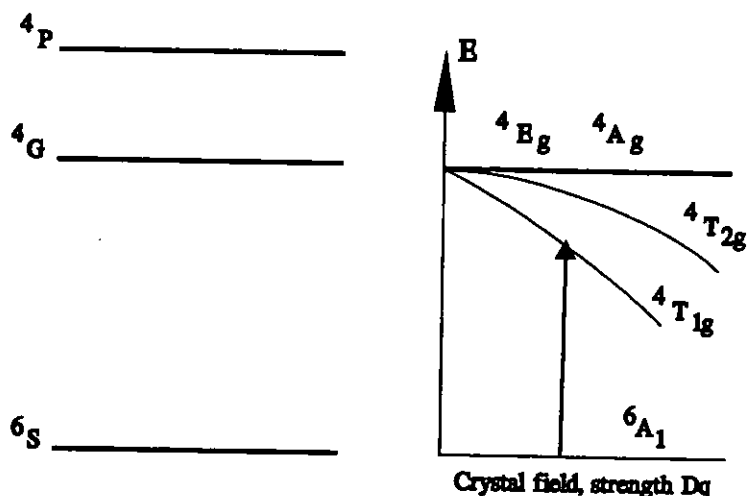


Figure 3.2 Energy levels of a free Mn^{2+} ion (left) and a Mn^{2+} ion in a crystal field of some strength, Dq . The energy terms are those commonly used in crystal field theory. (Adapted from [Mar-79]).

In a crystal field of strength Dq , the first excited state ^4G (actually four closely packed states of the 3d electrons) can be split into four levels named $^4\text{E}_g$, $^4\text{A}_g$, $^4\text{T}_{2g}$ and $^4\text{T}_{1g}$. The latter level is closer to the ground state and an optical transition can then be excited (Figure 3.2, right).

The calculation of Dq in different crystals can be done using some approximation methods. This is because the crystal (or ligand) field is a function of different parameters, like the valence state, the symmetry of the ion's environment (i.e., whether the crystal has a tetrahedral, octahedral, or any other polyhedral symmetry), distortions of the ideal polyhedral field due to crystal defects, and the nature and strength of the

crystal bonding. The statistical nature of the distribution of crystal defects, as well as of the Mn^{2+} impurities themselves, endows the spectral line with a probabilistic character in terms of light wavelength and a broad peak for the manganese-activated luminescence (Figure 3.5d). This is a general feature for the activation process by transition metal elements.

A different pattern arises when analysing the luminescence phenomenon activated by REE. This is a group of chemically very similar elements, also called lanthanides, with the following electronic configuration:

$$[1s^2 2s^2 2p^6 3s^2 3p^6 3d^{10} 4s^2 4p^6 4d^{10}] 4f^k [5s^2 5p^6] 5d^1 6s^2, \quad \text{where } k=1 \dots 14.$$

Most REE form trivalent ions but some of them, like Eu and Sm, can also form divalent ions. In the case of REE^{2+} , the $6s$ electrons are removed and the remaining $5d$ electron is the one most probably excited and hence participating in optical transitions. This electron is almost free and will be influenced by the environment, so REE^{2+} peaks are broad and depend on crystal parameters. Another reason for the broadening of these peaks is the fact that the transitions from level f to level d ($f \rightarrow d$) and the (less probable) $f \rightarrow f$ occur in the visible range, overlapping with each other.

In the general case of trivalent ions, REE^{3+} , a further $5d$ electron is stripped out of the ion and the only electrons that can participate in transitions come from the partially filled $4f$ inner shell. These electrons are shielded by two completely filled shells and they are not strongly influenced by the environment. REE^{3+} activated luminescence peaks show up rather sharp and are characteristic (Figure 3.5b). In this case the $f \rightarrow d$ transitions are in the UV region and do not overlap with the $f \rightarrow f$ transitions.

Co-activators or sensitisers

Sometimes the luminescent transitions in the activator impurities can only be excited efficiently by the de-excitation of another ion present also as impurity. In this case, the activator excitation by the proton beam is not an efficient process and a resonant transfer of energy from one ion to another (like in the cases of gas lasers) can pump the luminescent levels. Figure 3.3 shows the energy levels of a co-activator or sensitiser and the process of resonant transfer to the levels of an activator impurity.

Quenchers

The resonant matching of energy levels between two different impurities can sometimes constitute an impediment to the luminescence phenomenon. Indeed, quenching ions can siphon off the energy of an excited luminescent centre without any light emission. The most important quenching ion in minerals is Fe^{2+} . However, this ion can become an activator in other environments (Figure 3.5c) and quenching is only in relation to specific crystal environment and activator.

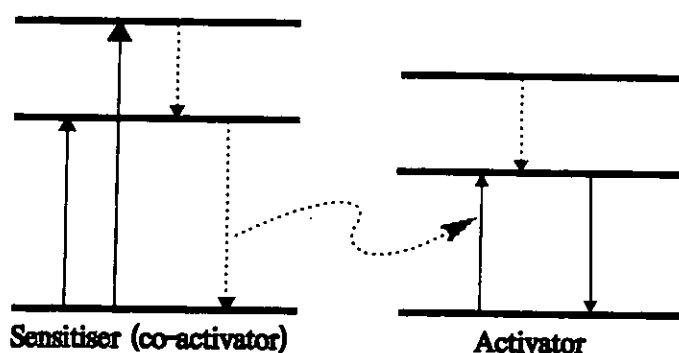


Figure 3.3. Process of resonant energy transfer from a sensitiser to an activator impurity. (Adapted from [Mar-79]).

Band theory and the colours

Unlike the crystal field theory, which applies for light-generating electrons bound to impurity ions, the band theory formalism regards all the electrons as belonging to the crystal as a whole. Semiconductors and insulators are good examples of where band theory can be applied. Their energy level exhibits a completely filled valence band separated from the empty conduction band by some energy gap, E_g (Figure 3.4). A very important class among these substances are the wide-band-gap minerals, which have $E_g > 3,5$ eV. This is the range of energy for the visible light and these materials cannot absorb any wavelength in that region and so, are colourless ([Nas-78]). This fact is also associated to their low conductivity since the environment thermal energy cannot pump up electrons to the conduction band.

However, with the addition of small amounts of impurities, both donors or acceptors can introduce new intermediate levels and make it possible to observe some optical transitions under proton bombardment. Very shallow acceptor levels or very deep donor levels can make it possible for optical transitions to be excited by visible light, so the mineral will exhibit some colour at light excitation as well.

Zircon (ZrSiO_4) is a good example of a wide-band-gap crystal in which small amounts of REE activators can induce a variety of luminescence lines in the visible and IR region.

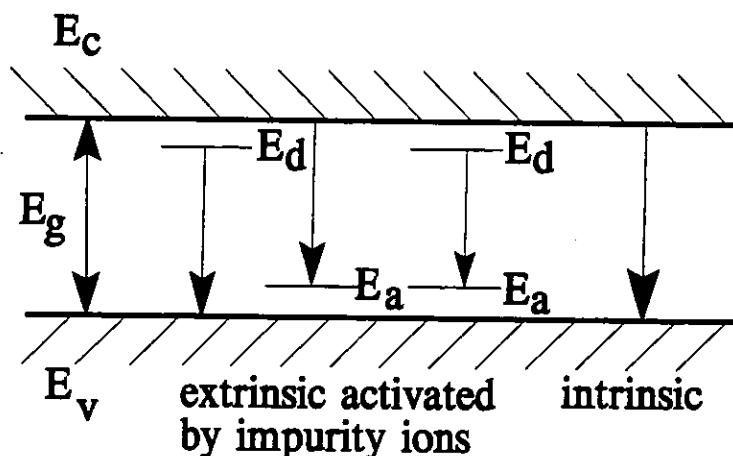


Figure 3.4. Illustration of the band theory approach to the luminescence of insulator and semiconductor material.

Intrinsic luminescence

As a rule of thumb, very pure minerals either do not luminesce or do it very weakly. However, crystal imperfection can induce distortions in energy levels of the whole lattice and eventually some optical transitions become available. The main aspects that increase the crystal imperfection are ([Mar-88]):

- non-stoichiometry;
- structural imperfections, caused by poor ordering of the crystals, radiation and shock damage;
- non-activator impurities.

The unpaired electron producing light emission under ion bombardment can be situated on a crystal defect or on a non-activator impurity. This is possible when Frenkel defects due to imperfections or damage exist in the crystal. Inside the crystal, some compensatory charge movement will occur in such cases, producing distorted energy levels that eventually can luminesce. Since many different mechanisms of compensation are possible, the intrinsic luminescence will exhibit broad peaks (Figure 3.5a).

3.2.6.2.3 Methods of detection of Ionoluminescence

The product of IL is visible, UV and IR light, so in principle, any optical detector can be used. The most simple optical detector is the naked eye and IL light has been used to quickly locate the sample position when analysing geological material. To an experienced operator, mineral identification can be made rather easily by observing the IL colours and using some other preliminary information about the sample.

Using a microscope on line (in transmitted or reflected light) gives a more detailed insight of the mineral assemblages present in the sample. The attachment of a photographic camera allows for making unique micrographs, in terms of amount of information about the sample and sometimes beautifully contrasting colours. The IL micrographs generally give more information than the conventional SEM images since, as stated before, buried structures can be shown in relative detail and in colour contrast. Competing petrographic images in polarised light do not show much of those details either.

Digital maps can normally be constructed when detecting the IL light in the so-called *pan-chromatic* mode. In this case, the whole light coming from the irradiated sample shines through the entrance window of a photomultiplier tube (PMT) and the electric signal coming out of it is processed by normal electronics. Provided that no sophisticated position-sensitive PMT's are used, this mode is accomplished in a NMP with a scanning proton beam. The light intensity of each pixel is recorded and the colour coded maps are produced. There is a concern, however, that eventual phosphorescent mineral phases can give spurious results in this case, since the delayed luminescence from one pixel can come along with the luminescence of the actually probed spot.

Sometimes it is interesting to do imaging in a specific wavelength. In this type of study, a filter monochromator can be interposed between the sample and the PMT, and the intensity of light at a specific

wavelength of every pixel (in the scanning mode) or a micrograph are recorded.

All of the methods described so far deal with the imaging capability of IL and can help in making some qualitative interpretation about the sample. Semi-quantitative results can be obtained in the spectroscopic mode of detection, where the light coming from a given point illuminates a scanning grating spectrometer and the different intensities at different wavelengths are recorded. Cheap spectrometers of the Czerni-Turner type with a scanning grating at a regulable speed coupled to a PMT detector can be used for this purpose. The main disadvantages of these systems are:

- low resolution;
- long measuring time (typically about 20 minutes to scan over 350 nm to 900 nm), which makes it impossible to follow some very dynamic transient processes and jeopardises the sample integrity because of beam damage, and
- high dark currents in a wide range of PMT's available.

A more elegant solution, though more expensive, can be the use of arrays of charge-coupled devices (CCD) coupled to a fixed-grating high resolution Czerni-Turner spectrometer. The resolution of CCD arrays for specific measurements can be reduced to units of Ångströms, with sampling times in the millisecond range.

3.2.6.2.4 Quantification and sensitivity

By observing IL spectra, it is possible to identify the peaks of the activator impurities fairly easily. For this purpose, one can use the wealth of information that is available from PL and CL. However, quantification of IL spectra is fraught with difficulties.

In general, the IL signal will depend both on sample properties like: concentration and efficiency of colour generating centres, opacity/trans-parency to different light wavelengths, concentration and efficiency of quenchers, and on system properties like the light collection efficiency and the detector solid angle. Unfortunately, the light generation process is much more complicated than this simplistic theory. The chemical state of the sample, the strength of the crystal field, the

variations in defect location and the lattice location of impurities can all change the intensity and wavelength of the induced light considerably.

Methods trying to extract as much quantitative information as possible from IL spectra point towards combination use of different signals, like PIXE and IL ([Mal-96], [Utu-95]) or multivariate statistical methods of analysis of information from different signals maps [Swi-93].

IL is a very sensitive technique. MDL are, in the best cases, in the ppb range for impurity activators. Endeavours envisaging to bring up a more clear theoretical picture of the light induction through ion bombardment must be undertaken in order to improve the analytical ability of IL. Moreover, studies of luminescence in different minerals can provide the necessary database for theoretical modelling.

3.2.6.2.5 Applications of IL in geological studies

Luminescence techniques are widely applied in geological studies since geological material normally luminesces, is less prone to beam induced damage and the results give easily interpretable information.

In NMP set-up's with geological applications, coupling an IL detection system can be rewarding and the following items can be readily addressed:

- i) Quick mineral assemblages identification by the colour of the emitted light in petrology and mineralogy studies;
- ii) Study of zoning patterns in minerals with applications in mineral exploration: normally some "gangue" minerals like quartz are associated with the penetration veins of some mineral forming fluids. The study of fluid inclusions then, can reveal the thermodynamic conditions that governed the hydrothermal deposition process and help in assessing their economic value. IL images give much detailed information about the zoned growth of the minerals.

Zoning patterns studies are also important in geological dating. Normally, accessory minerals like zircon ($ZrSiO_4$) are used as chronometers due to their ability to incorporate U and Th and the Pb decay products in the crystal. The mineral can eventually be formed at different ages through successive overgrowth by crystallisation of relatively "young" melts. Applying the dating to the whole mineral can lead to erroneous

results and each growth zone must be dated separately. IL helps in identifying the zoning structure of this mineral [Yan-94].

iii) Geochemical characterisation of minerals, through detection of trace presence of activator impurities (like transition metals and rare earth elements) in ppb - to - ppm levels. The combined use of IL with PIXE can provide the possibility of quantification of such impurities.

iv) Beam-induced damage studies in materials. IL is very sensitive to the crystal lattice conditions and to the chemical environment surrounding the activator and the quencher impurities. Beam irradiation conveys extra energy through collisions to the crystal which can significantly alter the chemical environment. The wavelength and intensity of the luminescence light can then change in time as more dose is absorbed by the mineral.

In insulator and semiconductor crystals, the ion beam can eventually induce some conductivity changes by increasing the carriers concentration in a very limited volume (at the ion projected range) and can, in a way, be regarded as a material science technique, aiming at material modification and monitoring [Jam-95].

3.2.6.3 Other NMP techniques

Focusing protons down to micrometer sized spots and measuring the different signals coming out from the bombarded specimen is the *modus operandi* in a NMP. It is generally accepted that a beam current of 100 pA is the minimal acceptable for any useful analytical work [Mal-95] except the STIM¹ technique that uses currents in the range of a few pA.

Achieving higher spatial resolution, i.e. smaller beam spot sizes, can be a handicap to the NMP techniques since it limits the fluency of the protons. In other hand, the high current densities attained at such conditions can be damaging to the samples. Therefore, NMP experiments are run at beam current values and spot sizes defined not only by the ultimate resolution achievable, but also by the specifics of the analysed

¹ Recently a detector holder for off-axis STIM was described [Sjö-96], which allows using "normal" high currents since the detector views the particles that are transmitted and scattered at an angle by the sample. Cross-sections for this process depend strongly on the angle of detection and the distance to the sample, so combined studies using off-axis STIM and other techniques can be made.

sample. Different techniques have been developed for specific applications in a NMP, where the signals in Figure 2.1 are detected.

Methods based on the detection of elastic scattered particles, nuclear reaction products, recoils and light have been used successfully.

In ion beam induced charge collection (IBIC), the damaging effects of an ion beam in the crystal structure can be used to induce electron-hole pairs in electrically active semiconductors. Since the efficiency for charge collection of a semiconductor (say a p-n junction) depends on the concentration of traps and recombination, the collected charge gives information about the presence of defects.

During the last two decades, several technique developments have been reported by different NMP groups and I do believe that the settling and developing phase for NMP techniques has already passed. Most emphasis must be placed on performing the correct applications of all these methods in different research fields. This fact will help in establishing some of the methods as routine analytical techniques for specific applications, and gathering new information that can be the necessary feedback to further improvements.

3.3 The Lund Nuclear Microprobe

The Lund Nuclear Microprobe (LNMP) is assembled around a single-ended Pelletron machine of the type NEC (3UH), completely dedicated to microprobe applications [Mal-93], with a terminal voltage of 3 MV. The beam line is kept under a vacuum better than 1×10^{-6} Torr by means of a turbo-molecular pump mounted at the exit of the accelerator and four diffusion pumps with liquid nitrogen traps, one of which is situated directly under the reaction chamber. Vacuum failure guarded valves were inserted immediately before each pump in the upstream direction.

The beam is generated by an RF ion source. Theoretical values for brilliance of such sources are in the range of $10 \text{ pAmrad}^{-2} \mu\text{m}^{-2}$, which can just be enough to get a $1 \mu\text{m}$ sized beam with analytical capability [Wat-87]. Smaller beam sizes, usable in applications like semiconductor industry, imply the development of high brilliance duoplasmatron or liquid metal ion sources.

The great disadvantage of single-ended machines is that the ion source is located at the high voltage end within the pressurised tank. Some improvements are underway in order to make it possible to change the ion gas from outside.

The general view of the beam line is illustrated in Figure 3.6. The beam at the exit of the accelerator tube is pre-defined by the exit slits, which reduce the amount of beam dumped downstream on the more precise object slits. After that the beam passes through a pre-focusing stage with a magnetic quadrupole doublet, and through the analysing and switching magnet, which bends it towards the 15° arm where the NMP is installed.

The beam position can be controlled by a magnetic steerer placed inside the accelerator tank and electrostatic steerers placed before the object-defining slits. Luminescent beam viewers and a closed-circuit TV system permit monitoring the beam position and size in three important nodes: before the object, after the aperture slits and just before the magnetic lens.

The object-forming slits can vary from 0 to 200 µm whilst the beam divergence limiting slits (just called aperture slits) vary from 0 to 500 µm. This range is suitable for the different applications currently running at the Lund NMP. The microprobe forming lens is a magnetic quadrupole triplet, which, together with an electrostatic quadrupole lens accommodated in its pole bores, forms an achromatic quadrupole triplet [Tap-89]. Normally only the magnetic triplet is used.

Beginning with the probe formation and ending at the specimen chamber, the system is hung upon solid concrete and iron piers, which sit on an anti-vibration floor. This is isolated from the low frequency vibrations of the accelerator, fore-vacuum pumps and the building in general. The accelerator tube is also covered by a metallic foil in order to minimise stray magnetic fields induced by the mains.

The beam is scanned post-lens by xy magnetic coils either manually or computer-controlled.

The data acquisition system

The data acquisition system (DAS) comprehends the scanning control system and the multi-parameter data collection and storage. The first task is accomplished by a VME multiprocessor module system to the bus of which different devices can be coupled ([Löf-89], [Tap-87]). The processor module controls the sequence of scanning patterns that are sent to a digital-to-analogue converter and the 0 - 5 V output signals drive the current generator that feeds the magnetic steering coils. A maximal resolution of 4096 x 4096 pixels is achievable.

The signals from the detectors are pre-processed by conventional electronic NIM™ modules and analysed by four ADC's and an eight-ports multichannel scaler (MCS). These are part of the Nuclear Data® DAS. The multi-parameter data composed of x and y coordinates and different signals from the detectors is conveyed to the mass storage units of a μ VAX II host computer.

Over the years, many revolutionary changes have occurred in the field of signal processing and digital computation. The availability of fast electronic CAMAC modules from standard particle physics experiments, gigantic low priced mass storage units and graphic-interfaced fast computation units allowed to enlarge the horizons in terms of user-friendliness and versatility of the DAS. A novel approach to the problem of data collection and processing is presently being implemented at the Lund NMP ([Elf-96]).

Continuous developments and improvements to the beam line are being made and the latest ones are described in Section 4.1. The major aim remains to approach compactness, easy-to-operate, automation of some routine steps and, hence, repeatability of beam location and size, as well as stability in relation to drifts during long runs.

3.4 Specifics of analysis of geological samples with a Nuclear Microprobe

Geological specimens are composed of a matrix of light elements, the so-called rock-forming minerals, and embedded high-Z minor, or trace elements. As discussed above, the latter constitute the object of analyses in geochemistry, since information about mineral formation and transformation conditions is encoded in their distribution patterns. Bearing this fact in mind, specific approach to the NMP set-up must be made if geological specimens are to be analysed with an acceptable degree of confidence.

Samples

In bulk PIXE analyses, the samples can be arranged as compressed powder pellets of previously ground rocks. The compression envisages increasing homogenisation in order to reduce errors in quantification procedures. The majority of NMP analyses of geological specimens, however, addresses many more aspects than the average concentration of trace elements, and the mineral assemblages are analysed as they appear

in the nature with minor changes. For this purpose, thin sections are normally used.

During sample preparation special care must be undertaken in order to avoid contamination. The final polishing to micrometer "smoothness" is normally done using diamond paste. Thin sections can be used with different analytical methods like petrographic microscopy, electron microscopy and microprobe and nuclear microprobe.

The majority of rock forming minerals are insulators, and during ion bombardment, the charge build-up can lead to deterioration of the energy spectrum of X-rays. The charge can be drained out, to the sample holder for example, by coating the sample surface with a conductive layer. Normally, carbon is used, since the soft X-rays from it are not detectable by a conventional Si(Li) detector.

The proton beam

Interesting features in geological samples are μm sized and one can feel tempted to use a very small beam size to insure higher spatial resolution. A lower limit of 100 pA must be sought for PIXE analysis but in real cases this limit can be much higher, going up to few nano-amperes. Higher currents are, logically, achieved at the expense of lower spatial resolution. Specific cases must be handled differently and the necessary compromises assumed. In making line-scans, for example, the resolution in one direction can be sacrificed in favour of the other (the scanning direction) with no major changes in current values.

Beam current measurements cannot be made by an on-line Faraday cup since the thin sections are normally mounted on a thick glass slide. The sample wheel itself can be used, if appropriately insulated, as a Faraday cup. Secondary electrons suppression by some negative voltage in front of the sample is a normal procedure in this case. More accurate charge measurements can be made by the rotator vane technique, as described above.

Artefacts

The first concern in analysing geological samples by PIXE arises from the nature of the samples themselves. High cross sections for K X-ray production yield high intensities for the major low-Z elements present in the matrix, which keeps the detection system busy, and the much lower intensity L lines of the heavier elements of interest will show

up in this "background" radiation. To reduce the intensity of such peaks, different kinds of absorbers are normally used. These can be:

- i) *funny filters*, which are absorbers with a pinhole in the middle. The solid angle for soft X-rays is drastically reduced, whilst keeping a higher detection efficiency for the higher energy X-rays;
- ii) *critical absorbers*, which are filters made of an element about two a.m.u. lighter than the one whose X-rays we want to suppress. The former element has an absorption edge coinciding with the energy of the X-rays of the latter one, and a strong reduction is then experienced. Unfortunately, this is accompanied with the emission of secondary X-rays induced in the material of the absorber and special care must be taken in order to avoid interference with the sample's X-rays.

Sometimes, two different detectors are used in parallel, one for major and the other for trace elements analysis. This is a rather easier and efficient technique but is conditioned to the availability of an extra Si(Li) detector. We have used such system in analyses of apatite samples, where the fast X-rays from phosphorus were detected by one detector and the second one, with suitable filters, detected REE [Utu-95].

Some matrix elements in geological samples like fluorine, present in fluorite and sodium, present in plagioclases, can display high cross sections for proton activation and emit copious fluxes of γ - rays under bombardment. Despite the fact that the energy of these γ -rays lies far above the sensitive region of the Si(Li) detector, multiple scattering processes can introduce an extra-source of continuous background, worsening the detection limits for REE. An anti-Compton shield can reduce these problems but some more sophistication of the signal processing electronics is needed.

Large X-ray peaks normally display a low energy tail that affects the peaks of heavier elements. This is the case of the Zr $K\alpha$ peak in analysing zircon crystals, on whose tail "sits" the normally smaller Y $K\alpha$ peak. Lead peaks are also affected making thereby, the quantification of Pb for datation, very difficult.

Spectra fitting

The above numbered phenomena must be taken into account when analysing the spectra of geological samples. Throughout this work, the

GEOPIXE package, developed at CSIRO [Rya-90], Australia, has been used. This program takes care of the major artefacts arising in the analysis of geological samples. The commissioning of a new DEC 3000 ALPHA workstation enabled working practically on-line during spectra evaluation, increasing the throughput of the analytical procedures.

Adaptations of the specimen chamber

The general layout of the specimen chamber during PIXE and IL measurements is shown in Figure 3.7. A rear-view microscope with interchangeable objective lenses enables quick sample location when transparent specimens are analysed. The sample wheel is x, y, and z movable, i.e., can be translated in any axis which permits focusing of the beam spot onto the wanted position. It is also electrically insulated to facilitate beam charge measurements made.

When analysing opaque samples, a top microscope equipped with optional CCD camera and video monitor can be used to view the front part of the samples through the reflected light from a mirror. The beam can pass through a small hole in the mirror so that it is possible to view the sample during analysis.

Two detector ports, one on each side at a 135° angle to the beam direction are used for the X-ray and the IL detectors. In some applications, two X-ray detectors can be used simultaneously. The Si(Li) detector normally used for PIXE has an active area of 50 mm² and a resolution of 155 eV at the 5,9 keV Mn K α peak.

The arrangement for IL detection can be seen on the right side of Figure 3.7. In the imaging mode, the light collected by a special collimator lens, is bent by a 45° mirror into the Hamamatsu® R585 PMT. This tube has a low dark current and a narrow dynamic range (160 to 650 nm). When imaging at a specific wavelength is envisaged, a filter monochromator can be interposed in the light path to the PMT detector. In spectroscopic measurements, a Hamamatsu® R943-02 PMT is used. This one has a larger dynamic range (160 - 940 nm) and a higher dark current. During measurements, it was cooled down to -30° C, thereby reducing the dark current to 1 cps.

Part of this thesis was made using a new IL detection system based on a CCD detector procured from Hamamatsu® of the PMA-50 type. This is a 1024 array detector with Peltier cooling to reduce noise. The spectrometer allows using a PMT in a second port instead of the semiconductor detector and has a turret with three different gratings so

that different resolving powers can be used at different wavelength ranges. The main advantages of this detection system are higher resolution and fast measuring (down to several tens of milliseconds).

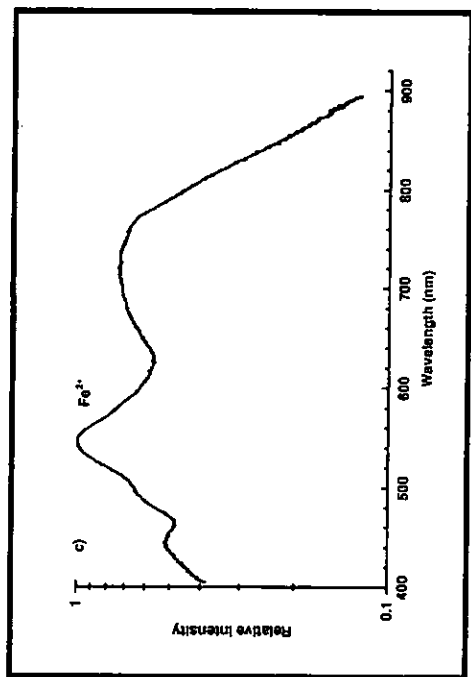
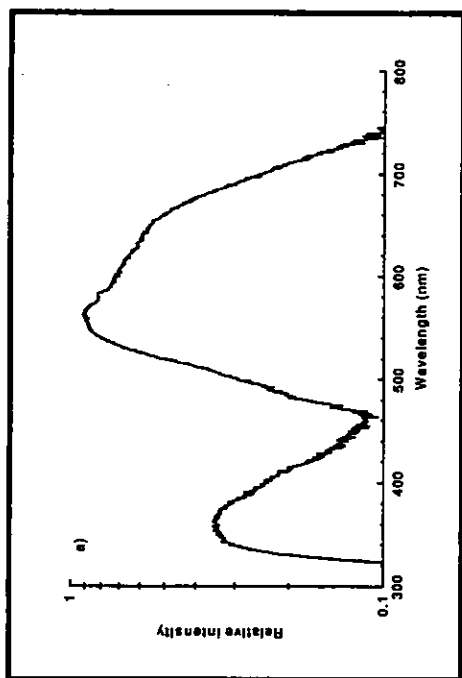
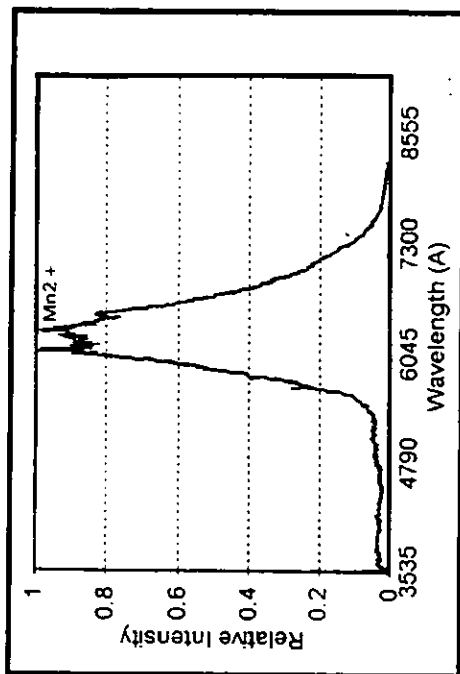
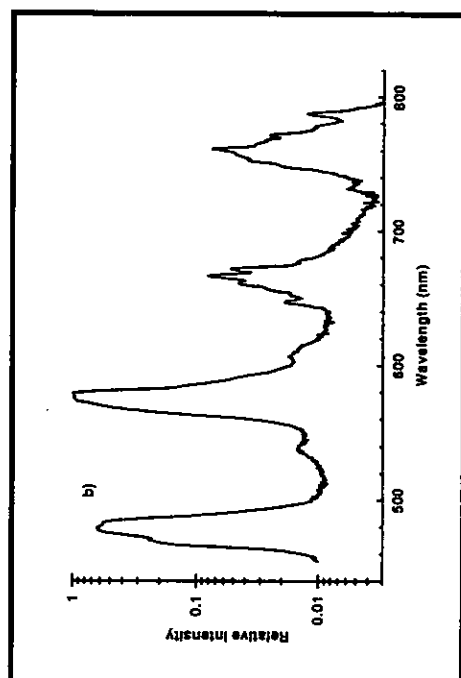


Figure 3.5. IL spectra of: a) pure synthetic zircon mineral; b) dysprosium doped synthetic zircon; c) natural zircon, and d) apatite (Mn^{2+} activated).



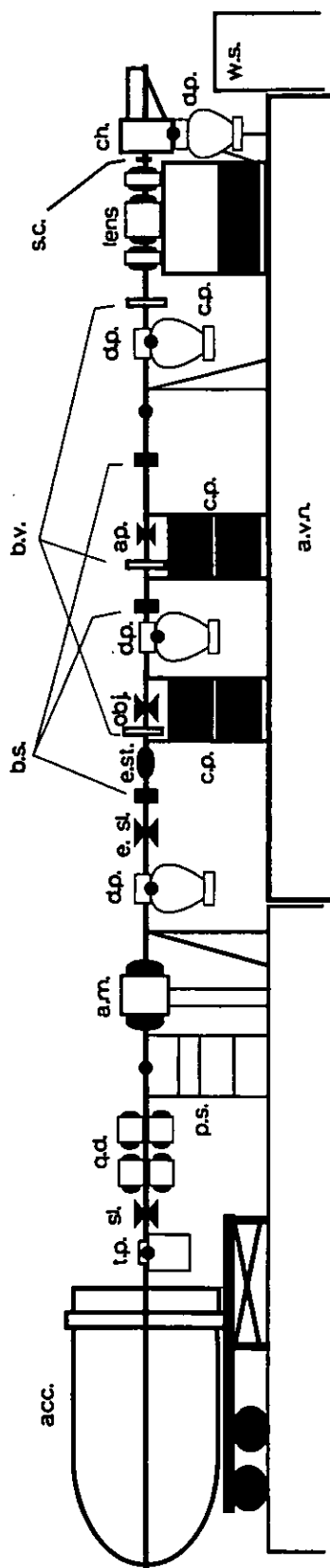


Figure 3.6. Layout of the beam line of the Lund Nuclear Microprobe.

Legend:

- acc. - single-ended 3 MV Pelletron accelerator;
- t.p. - turbo-molecular vacuum pump;
- sl. - beam defining exit slits;
- q.d. - pre-focusing magnetic quadrupole doublet;
- p.s. - power supply and control of the turbo pump;
- a.m. - analysing and switching magnet;
- d.p. - oil vapour diffusion vacuum pump;
- e.sl. - energy stabilising slits;
- b.s. - beam stop;
- b.v. - beam viewers;

- obj. - object forming slits;
- ap. - beam divergence limiting slits;
- lens - achromatic magnetic quadrupole triplet lens;
- s.c. - magnetic scanning coils;
- ch. - specimen chamber;
- c.p. - concrete / iron piers;
- w.s. - working stage;
- a.v.n. - anti-vibration niche;
- - guarded high vacuum valves.
- e.sl. - electrostatic steerers.

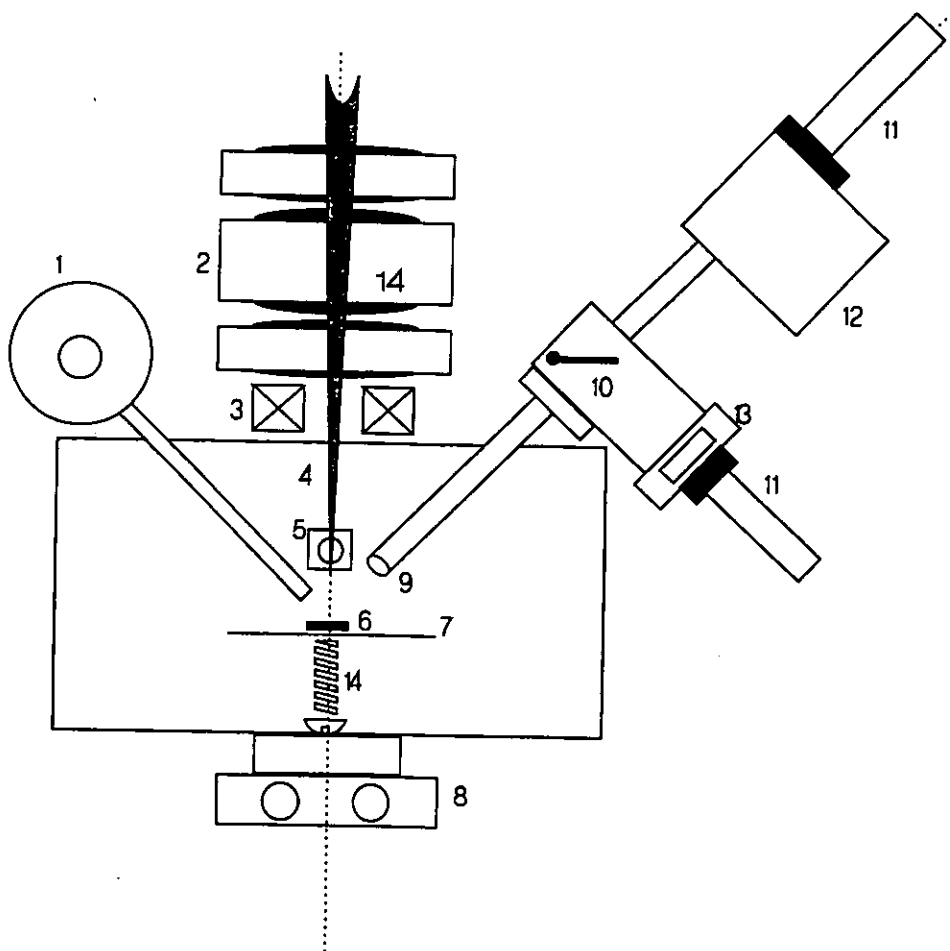


Figure 3.7. Top view of the specimen chamber with the equipment for geological studies mounted.

Legend:

- 1 - Si(Li) X-ray detector;
- 2 - Magnetic quadrupole lens;
- 3 - magnetic scanning coils;
- 4 - proton microprobe;
- 5 - 45° mirror with a central hole;
- 6 - geological sample;
- 7 - aluminium sample wheel;
- 8 - rear view microscope;
- 9 - VIS-UV collimator lens

- 10 - mirror;
- 11 - PMT;
- 12 - Optical spectrometer;
- 13 - filter monochromator;
- 14 - xyz movable stage;

Note: a top microscope is used to view opaque samples from the front using the reflection from the front mirror.

4. Results of geological studies using Nuclear Microprobe Techniques

4.1 A procedure for beam line alignment

The ultimate resolution of a NMP is defined by the smallest beam spot size that can be achieved on the focal plane of the lens still with analytical capability (at least 100 pA for PIXE analysis). In geological applications, normally a few nA currents are required in order to conduct the experiment in a reasonable time. To achieve such fluency with small beam size, careful optimisation of the transmittance of the whole system must be performed.

Parameters that affect the beam spot size include:

- i) lens aberrations : astigmatism, chromatic and spherical;
- ii) rotational and translational misalignment of the lens;
- iii) multipole field contamination in the lens;
- iv) beam brightness;
- v) accelerator stability;
- vi) scattering in the slits' opening, and
- vii) stray electric and magnetic fields.

Aspects related to the intrinsic aberrations of the lens package were dealt with in previous works [Tap-89], [Tap-89a]. In order to reduce stray electric fields, the beam line and some electrical cables were covered by a Faraday cage μ -metal foil. Accelerator energy stability is in the 10^{-4} range and beam energy stability can be made even higher by using energy stabilising slits that cut away the "non-monochromatic" particles downstream, after energy analysis.

In the recent accelerator servicing, we have addressed questions related to rotational and translational misalignment of the lens package and improvement of the beam brightness by making a better beam line alignment. For this purpose, the following changes were made:

- i) insertion of rugged exit slits to take on the beam halo and increase protection of the object slits downstream;
- ii) insertion of a x, y, θ stage for the pre-focusing quadrupole doublet, thereby enabling correction of translational and rotational misalignments on it;
- iii) insertion of x, y stages for both the object and the aperture slits allowing for a quick change of their relative position for fine-tuning in the alignment procedure, and

- iv) reduction of the distance between the object and the aperture slits from 2180 mm to 1564 mm in order to increase the transmittance of the system.

A careful alignment of the beam line was then performed in accordance to the following procedures:

Optical alignment

The whole beam line and components are aligned relative to the position of the ion source, using fixed reference marks and a precise theodolite. A light source was shined behind the slits and their position changed to millimeter accuracy using the xy stages.

Pre-focusing quadrupole doublet

The beam envelope proved to be very sensitive to rotational and translational misalignment of the pre-focusing lens. The new stage inserted below it enabled correction of these parasitic aberrations and better focusing.

Alignment with the proton beam

The relative positions of the object and aperture slits were fine-tuned in order to maximise the beam current in the sample position. We could qualitatively judge the degree of correctness of the alignment by the amount of bias needed in the electrostatic and magnetic steering (Figure 3.6).

Lens alignment

First, the quadrupole magnets are excited one by one, and misalignments in the x and y directions are corrected, relative to a fixed point in the cross-hair of the back microscope. This is a rather painstaking procedure and must be done in order: align the x direction and then the y direction with micrometer precision, for the first quadrupole lens and then pass to another.

The rotational misalignment is corrected for each possible combination of two quadrupole magnets. A luminescent target is used and is viewed at high magnification by the front view microscope (Figure 3.7) coupled to a TV camera. The lens is rotated on micrometer scale, while dynamically changing from the focused to defocused position and monitoring the change in the shape of the beam envelope. The system is

considered correct when in both focused and defocused positions, the beam remains in the optical axis and the shape of the beam envelope does not change.

As a result, the beam brightness could be improved up to a factor of three (Figure 4.1). Beam size estimation by scanning a 2000 mesh per inch silver grid gave a rough result of better than $2,5 \mu\text{m} \times 2,5 \mu\text{m}$ for a beam current of 100 pA.

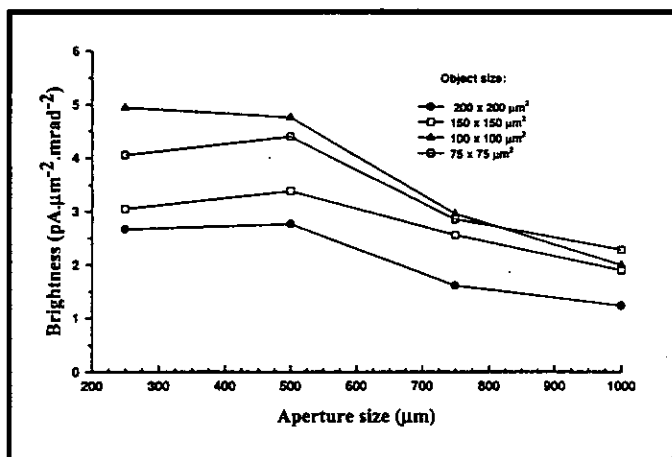
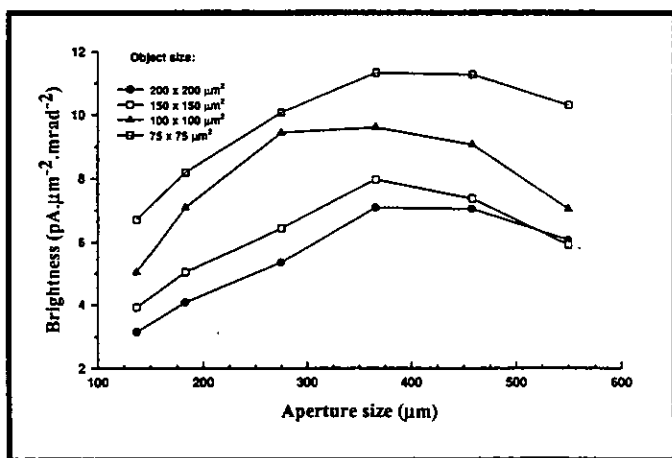


Figure 4.1. Graphics showing the brilliance measurements done at the Lund NMP before (upper) and after (lower) the servicing and alignment procedures described above. An overall improvement of more than a factor of three can be noticed.



The values of brightness illustrated in figure 4.1 are close to the theoretical limit for a RF ion source [Wat-87]. We expect that a beam size approaching one micro-meter will be attainable at low current modes,

for STIM measurements.

4.2 Characterisation of inorganic material using IL method

Ionoluminescence is a newly developed technique among NMP users. Different works presented hitherto point to the advantages of using IL in geological studies, much the same way as its electron equivalent, the cathodoluminescence. A wealth of information on the CL of

minerals is available, which can be used for IL in the majority of the cases. However, serious discrepancies arise when using proton excitation (IL) instead of electrons, by virtue of the differences in stopping and ionising powers. Careful and systematic studies must be done aiming at

- i) the creation of a database for mineral studies with IL;
- ii) comparison of the results for CL and IL, and
- iii) setting up routine procedures for analysis of different geological samples.

These three issues have been addressed in continuous studies at the Lund NMP, enlarging the scope to include bio-medical and industrial samples.

Synthetic zircon crystals doped with REE were analysed for identification of luminescence lines in the UV, VIS and IR using a new CCD array detector. Some of the spectra are displayed in Figure 4.2. Some of them (Yb, Gd and Ho) exhibit the characteristic narrow peaks for trivalent REE on top of the broad intrinsic band of Zr. This can be due to difference in the sites occupied by these activators in the lattice or differences in the process of growing the crystals (degree of saturation of the melt from which the crystals solidified).

Beam damage and modification of the materials

A particular feature arises when exciting luminescence with energetic particles. Their energy is commonly much higher than the energy gaps between the excited and ground state of a luminescence generating centre and the surplus will be lost in the crystal, causing damage. The amount of beam damage depends on the energy and momentum of the incident particles. For MeV protons used in IL studies, this damage is more pronounced at depths of 30 - 60 μm , which is the range of these particles in different minerals.

The observable symptoms of beam damage are the fading of the luminescence peak, wavelength shift of the emitted light and charring of the bombarded spot caused by heating. In Figure 4.3, the decay of a IL spectrum of tooth sample is displayed. Tooth is mainly composed by the mineral fluorapatite and some trace elements. The Fe^{2+} activated luminescence peak is visible at about 540 nm. The decay of three different peaks of this spectrum was fitted to two different exponential functions and is presented in Figure 4.4 (left). The high sampling speed

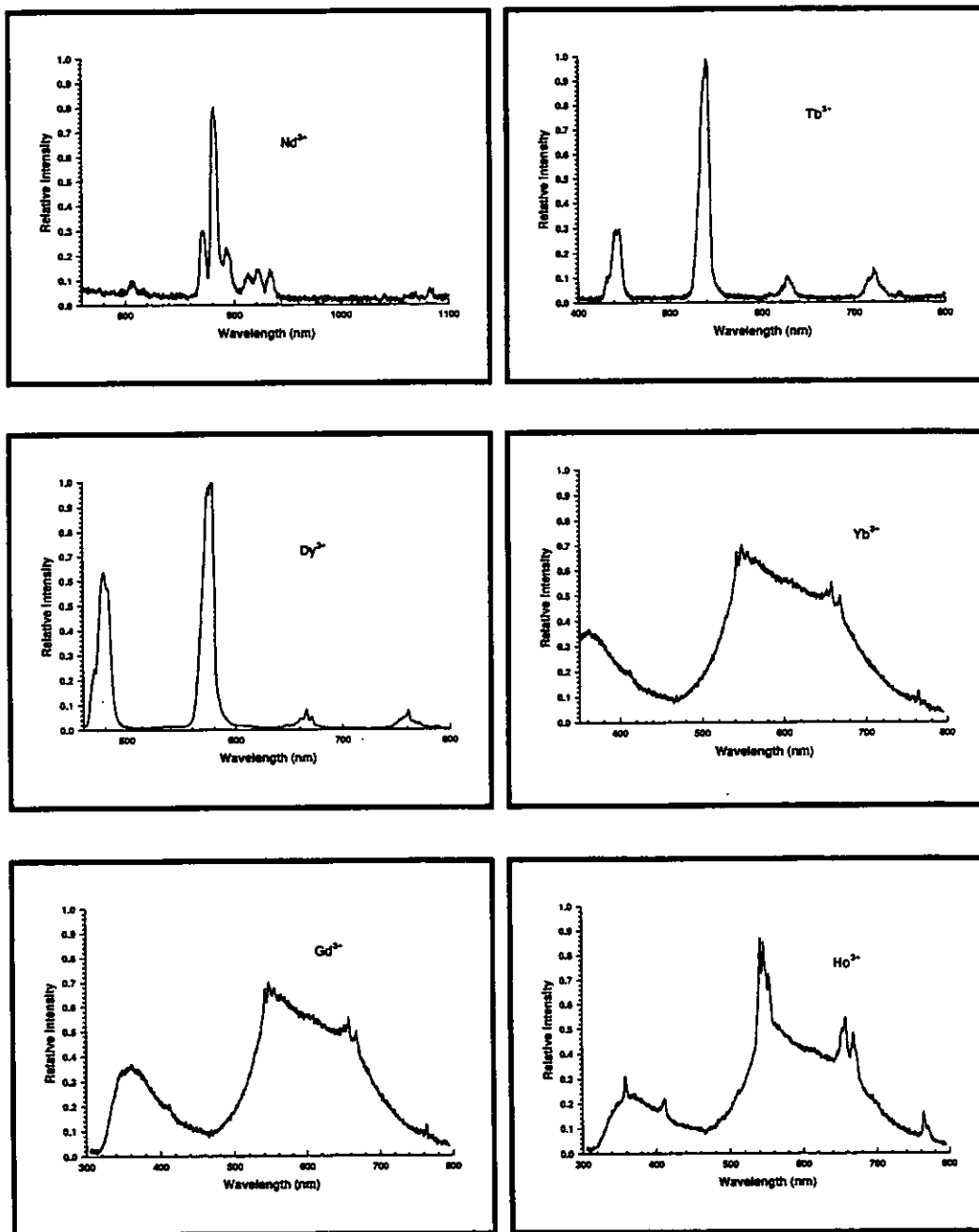


Figure 4.2. IL spectra of a synthetic zircon ($ZrSiO_4$) mineral doped with different REE, taken with a CCD array detector cooled down to 0° . Experimental conditions were: 2.55 MeV protons; current - 2.5 nA; beam spot size $10 \times 10 \mu m^2$. The slits opening of the spectrometer was $200 \mu m$ and the detector exposure time was 300 ms.

of the new CCD detector permitted the registering of this decay in a dynamic mode.

In large-band-gap crystals like diamond and zircon, proton bombardment can be regarded as a process by which positive charges are buried at a depth equal to the range of the protons in those materials. The electrical conductivity of the sample may then change [Tri-96]. In Figure 4.4 (right), an IL spectrum of pure synthetic zircon is presented, in which the process of internal charging up shows up as narrow peaks randomly separated on the top of the characteristic Zr broad peak. Using the new CCD system we could dynamically follow the changes in the IL peaks' shapes: the internal charging up disappears after about 30 s of bombardment (accumulated dose of $1,2 \times 10^{18}$ protons/cm²). This could indicate that a conductive path was set in the crystal and the protons, which mainly accumulated at the depth equal to their range in zircon (35 μ m) and could then be channelled out.

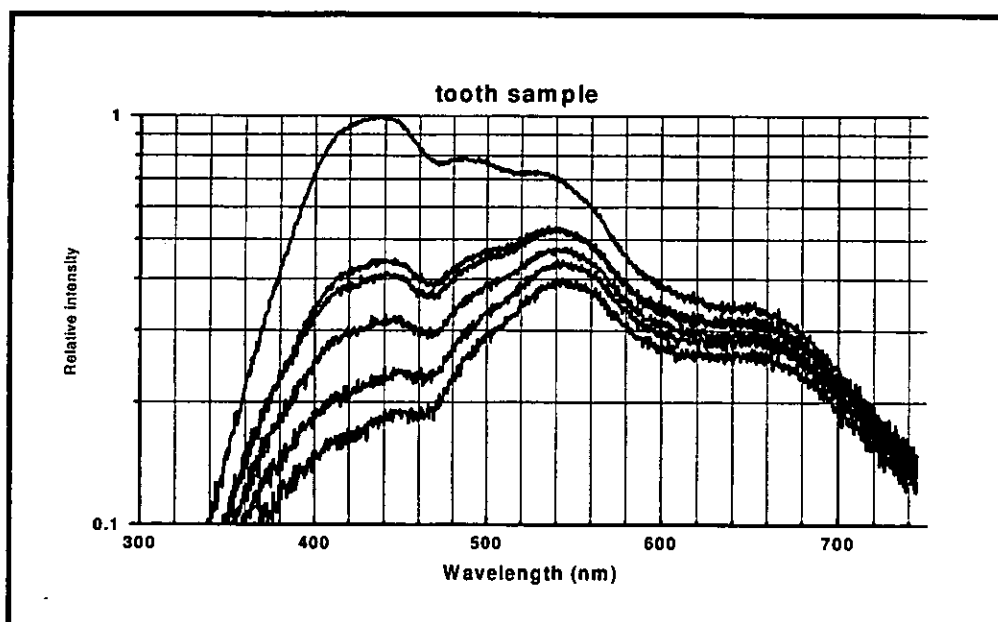


Figure 4.3. Sequence of IL spectra of a tooth sample showing the decay on peak intensity due to beam induced damage. The experimental conditions are the same as in Figure 4.2. The highest peak was first recorded shortly after moving the sample to a fresh area and each of the following spectra presented in decreasing order was delayed 1300 ms relative to the antecedent one. The luminescence colour was yellowish-reddish. As it can be seen, the beam damage is a very dynamic process : the peak in the blue region (at 420 nm) decreased its intensity to half in 2 s, which corresponds to an accumulated dose of about 8×10^{16} protons/cm².

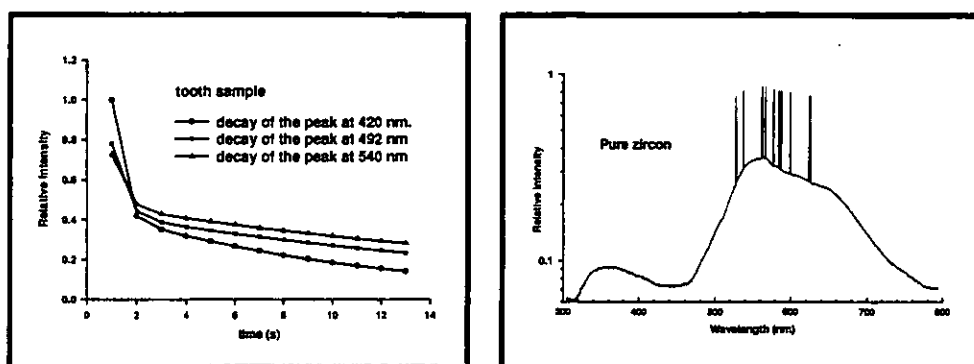


Figure 4.4. (left) : Exponential fit to the decay of the three peaks of Figure 4.3; (right) : IL spectrum of a pure synthetic zircon displaying some charging up in the form of randomly spaced sharp peaks on top of the characteristic broad Zr IL peak (see e.g., Figure 3.5a).

4.3 Study of mineral apatites by combined IL / μ PIXE methods

Apatite is one of the most common accessory minerals found in crustal rocks and its presence and distribution are used for geological modelling of different processes like mantle melting and differentiation in mantle chambers ([Roe-87]). In addition, apatites are commonly found associated to carbonatites and retain REE in their structure by the combined substitution of Ca + P by REE³⁺ + Si in the initial formula Ca₅(PO₄)₃F. Moreover they are the most important ore deposits of phosphates.

In this study we aimed at:

- i) determination of the bulk concentration of phosphorus;
- ii) mapping REE distribution in order to provide information for petrology studies of the Evate deposit;
- iii) studying REE and transition metals activated luminescence in apatites.

The quantification was made against a Wilberforce® standard and the two Si(Li) detectors were used: one with an active area of 30 mm² for the detection of phosphorus and the other subtending a larger solid angle, with an area of 50 mm² for trace elements detection. Phosphate (P₂O₄) concentrations higher than 18 % were found for all of the analysed samples, which makes it viable for use as cheap fertilisers by local farmers.

The REE distribution shows an enrichment of the apatites by light rare earth elements (LREE) relative to heavy ones (HREE). Normally the ratio Ce/Y is used to describe this tendency. Ce is a LREE and Y, despite the fact that it is not a REE, its ion, Y^{3+} , has the same charge and the same radius as Ho^{3+} . Also, that Y is more abundant so it will show up preferentially whenever a HREE occurs. In the Evate apatites, this ratio was about 4 in average. This points to the fact that the apatites have crystallised from a melt enriched with LREE, which is common to carbonatites. These results are consistent with different studies in apatites ([Fle-82]) and with the previously performed petrographic description of the deposit ([Tem-90]).

The importance of studying luminescence in apatites springs from the fact that apatite is a good host for different phosphorescent materials used the luminescence yield for different activators is much higher in these crystals ([Mor-70]). The fact that apatites retain REE in substitutional positions for Ca, makes possible to study the IL spectra of these elements for comparison with other geological materials, on an attempt to create a database of geological ionoluminescent material. On our studies, the typical Mn^{2+} and REE^{3+} activated luminescence transitions were observed and were found to be similar to the CL ones. The high sensitivity of IL to activator impurities helped in identifying REE peaks, which were below the detection limits by μ PIXE method.

The combination of IL and μ PIXE showed its powerfulness in geological studies.

4.4 Study of mineral zonation by IL / μ PIXE

As it was described in Section 3.1, zonation occurs during fractional crystallisation of melts. The study of zoning patterns in accessory minerals provides a window into the physicochemical conditions at which the minerals were formed. The information inferred from such analysis helps geologists to establish models for the dynamics of the ore-forming liquids, with applications in geological prospecting or the pressure and temperature conditions that governed the process of crystallisation, with application in tectonic and petrologic studies in general. However, in real samples, the zoning patterns are commonly invisible to light microscope (Figure 4.5, bottom) or even electron microscope, when buried deep in the sample. Since there is a difference in activator impurities concentrations among the zones in a mineral, the IL method can easily map these features with high contrast (Figure 4.5, upper). The IL method helps to target the zone to be probed during NMP

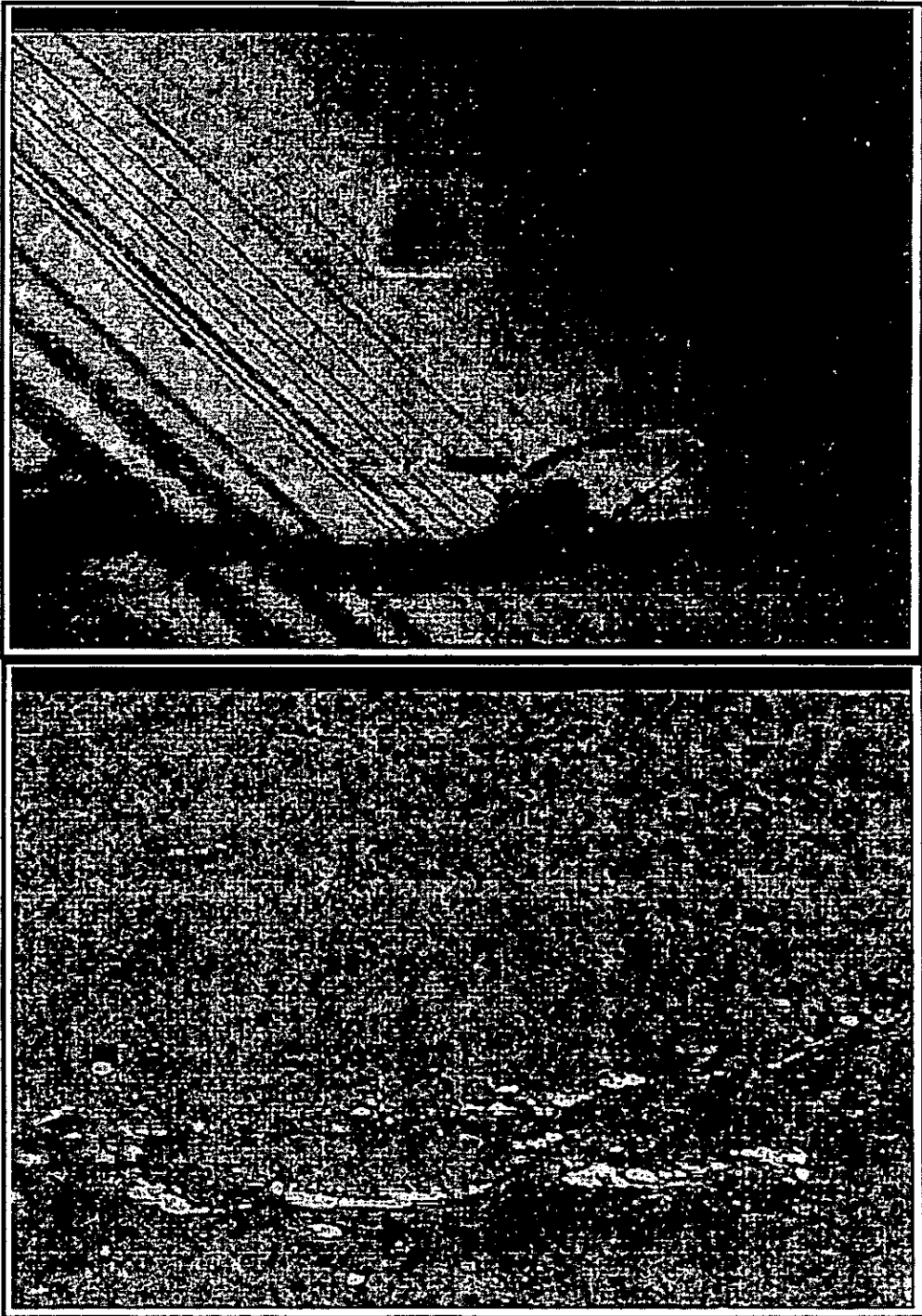


Figure 4.5. IL (top) and reflected light (bottom) images of the same spot on a natural zircon mineral. For the IL micrograph a proton beam of 2,55 MeV with current $\sim 5nA$ and exposure time of few seconds were used. (From [Mal-96]).

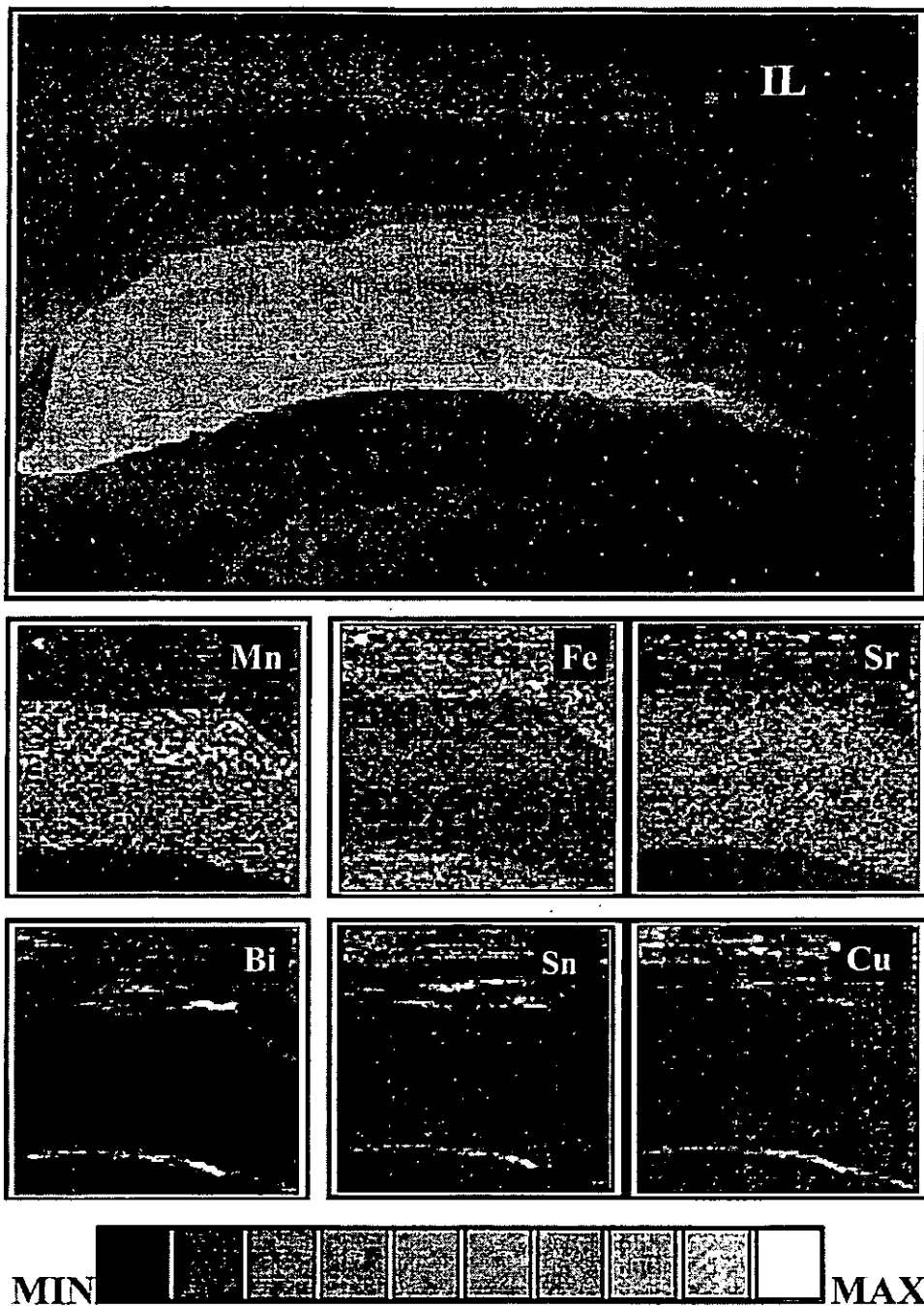


Figure 4.6. Illustration of combined use of IL (upper image) and μ PIXE for elemental imaging of an ancient Roman glass sample. The area mapped by PIXE is the dark square on the IL map ($1 \times 1 \text{ mm}^2$) caused by beam damage. A 2.55 MeV proton beam with spot size $10 \times 10 \text{ }\mu\text{m}^2$ was used. (From [Jan-96]).

analysis of geological samples, by locating quickly the interesting structures.

The combined use of IL and μ PIXE is also displayed in Figure 4.6. Presented are elemental maps of a leached region on an ancient Roman glass sample of Qumran, Jordan ([Jan-96]). The glasses were found in archaeological diggings, so they were exposed to severe weathering for a long time. Using IL imaging, we could identify the different regions by their light emission. The strong luminescence is Mn^{2+} activated (correlates very well with the Mn distribution) and it can be noted that the presence of Fe is reduced in that zone. Fe^{2+} is normally a quencher.

4.5 μ PIXE studies of pyrites

The microscopic ability imparted to the PIXE method by a Nuclear Microprobe makes it possible to analysis of geological samples aiming at the study of distribution patterns of trace elements in mineral grains on a micrometer scale. These patterns are telltales of the mineralisation conditions and/or the different geological metamorphic events, to which the minerals were subjected.

We have systematically studied pyrite (FeS_2) grains from rocks of the northern part of Sweden, for their trace elements content and distribution profile. Pyrite was chosen with the idea to use the results as a geochemical method for prospecting for ores, since it was found to be the most abundant and widespread of the sulfides in different kinds of bedrocks. Furthermore, its extensive stability range ensures that it will survive all but the highest grade of metamorphism and so, the distribution of trace elements in the grains can give valuable insights into the dynamic changes of the geological environment.

In PIXE analysis of pyrite samples, we have used a 425 μm thick mylar and a 300 μm thick aluminium absorbers, to suppress the intense peak of Fe K X-rays. We could increase the beam current up to 17 nA, whilst keeping a reasonable count-rate. This technique enabled us to attain detection limits as low as 7 ppm (1σ) for Au with an accumulated charge of 360 nC/pixel.

Several tens of grains were analysed and the processing of the results is still underway. However, PIXE studies showed a high concentration of Co in the pyrites from the Karelian Block (e.g., Figure 4.7), when compared with the Svecofennian Block, which suggests that the first region is part of a cobalt province.

A second possibility is that, the availability of Co in the geological cycle may have changed during the geological time, resulting in the obs-

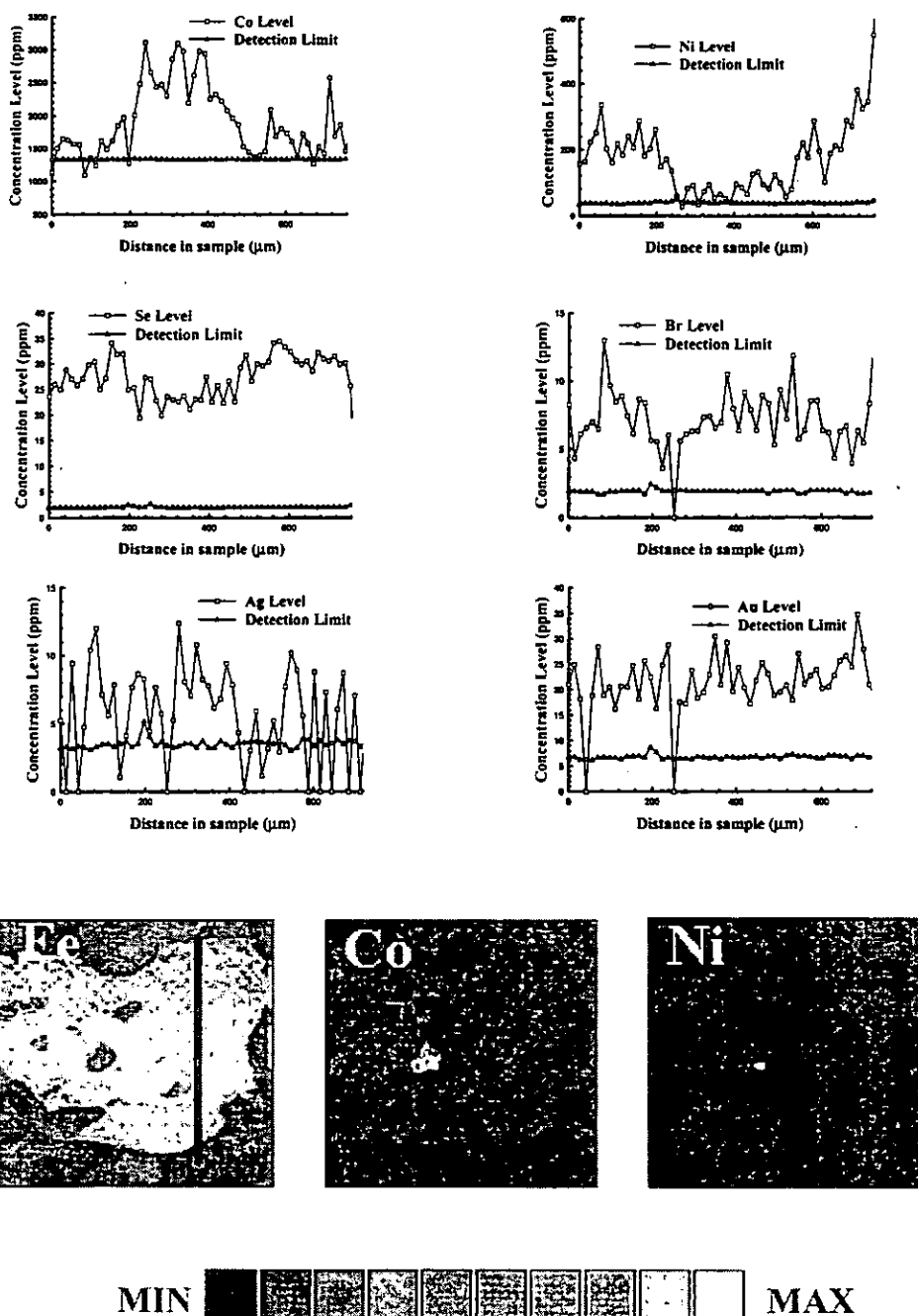


Figure 4.7. Trace elements concentration profiles and X-rays maps of Fe, Co and Ni of grain number 55185 A, from the Karelian Block, northern Sweden. The traverse analysis was made along the line in the Fe map. All images are $800 \times 800 \mu\text{m}^2$ across.

erverd patterns in the grains. Geological dating shows that the Karelian Block is younger than the Svecofennian. In Figure 4.8 X-ray maps of different trace elements in pyrite grains from the Karelian Block, are depicted, revealing oscillating zonation patterns.

The main aim of this project is to model the dynamics of the ore-forming processes, to help in geological prospecting. Noble metals like gold and platinum group elements are commonly associated to different sulfides and micro-analytical methods like μ PIXE, help to describe the partitioning of trace elements in different coexisting sulfide minerals.

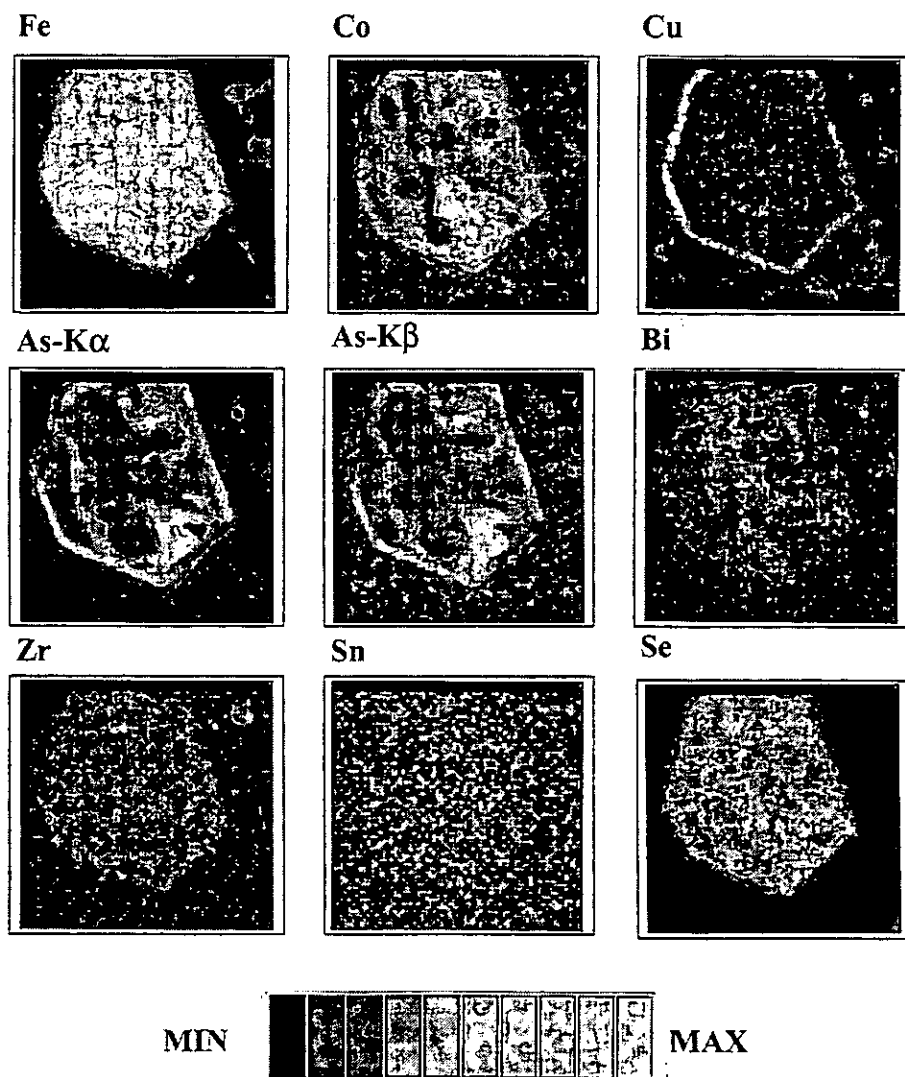


Figure 4.8. X-ray elemental maps in pyrite grain number N162901_Q showing oscillatory zonation patterns of Co, Cu, As and Se. Co seems to be correlated with As (arsenopyrite), which overgrew around a pyrite grain.

4.6 Geothermometry using μ PIXE

The pressure and temperature conditions prevalent during the evolution of a geological assemblage, dictate the physicochemical processes that will take place and, hence, the chemical composition of the resulting different mineral assemblages. The distribution of some elements in solid solutions is very sensitive to pressure or temperature and they can be used as geothermometers or geobarometers.

Using EMPA or NMP it is possible to measure the partitioning of the different elements in coexisting mineral assemblages and, thus, infer the P-T conditions of the rock through the geological time. Geothermobarometry is used to unravel the history of metamorphic transformations that took place in the rock and helps understanding the tectonic events responsible for the orogenesis of a terrain and the dynamics of ore-forming fluids [Spe-89].

We have used NMP to characterise metamorphic rocks of the Namama metamorphic thrust belt, northern Mozambique, by studying minerals commonly used as geothermometers.

Iron meteorites

The same concept of geothermometry is used to study the cooling history of iron meteorites. These ones, are samples of the core of a planetary-sized body that was formed 4,6 billion of years ago. Studying iron meteorites is very important for understanding the formation and development of the terrestrial planets (Venus, Earth and Mars).

The cooling rate of an iron meteorite is inferred through the partitioning pattern of Ni in the two coexisting kamacite and taenite facies. However, the "Ni-thermometer" describes the cooling rate over a narrow temperature interval around 500 °C. In order to cover the whole cooling range between 750 °C and 300 °C, some other thermometers, with different diffusivity in kamacite and taenite must be used. We have started a search for these new cooling rate indicators using a NMP. The idea is that the concentration in the centre of the taenite lamellae of the element used as thermometer must display the same dependence on the lamellar width as does Ni. Then the element can be used to indicate cooling rates in different temperature intervals.

The study is still ongoing but we have found that Ru and Pd show the same trend as Ni (Figure 4.9) and presumably may record the cooling rate of iron meteorites in a higher temperature range [Mei-96].

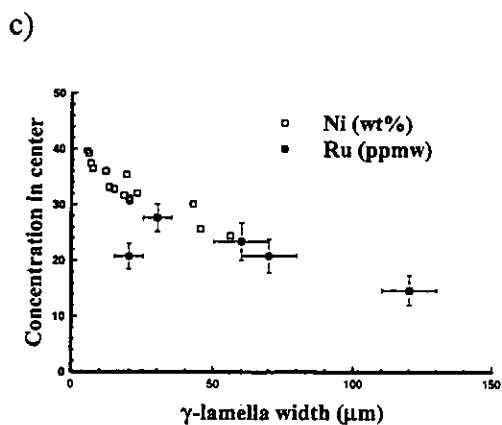
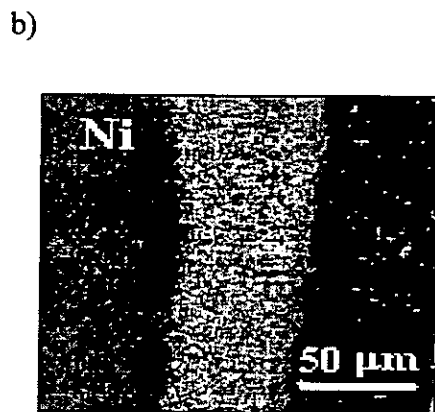
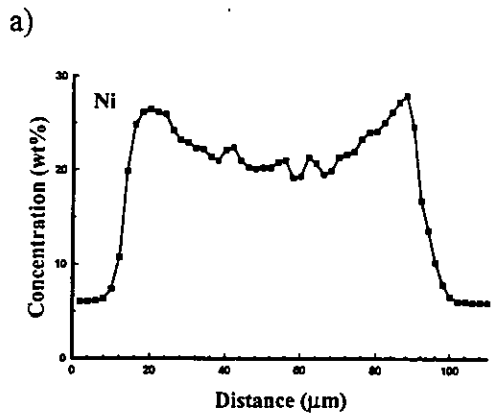


Figure 4.9. a) Typical M-shaped distribution pattern of Ni across the kamacite phase and taenite lamella (b). In c), the concentration of Ru as a function of lamellae width displayed against the Ni's. Ru shows the same negative trend and possibly can be used as a new cooling rate indicator in iron meteorites. (From [Mei-96]).

5. Conclusions.

In an attempt to summarise the findings and achievements attained at the present work, the following conclusions can be drawn:

- i) a low energy ion beam analysis facility based on a 500 keV particle accelerator was installed at the Maputo University and is being experimentally tested;
- ii) a long term research capacity building in order to upgrade the Department of Physics of Eduardo Mondlane University and manpower training to form a group of multidisciplinary researchers utilising the IBA facility is ongoing;
- iii) a team work at the Lund Nuclear Microprobe has been carried out addressing mainly:
 - the improvement of the apparatus performance in terms of spatial resolution, easiness of operation, reliability and long term stability;
 - the development of new techniques for specific uses of a NMP;
 - consolidation and application of well established IBA techniques.
- iv) the newly developed Ionoluminescence technique was used in geological applications. The studies envisaged:
 - setting up a new CCD array detection system;
 - systematically studying minerals in order to add new information to the database of IL, and
 - establish some routine procedures for geological studies using IL combined with PIXE.
- v) the combination of IL and μ PIXE methods proved to be very powerful and suited to geological studies in a NMP. Specific applications included characterisation of minerals and materials by IL, study of trace elements distribution in apatites and pyrites, study of geological thermometers.

6. Bibliography

- [Aig-74] Aiginger H. and Wobrauschek P., Nucl. Instr. & Methods 114 (1974) 157.
- [Aga-90] Agawa Y., Uchiyama T., Hoshino A., Tsuboi H., Fukui R., Takagi K., Yamakawa H., Matsuo T., Takai M. and Namba S., Nucl. Instr. & Methods B45 (1990) 540.
- [And-81] Andrae M.O. and Barnard W.R., Nucl. Instr. & Methods 181 (1981) 383.
- [Bat-92] Battistig G., Amsel G., d'Artemare E. and Vickridge I, Nucl. Instr. & Methods B66 (1992) 1.
- [Bet-94] Bettiol A.A., Jamieson D.N., Prawer S. and Allen M.G., Nucl. Instr. & Methods B85 (1994) 775.
- [Bev-86] Bever M.B., editor, Encyclopedia of Materials Science and Engineering, (The MIT Press, MA, 1986).
- [Bla-88] Blackburn W.H. and Dennen W.H., Principles of Mineralogy, (Wm. C. Brown Publishers, 1988).
- [Bor-75] Boro R.T. and Cipolla S.J, Nucl. Instr. & Methods 131 (1975) 343.
- [Bro-78] Brown P.E., Essene E.J. and Kelly W.C., Amer. Mineral. 63 (1978) 250.
- [Bru-84] Brunner G. and Rössiger V, Nucl. Instr. & Methods B3 (1984) 275.
- [Bud-84] Budnar M., Nucl. Instr. & Methods B4 (1984) 303.
- [Cab-91] Cabri L.J., Chryssoulis S.L., Campbell J.L. and Teesdale W., Appl. Geochem. 6 (1991) 225.
- [Cah-84] Cahill T.A., Matsuda Y, Shadoan D., Eldred R.A. and Kusko B.H., Nucl. Instr. & Methods B3 (1984) 263.
- [Cam-89] Campbell J.L., Wang J.-X., Maxwell J.A. and Teesdale W.J., Nucl. Instr. & Methods B43 (1989) 539.
- [Che-80] Chen M.H., Crasemann B. and Mark. H., Physical Rev. A21 (1980) 436.
- [Chu-78] Chu W.K., Mayer J.W. and Nicolet M.-A., Backscattering Spectrometry,

(Academic Press, Inc., 1978).

- [Doy-79] Doyle B.L., Peercy P.S., *Appl. Phys. Letters* 34(11) (1979) 811.
- [Elf-95] Elfman M., Homman N.P.-O. and Kristiansson P., *Nucl. Instr. & Methods B95* (1995) 122.
- [Elf-96] Elfman M, Kristiansson P., Malmqvist K.G., Pallon J., Sjöland K.A., Utui R.J. and Yang C., submitted to *Nucl. Instr. & Methods* (1996)
- [ElG-92] El-Ghawi U.M., Bahal B.M. and Al-Arbi S.K., *Rad. Res.* 131 (1992) 243.
- [Eng-84] England P.C. and Thompson A.B., *J. of Petrology* 25(4) (1984) 894.
- [Eng-84a] England P.C. and Thompson A.B., *J. of Petrology* 25(4) (1984) 929.
- [Fab-79] Fabriès J., *Contrib. Mineral. Petrol.* 69 (1979) 329.
- [Fel-77] Feldmann L.C. and Picraux S.T., from Mayer J. and Rimini E. (editors), *Ion Beam Handbook for Material Analysis* (Academic Press, New York, 1977).
- [Fle-82] Fleischer M. and Althschuler Z.S., *The lanthanides and yttrium in minerals of apatite group: A review.* U.S. Geological Survey Open-File Report, (1982) 82.
- [Fra-88] Frantz J.D., Mao H.K., Zhang Y.-G., Wu Y., Thompson A.C., Underwood J.H., Giauque R.D., Jones K.W. and Rivers M.L., *Chemical Geology* 69 (1988) 235.
- [Fra-91] Frauenfelder H. and Henley E.M., *Subatomic Physics*, (Prentice , Hall, Inc., 1991).
- [Fuc-90] Fuchs E, Oppolzer H. and Rehme H., *Particle Beam Microanalysis - Fundamentals, Methods and Applications*, (VCH Verlagsgesellschaft mbH, 1990).
- [Gil-90] Gilfrich J.V., *X-ray Spectrometry* 19(2) (1990) 45.
- [Gip-81] Gippner P., Bauer C., Hohmuth K., Mann R. and Rudolph W., *Nucl. Instr. & Methods* 191 (1981) 341.
- [Git-79] Gittins J., *Contib. Mineral. Petrol.* 69 (1979) 1.
- [God-88] Goodhew P.J. and Humphreys F.J., *Electron Microscopy and Analysis*, (Taylor & Francis, 1988).

- [Göt-88] Götz G. and Gärtner K., editors, High Energy Ion Beam Analysis of Solids, (Akademie - Verlag Berlin, 1988).
- [Gri-89] Griffin W.L., Smith D., Boyd F.R., Cousens D.R., Ryan C.G., Sie S.H. and Suter G.F., *Geoch. et Cosmoch. Acta* 53 (1989) 561.
- [Gri-89a] Griffin W.L., Cousens D.R., Ryan C.G., Sie S.H. and Suter G.F., *Contrib. Mineral. Petrol.* 103 (1989) 199.
- [Gri-92] Grieken R.E., Markowicz A.A., *Handbook of X-ray Spectrometry - Methods and Techniques*, (Marcel Dekker, Inc, 1992).
- [Gro-95] Grodzins L., Boisseau P., Glavish H., Klinkowstein R., Nett W. and Shefer R., *Nucl. Instr. & Methods B104* (1995) 1.
- [Hay-88] Hayat U., Bartlett P.N., Dodd G.H. and Lewis M.H., *Journal of Polymer Science A26* (1988) 201.
- [Hom-94] Homman N.P.-O., Yang C. and Malmqvist K., *Nucl. Instr. & Methods A353* (1994) 610.
- [Hom-94a] Homman N.P.-O., PhD Thesis, (KF-Sigma, 1994).
- [Hop-90] Hopson R.F. and Ramseyer K., *Geology* 18 (1990) 336.
- [Hsu-90] Hsu C.C, Chang Y.C. and Chu T.C., *Int. Journal of PIXE*, 1(1) (1990) 55.
- [Hub-80] Hubbes H.H., Schmiedeskamp B., Roosendaal H.E. and Lutz H.O., *Nucl. Instr. & Methods* 168 (1980) 313.
- [Iid-85] Iida A., Sakurai K., Matsushita T. and Gohshi Y., *Nucl. Instr. & Methods* 228 (1985) 556.
- [Ind-85] Indares A. and Martignole J., *Amer. Mineral.* 70 (1985) 275.
- [Izm-80] Izmailov Sh.Z., Sirotinin E.I., Tulinov A.F. and Chumanov V.Ya, *Nucl. Instr. & Methods* 170 (1980) 123.
- [Jam-95] Jamieson D.N., *Nucl. Instr. & Methods B104* (1995) 533.
- [Jan-96] Janssens K., Aerts A., Vincze L., Adams F., Yang C., Utui R., Malmqvist K., Jones K.W., Radtke M., Garbe S., Lechtenberg F., Knöchel A. and Wouters H., *Nucl. Instr. & Methods B109/110* (1996) 690.
- [Jaq-81] Jaque F. and Townsend P.D., *Nucl. Instr. & Methods* 182/183 (1981) 781.
- [Jen-81] Jenkins R., Gould R.W. and Gedcke D., *Quantitative X-ray Spectrometry*, (Marcel Dekker, Inc., NY and Bassel, 1981).
- [Joh-81] Johansson G.I., Pallon J., Malmqvist K.G., and Akselsson K.R., *Nucl. Instrum.*

& Methods 181 (1981) 81.

- [Joh-88] Johansson S.A.E. and Campbell J.L., PIXE: A Novel Technique for Elemental Analysis (Wiley, Chichester, 1988).
- [Joh-95] Johansson S.A.E., Campbell J.L. and Malmqvist K.G., Particle-Induced X-ray Emission Spectrometry (PIXE), (John Wiley and Sons, 1995).
- [Joh-70] Johansson T.B., Akselsson R., and Johansson S.A.E., Nucl. Instr. & Methods 84 (1970) 141.
- [Kea-88] Kearsley A. and Wright P., Microscopy and Analysis, Sept. 1988, pp 49 - 51.
- [Kis-95] Kishimoto T., Mimura R., Sawaragi H., Aihara R. and Takai M., Nucl. Instr. & Methods B104 (1995) 52.
- [Klo-96] Klockenkämper R.K. and von Bohlen A., X - Ray Spectrometry, 24(4) (1996) 156.
- [Kri-83] Krist T. and Merten P., Nucl. Instr. & Methods 218 (1983) 821.
- [Kri-90] Kristiansson P. and Swietlicki E., Nucl. Instr. & Methods B49 (1990) 98.
- [L'Ecu-78] L'Ecuyer J., Brassard C., Cardinal C. and Terreault, Nucl. Instr. & Methods 149 (1978) 271.
- [Lin-84] Lindner G., Nucl. Instr. & Methods B3 (1984) 130.
- [Löv-89] Lövestam N.E.G., Nucl. Instr. & Methods B36 (1989) 455.
- [Mal-82] Malmqvist K.G., Johansson G.I. and Akselsson K.R., J. Rad. Chem. 74 (1982) 125.
- [Mal-93] Malmqvist K.G., Hyltén G., Hult M., Håkansson K., Knox J.M., Larsson N.P.-O., Nilsson C., Pallon J., Schofield R., Swietlicki E., Tapper U.A.S. and Yang C., Nucl. Instr. & Methods B77 (1993) 3.
- [Mal-95] Malmqvist K.G., Nucl Instr. & Methods B104 (1995) 138.
- [Mal-96] Malmqvist K., Elfman M., Remond G. and Yang C., Nucl Instr. & Methods B109/110 (1996) 227.
- [Mar-79] Marfunin A.S., Spectroscopy, Luminescence and Radiation Centers in Minerals, (Springer-Verlag, Berlin, 1979).
- [Mar-88a] Marshall D.J., Cathodoluminescence of Geological Materials, (Boston, UNWIN, HYMAN, 1988).
- [Mar-93a] Marshall D.J., Scanning Microscopy 7(3) (1993) 861.
- [Mar-86] Martinsson B.G., Nucl. Instr. & Methods B15 (1986) 636.

- [Mar-88b] Martinsson B.G. and Hansson H-C., Nucl. Instr. & Methods B34 (1988) 203.
- [Mar-93] Martinsson B.G. and Kristiansson P., Nucl. Instr. & Methods B82(1993)589.
- [Mau-83] Maurel B. and Amsel G., Nucl. Instr. & Methods 218 (1983) 159.
- [Mei-96] Meibom A., Utui R., Yang C. and Elfman M. "*Iron Meteorites: searching for new cooling rate indicators using μ PIXE*" (In the Proceedings of the Fourteenth International Conference on Applications of Accelerators in Research and Industry, 1996, University of North Texas, Denton, on press).
- [Men-96] Menten B., Elfman M., Martinsson B., Nucl. Instr. & Methods B109/110 (1996) 511.
- [Mer-80] Mertens P. and Krist T., Nucl. Instr. & Methods 168 (1980) 33.
- [Mon-92] Moncoffre N., Nucl. Instr. & Methods B66 (1992) 126.
- [Mon-79] Montgomery C.W., Contrib. Mineral. Petrol. 69 (1979) 167.
- [Mor-78] Moriya Y., Ato Y. and Miyagawa S., Nucl. Instr. & Methods 150(1978) 523.
- [Mor-70] Morozov A.M., Morozova L.G., Trofimov A.K. and Feofilov P.P., Optika i Spektroskopiya, XXIX(6) (1970) 1107. (My own translation from Russian).
- [Muk-81] Mukoyama T. and Sarkadi L., Nucl. Instr. & Methods 190 (1981) 619.
- [Mus-72] Musket R.G. and Bauer W., J. Appl. Phys., 43(11) (1972) 4786.
- [Mus-73] Musket R.G. and Bauer W., Nucl. Instr. & Methods 109 (1973) 449.
- [Mus-74] Musket R.G., Nucl. Instr. & Methods 117 (1974) 385.
- [Nas-78] Nassau K., American Mineralogist 63 (1978) 219.
- [Nel-77] Nelson J.M. and Courtney W.J., Nucl. Instr. & Methods 142 (1977) 127.
- [Nix-87] Nixon P.H., Mantle Xenoliths (John Wiley & Sons Ltd, 1987).
- [O'Ne-79] O'Neil H.St.C. and Wood B.J., Contrib. Mineral. Petrol. 70 (1979) 59.
- [Osi-91] Osipowicz T. and Lieb K.-P., Thin Solid Films 203 (1991) 357.
- [Pau-84] Paul M., Nucl. Instr. & Methods B3 (1984) 5.
- [Pri-79] Priem H.N.A., Boelrijk N.A.I.M., Hebeda E.H., Oen I.S., Verdurmen E.A.Th. and Verschure R.H., Contrib. Mineral. Petrol. 70 (1979) 103.

- [Rei-93] Reid Jr. J.B., Murray D.P., Hermes O.D, and Steig E.J., *Geology* 21 (1993) 587.
- [Rem-92] Remond G., Cesbron F., Chapoulie R., Ohnenstetter D., Roques-Carmes C. and Schvoerer M., *Scanning Microscopy* 6(1) (1992) 23.
- [Ric-90] Rickards J., Oliver A., Miranda J. and Zironi E.P., *Appl. Surf. Sci.* 45 (1990) 155.
- [Rod-94] Rodriguez-Fernandez L., Miranda J. and Oliver.A., *Nucl. Instr. & Methods B85* (1994) 150.
- [Roe-87] Roeder P.L., MacArthur D., Ma X.-P., Palmer R. and Mariano A.N., *Am. Mineral.* 72 (1987) 801.
- [Ros-90] Ross G.G. and Leblanc L., *Nucl. Instr. & Methods B48* (1990) 134.
- [Ros-84] Ross G.G., Terreault B., Gobeil G., Abel G., Boucher C. and Veilleux G., *J. of Nucl. Materials* 128 & 129 (1984) 730.
- [Rup-88] Ruppel C., Royden L. and Hodges K.V., *Tectonics* 7(5) (1988) 947.
- [Rya-90] Ryan C.G., Cousens D.R., Sie S.H. Griffin W.L., Suter G.G., and Clayton E., *Nucl. Instrum. & Methods B47* (1990) 55.
- [Rya-93] Ryan C.G. and Griffin W.L., *Nucl. Instr. & Methods B77* (1993) 381.
- [Rya-93a] Ryan C.G., Heinrich C.A. and Mernagh T.P., *Nucl. Instr. & Methods B77* (1993) 463.
- [Rya-95] Ryan C.G., *Nucl. Instr. & Methods B104* (1995) 377.
- [Rya-95a] Ryan C.G., Heinrich C.A., van Achterbergh E., Ballhaus C. and Mernagh T.P., *Nucl. Instr. & Methods B104* (1995) 182.
- [Rya-96] Ryan C.G., Griffin W.L. and Win T.T. *Nucl. Instr. & Methods B109/110* (1996) 601.
- [San-86] Sandiford M. and Powell R., *Earth and Planet. Sc. Letters* 79 (1986) 151.
- [Sax-79] Saxema S.K., *Contrib. Mineral. Petrol.* 70 (1979) 279.
- [Say-94] Sayama H., Kimura H., Ohno Y., Sonoda K., Kotani N., Satoh S. and Takai M., *Nucl. Instr. & Methods B85* (1994) 703.
- [Sel-90] Selverstone J. and Chamberlain C.P., *Geology* 18 (1990) 307.
- [Sie-87] Sie S.H., Ryan C.G., Cousens D.R. and Griffin W.L., *Proceedings of the 5th Australian Institute of Nuclear Science & Engineering Conference on Nuclear Techniques of Analysis*, Lucas Heights, NSW, Nov. 1987.
- [Sie-89] Sie S.H., Ryan C.G., Cousens D.R. and Griffin W.L., *Nucl. Instr. & Methods*

B40 (1989) 690.

- [Sie-96] Sie S.H., Murao S. and Suter G.F., Nucl. Instr. & Methods B109/110 (1996) 633.
- [She-85] Shepherd T.J, Rankin A.H. and Alderton D.H.M., A Practical Guide to Fluid Inclusion Studies (Blackie & Son Ltd, 1985).
- [Sjö-95] Sjöland K.A., Kristiansson P. and Tallone P., Nucl. Instr. & Methods B104 (1995) 255.
- [Sjö-96] Sjöland K.A. and Kristiansson P., Off-axis STIM nuclear microprobe analysis, Nucl. Instr. & Methods, on press.
- [Ski-87] Skinner B.J. and Porter S. C., Physical Geology, (John Wiley & Sons, 1987).
- [Sko-92] Skoog D.A. and Leary J.J., Principles of Instrumental Analysis, (Saunders College Publishing, 1992).
- [Smi-85] Smith D. and Wilson C.R., Amer. Mineral. 70 (1985) 30.
- [Smi-91] Smith D., Griffin W.L., Ryan C.G. and Sie S.H., Contrib. Mineral. and Petrol. 107 (1991) 60.
- [Sow-94] Sow C.H., Orlic I., Osipowicz T. and Tang S.M., Nucl. Instr. & Methods B85 (1994) 133.
- [Spe-89] Spear F.S. and Peacock S.M., Metamorphic Pressure-Temperature-Time paths, in Short Course of Geology, vol. 7, (Washington DC, Am. Geoph. Union, 1989).
- [Sva-92] Svanberg S., Atomic and Molecular Spectroscopy - Basic Aspects and Practical Applications, (Springer-Verlag, 1992).
- [Swi-84] Swietlicki E. and Bohgard M., Nucl. Instr. & Methods B (1984)441.
- [Swi-93] Swietlicki E., Larsson N.P.-O. and Yang C., Nucl. Instr. & Methods B77 (1993) 195.
- [Tak-95] Takai M., Nucl. Instr. & Methods B104 (1995) 501.
- [Tap-87] Tapper U.A.S., Lövestam N.E.G., Karlsson E. and Malmqvist K.G., Nucl. Instr. & Methods B28 (1987) 317.
- [Tap-89] Tapper U.A.S. and Nielsen B.R., Nucl. Instr. & Methods B44 (1989) 219.
- [Tap-89a] Tapper U.A.S. and Jamieson D.N., Nucl. Instr. & Methods B44 (1989) 227.
- [Tap-91] Tapper U.A.S. and Malmqvist K.G., Anal. Chemistry 63(14) (1991) 715.
- [Tel-78] Telfer D.J. and Walker G., Modern Geology 6 (1978) 199.

- [Tem-90] Tembe S.S., Evate apatites: project proposal, National Geological Survey of Mozambique, (1990), not published.
- [Tho-81] Thompson D.A., Poehlman W.F.S., Presunka P. and Davies J.A., Nucl. Instrum. & Methods 191 (1981) 469.
- [Tri-96] Trigaud T., Moliton J.P., Mazière B., Jussiaux C. and Chiron D., Nucl. Instrum. & Methods B111 (1996) 254.
- [Utu-94] Utui R.J., unpublished, Project progress report to SAREC (1994).
- [Utu-96] Utui R.J., Homman N.P.-O. and Malmqvist K.G., submitted to Int. Journal of Pixe (1996).
- [Utu-95] Utui R.J., Homman N.P.-O., Yang C., Malmqvist K.G. and Tembe S.S., Nucl. Instr. & Methods B104 (1995) 432.
- [Wal-90] Walls J.M., editor, Methods of Surface Analysis: techniques and applications (Cambridge University Press, 1990).
- [Wat-87] Watt F. and Grime G.W. , editors, Principles and Applications of High - Energy Ion Microbeam (Adam Higler, Bristol 1987).
- [Whi-90] Whitlow H.J, Materials Res. Soc., Proc. High Energy and Heavy Ion Beams in Materials Analysis (1990).
- [Wil-91] Willemsen M.F.C. and Kuiper A.E.T., Nucl. Instr. & Methods B61 (1991) 213.
- [Wob-96] Wobrauschek P., Strelci C., Kregsamer P., Ladisich W. and Rieder R., Journal of Trace and Microprobe Tech. 14(1) (1996) 103.
- [Wog-92] Wogelius R.A., Fraser D.D., Feltham D.J. and Whiteman M.I., Geochim. Et Cosmoch. Acta 56 (1992) 319.
- [Yan-94] Yang C., Homman N.P.-O., Johansson L. and Malmqvist K.G., Nucl. Instr. & Methods B85 (1994) 808.
- [Yan-95] Yang C., Homman N.P.-O., Malmqvist K.G., Johansson L., Halden N.M. and Barbin V., Scann. Microscopy 9(1) (1995) 43.
- [Yan-95a] Yang C., PhD Thesis, (Lund University, 1995).
- [Zie-92] Ziegler J.F. ,Handbook of Ion Implantation Technology (North Holland1992).
- [Zie-95] Ziegler J.F. , TRIM ver.95 (IBA Research, Yorktown, NY 10598, 1995).

10123

7. Thesis.

The thesis comprehends the following papers:

- I. R.J. Utui, N.P.-O. Homman and K.G. Malmqvist "*A new low energy Ion Beam Analysis facility at the Eduardo Mondlane University*". (Submitted to the Int. Journal of PIXE, 1996).
- II. R.J. Utui, N.P.-O. Homman, C. Yang, K.G. Malmqvist and S.S. Tembe "*Nuclear Microprobe analysis of Evate (Mozambique) apatites*". (Published in Nucl. Instrum. & Methods B104 (1995) 432 - 436).
- III. C. Yang, K.G. Malmqvist, J.M. Hanchar, R. J. Utui, M. Elfman, P. Kristiansson, J. Pallon and A. Sjöland "*Ionoluminescence combined with PIXE in the Nuclear Microprobe for the study of inorganic material*". (In the Proceedings of the Fourteenth International Conference on Applications of Accelerators in Research and Industry, 1996, University of North Texas, Denton, on press).
- IV. K. Janssens, A. Aerts, L. Vincze, F. Adams, C. Yang, R. Utui, K. Malmqvist, K.W. Jones, M. Radtke, S. Garbe, F. Lechtenberg, A. Knöchel and H. Wouters "*Corrosion phenomena in electron, proton and synchrotron X-ray microprobe analysis of Roman glass from Qumran, Jordan*" (Published in Nuclear Instruments and Methods B 109/110 (1996) 690-695).
- V. R.J. Utui, X. Wang, F.M. Guerreiro, M. Elfman, P. Kristiansson, K.G. Malmqvist, J. Pallon, A. Sjöland and C. Yang "*Application of Nuclear Microprobe in the study of granulite facies rocks from the Namama Thrust Belt*" (Submitted to Nucl. Instrum. & Methods Section B, 1996).

The author is responsible for all the aspects of papers I, II and V, regarding the installation of the laboratory (paper I), the performance of experiments and analysis of data (papers II and V). In papers III and IV the author participated in experimental analysis of the samples and data evaluation.

The author contributed to the following paper, whose subject is related to geological applications, but is not included in the thesis:

- I. A. Meibom, R.J. Utui, C. Yang and M. Elfman "*Iron Meteorites: searching for new cooling rate indicators using μ PIXE*" (In the Proceedings of the Fourteenth International Conference on Applications of Accelerators in Research and Industry, 1996, University of North Texas, Denton, on press).

Other papers exist, published or on press, in which the author either contributed in a lesser extent or the subject falls outside the scope of the present work, so they are not referred to here.

R.J. Utui, N.P.-O. Homman and K.G. Malmqvist "*A new low energy Ion Beam Analysis facility at the Eduardo Mondlane University*".
(Submitted to the Int. Journal of PIXE, 1996).

THE NEW LOW ENERGY ION BEAM ANALYSIS FACILITY AT MAPUTO UNIVERSITY

R.J. UTUI^a

*Department of Physics, Eduardo Mondlane University,
P.O.Box 257, Maputo, Mozambique*

N.P.O. HOMMAN, AND K.G. MALMQVIST

*Department of Nuclear Physics, Lund University and Lund
Institute of Technology, Sölvegatan 14, S - 223 62, Lund, Sweden.*

ABSTRACT

A new Ion Beam Analysis (IBA) facility which was recently installed in the Department of Physics of the Eduardo Mondlane University of Maputo, Mozambique, is described. The set up is based on a low energy (500 keV) Van de Graaff proton accelerator and is intended to be used in particle induced X-ray emission (PIXE), Rutherford Backscattering (RBS) and nuclear reaction analysis (NRA).

Preliminary experiments on beam diagnostics were performed successfully and the followed procedure is described.

1. Introduction

The PIXE method, which combines X-ray excitation by charged particles and detection with a Si(Li) detector constitutes a well established method of multi-elemental analysis with sensitivity down to the ppm level¹. The fact that only small quantities of sample are required allied to the non-destructiveness makes this method suitable for rapid survey of many samples². For a well calibrated apparatus, absolute concentrations at ppm level can be easily obtained for the elements present in the sample. However, to exploit these advantages it should require a minimum of set up time, provide a possibility for on-line data analysis as well as allow optimisation of the sensitivity for different elements by variation of beam energy and the use of selective X-ray absorbers^{3,4}. Further, beam energy, beam charge and detector response must be reproducible in order to obtain reliable quantitative results⁴.

^a Corresponding author; e-mail: roger@nambu.uem.mz.

The quantification of thin samples, i.e. samples with thickness lower than the range of the protons in the material, is done by comparing the X-ray spectra to those of standards with known composition⁵, whilst for thick samples many factors must be taken into account. In this case an initial guess of the matrix composition is used to calculate the variation of cross sections for X-ray production with the energy of protons, the attenuation of X-rays in the material and the enhancement of some spectral lines through secondary X-ray fluorescence. Nowadays there exist a lot of spectral analysis computer codes in which all these factors are taken into account in order to fit spectra with good accuracy.

The minimum detectable amount varies in one to two orders of magnitude for different elements of the periodic table due to factors like cross section for X-ray production, attenuation of the X-rays by the detector window, induction of nuclear reactions which give raise to gamma-ray noise. Light elements, for example, cannot be detected at all by PIXE and then a complementary technique - Rutherford Backscattering (RBS) - which does not imply additional requisites to the set up is used. In this technique the energy spectrum of the back scattered particles is used to calculate the composition of the sample using simple kinematic relations. The high yield of gamma rays from selected nuclear reactions in several light nuclei on other hand makes possible the use of another complementary technique, nuclear reaction analysis (NRA), which, together with PIXE and RBS can provide a powerful accelerator based analytical tool.

The aim of the present work can be seen within the framework of a research project intending to introduce accelerator based ion beam analysis techniques in the Eduardo Mondlane University, Maputo. After a long period of stagnation the university lacks updated research equipment in basic sciences and attempts to build some infrastructure that can be used by multi-disciplinary teams of researchers at low investment are regarded. For this project we made use of the already availavble 500 keV Van de Graaff proton accelerator commissioned in the late sixties. The assembling of such a system in the present conditions was quite sinuous and implied setting up or reconditioning almost all the basic infrastructure .

Basic fundamental work on PIXE at sub-MeV energies have been reported by a number of authors⁷⁻¹² and all the applications that were found for this method in this "not usual" energy range point out at its high sensitivity for detecting low Z elements in heavy elements matrix^{13,14} and high detection limits for elements with $Z > 25$. The use of extra thin window X-ray detectors makes this technique competitive for detecting elements down to carbon. Nuclear reaction analysis at these energies for detection of light elements have found large application in material sciences, medicine and biology^{16,17,18}.

The new ion beam analysis facility featuring these three methods is intended to be used in geological, biological and environmental sciences serving an interdisciplinary team of researchers.

2. Description of the Experimental Set-up

2.1. The beam line

The diagram of the experimental set-up can be seen in Fig. 1. The 500 keV Van de Graaff accelerator manufactured by High Voltage Engineering® delivers a proton beam of up to 100 nA on target with voltage stability better than 10^{-4} . The beam passes through an object aperture and is energy defined by an analysing and switching magnet. The IBA line was assembled at 30° . Downstream we have a quadrupole doublet focusing lens, a beam viewer, the reaction chamber and the Faraday cup.

Three oil diffusion pumps keep the beam line at a vacuum better than 5×10^{-6} Torr and the working pressure at the chamber is better than 4×10^{-5} Torr.

2.2 The reaction chamber

The reaction chamber has been described elsewhere¹⁹. Two collimators with 5 mm in diameter define the beam at the entrance. The Si(Li) detector views the target at a distance of 4 cm and is mounted at an angle of 135° relative to the beam for lower secondary bremsstrahlung intensity. The front wall of the chamber is made of Plexiglas with a port for a gamma ray detector. Charge measurements for thin samples are made at the Faraday cup and for thick samples at the chamber that is, for this purpose, insulated from the beam line. The charge measurement system comprises also a secondary electron suppression by applying +30V to the last collimator and -50 V to the electron shield between the sample and the last collimator.

2.3. The detection systems and electronics

For X-ray detection we are using a Kevex® Si(Li) detector with 10 mm² area, 8µm thick beryllium window and a measured resolution of 150 eV FWHM at 5,9 keV. The back scattered protons are detected by a ruggedized® surface barrier detector with a total area of 50 mm², 100 µm of minimal depletion depth and measured resolution of 18 keV at 5,49 MeV alphas, mounted at 170° relative to the beam.

The gamma detector, an ORTEC[®] Hp-Ge with 30% reported efficiency can be placed into a port viewing the sample at 90°.

A minimum set of NIM modules is available that includes bias voltage supply, pre-amplifiers and amplifiers, current digitiser, a pulse generator, ratemeters, counters and timers. Two MCA slot cards coupled to a PC form the data acquisition system.

3. First Results

The first experiments performed at the new IBA set up were intended to calibrate the beam optics, to set the optimal beam current and shape and to test the whole system. After placing an object aperture of 1 cm diameter (see fig. 1) and calibrating the magnets power supplies we adjusted the generator current in order to get a 2 μ A beam current ant the beam viewer/stop. A 5 mm diameter carbon slit was placed right behind the beam viewer and the current at the focusing lenses adjusted in order to have a beam cross over at the slit to warrant more beam transmission. As result we could get a beam spot of about 8 to 10 mm diameter on target with a current of 100 nA..

A PIXE spectrum of a geological sample collected in this set up with 475 keV protons is shown in fig. 2 for an integrated charge of 3 μ C.

4. Summary

A new ion beam analysis facility at the Eduardo Mondlane University, Maputo, was installed and tested. Preliminary calibration experiments were performed and the set up is now operational. PIXE, RBS and NRA are the three methods installed to serve a multidisciplinary team of users.

Acknowledgements

The authors would like to thank the Swedish Authority for Research co-operation with Developing Countries (SAREC) for supporting this project and the Department of Nuclear Physics of the Lund Institute of Technology for providing some useful parts of the beam line.

References

1. S.A.E. Johansson and T.B. Johansson, Nucl. Instrum. & Methods 137 (1976) 473.
2. S.A.E. Johansson and J.L. Campbell, *Pixe a Novel Technique for Elemental Analysis* (Wiley 1988).
3. P.F. Hinrichsen, A. Houdayer, G. Kajrys and A. Belhadfa, Revue Phys. Appl. 23 (1988) 1557.
4. R. Leconte, P. Paradis, S. Monaro, M. Barrete, G. Lamoureux and H.A. Menard, Nucl. Instrum. & Methods 150 (1978) 289.
5. G.I. Johansson, J. Pallon, K.G. Malmqvist and K.R. Akelsson, Nucl. Instrum. & Methods 181 (1981) 81.
6. W.K. Chu, J.M. Mayer and M.A. Nicolet, *Backscattering Spectrometry*, (Academic Press, 1978).
7. L.Rodriguez-Fernandez, J. Miranda and A. Oliver, Nucl. Instrum. & Methods B85 (1994) 150.
8. C.H. Sow, I. Orlic, T. Osipowicz, M. Tang, Nucl. Instrum. & Methods B85 (1994) 133.
9. C.C. Hsu, Y.C. Chang and T.C. Chu, *International Journal of PIXE*, vol.1 no.1 (1990) 55.
10. M. Budnar, Nucl. Instrum. & Methods B4 (1984) 303.
11. D.A. Thompson, W.F.S. Pochlman, P. Presunka and J.A. Davie, Nucl. Instr. & Methods 191 (1981) 469.
12. T. Krist and P. Merten, Nucl. Instrum. & Methods 218 (1983) 821.
13. J. Rickards, A. Oliver, J. Miranda and E.P. Zironi, *Appl. Surface Science* 45 (1990) 155.
14. U.M. El-Ghawi, B.M. Bahal and S.K. Al-Arbi, *Radiation Research* 131 (1992) 243.
15. M.F.C. Willemsen and A.E.T. Kuiper, Nucl. Instrum. & Methods B61 (1991) 213.
16. P.Gippner, C. Bauer, K. Hohmuth, R. Mann and W. Rudolph, Nucl. Instrum. & Methods 191 (1981) 341.
17. M.A. Chaundri and A. Crawford, Nucl. Instrum. & Methods 181 (1981) 327.
18. J.D. MacArthur, G.R. Palmer, W.E. Hekman and K. Budd, Nucl. Instrum. & Methods 218 (1983) 519.
19. K.G. Malmqvist, G.I. Johansson and K.R. Akelsson, *Journal of Radioanal. Chem.* 74 (1982) 125.

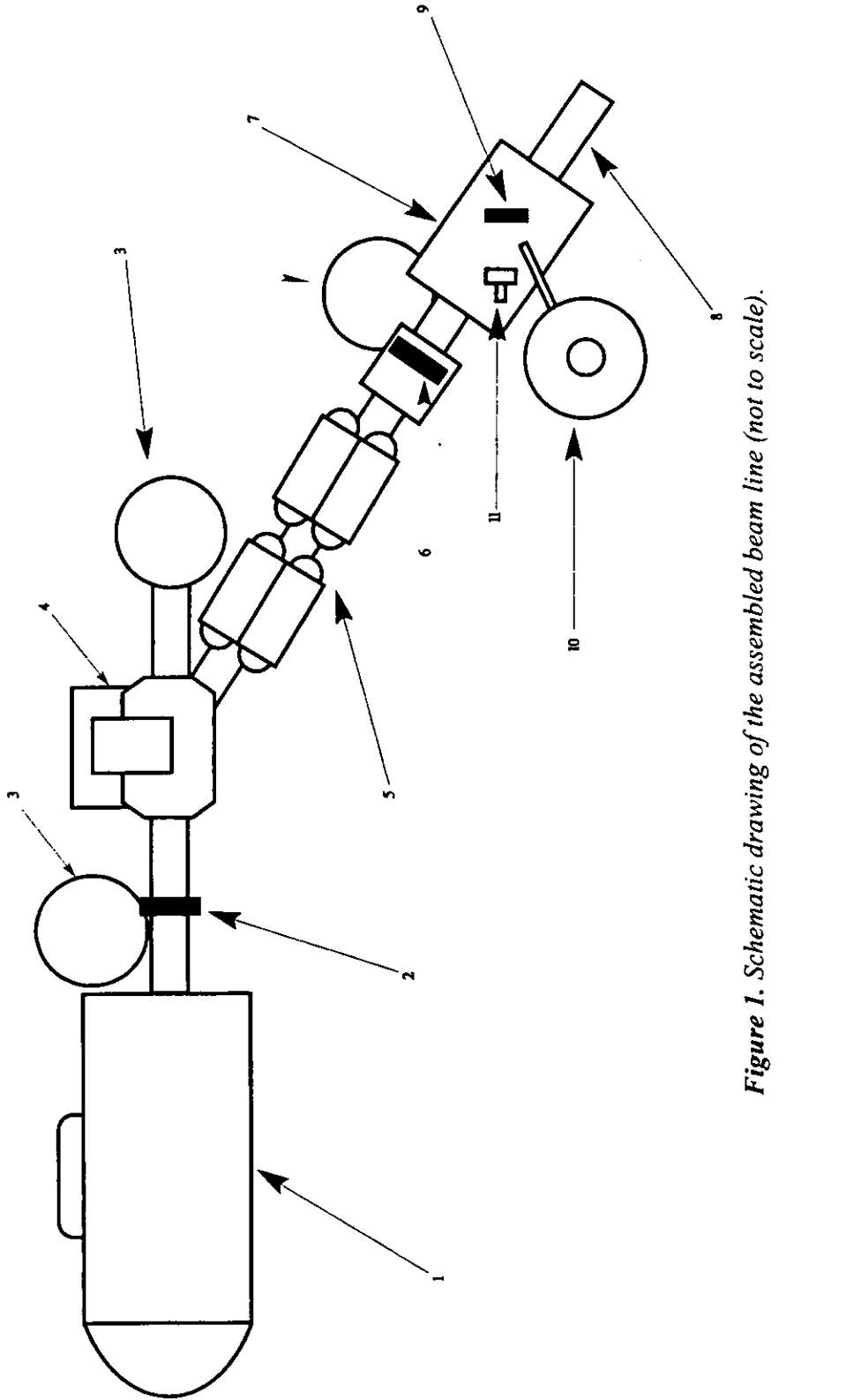


Figure 1. Schematic drawing of the assembled beam line (not to scale).

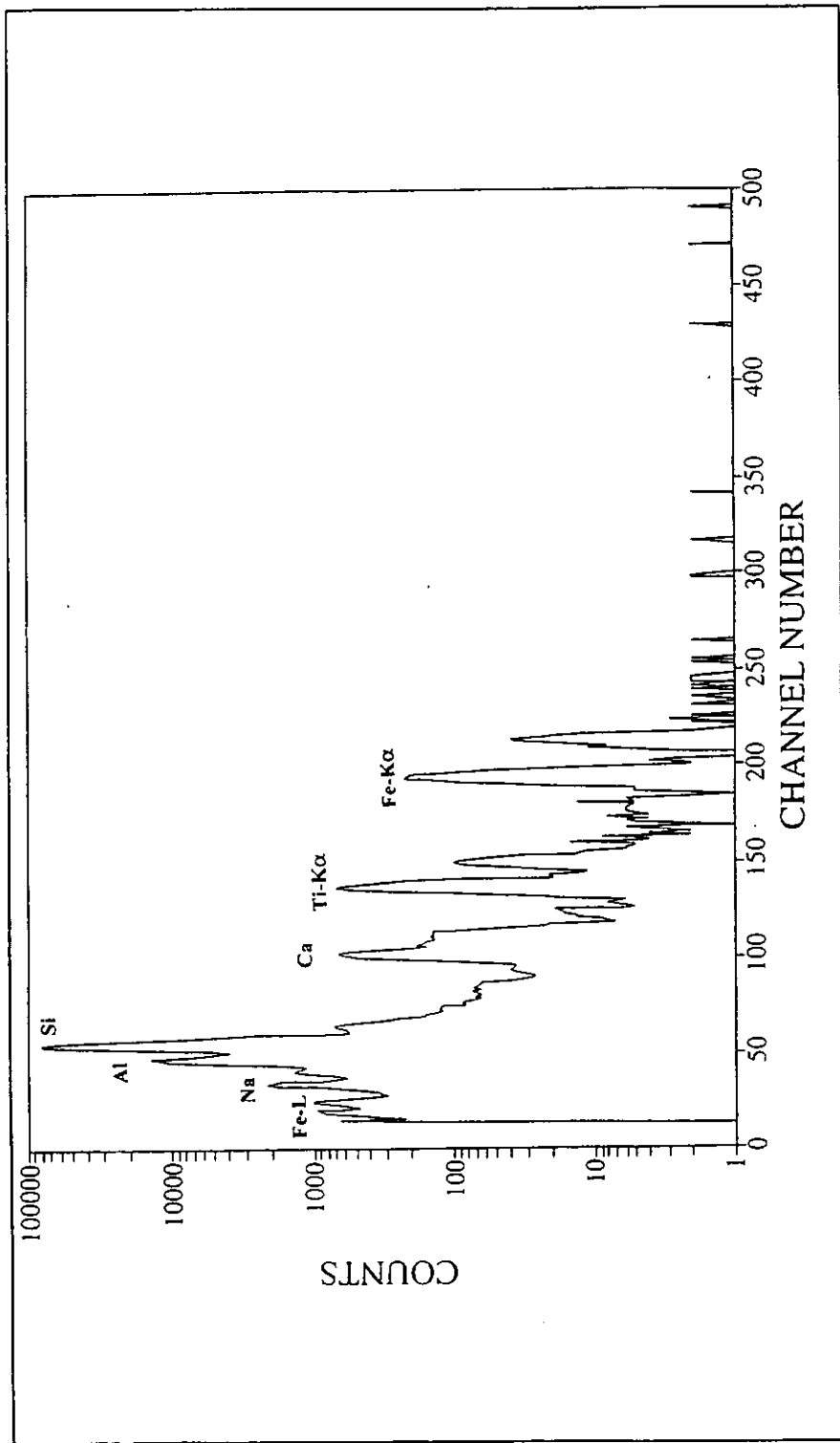


Figure 2. PIXE spectrum of a bentonite sample for a proton energy of 475 keV and 3 μ C of integrated charge.

R.J. Utui, N.P.-O. Homman, C. Yang, K.G. Malmqvist and S.S. Tembe
"Nuclear Microprobe analysis of Evate (Mozambique) apatites".
(Published in Nucl. Instrum. & Methods B104 (1995) 432 - 436).

With permission of Elsevier Science B.V.

Nuclear microprobe analysis of Evate (Mozambique) apatites

R.J. Utui^{a,*}, N.P.-O. Homman^b, C. Yang^b, K.G. Malmqvist^b, S.S. Tembe^c

^aDepartment of Physics, Eduardo Mondlane University, P.O. Box 257, Maputo, Mozambique

^bDepartment of Nuclear Physics, Lund University and Lund Institute of Technology, Sölvegatan 14, S-223 62, Lund, Sweden

^cInstituto Nacional de Geologia, Praca 25 de Junho, Maputo, Mozambique

Abstract

A characterization of mineral apatite samples using Nuclear Microprobe techniques was made. Thin polished sections of apatite in calcite matrix were analyzed by PIXE (particle-induced X-ray emission) and IL (ion luminescence) for major and trace elements quantification. Some Rare Earth Elements (REE), which are IL activators mainly in the UV and visible region, present in the sample in concentrations far below the minimum detectable limit by PIXE method, could still display characteristic luminescence spectra. Hence, IL is a very useful complementary method to traditional ion beam analytical techniques such as PIXE, and NRA (nuclear reaction analysis) for application in geology.

The results are in perfect agreement with some available information about previous tectonic studies performed in the Nampula geological province and show some possibility of beginning a semi-artesian exploitation of the apatite for use in local subsistence farming as a cheap fertilizer.

1. Introduction

For many years, focused MeV ion beams have been successfully used in geological research. PIXE and PIGE (particle-induced gamma-ray emission) are the most common techniques for multi-elemental quantification [1, 2] and elemental mapping, when combined with suitable scanning systems. Recently, the usefulness of another ion beam analysis (IBA) technique, ion luminescence, was demonstrated [3]. The IL spectrum is partly determined by the presence of *activator* impurities in the sample and can be simply measured by photon counting methods in the UV and visible regions.

A comprehensive study of light-induced luminescence in fluorapatite $\text{Ca}_5(\text{PO}_4)_3\text{F}$ monocrystals artificially doped with elements from Ce through Yb was made by Morozov et al. [4]. They demonstrated that the probability of radiative transitions between excited terms of REE 3+ ions was higher in those crystals than in any other matrices [4].

In the present work both PIXE and IL were used, providing useful information about trace elements concentration and distribution in apatite samples. These techniques facilitated (1) the mineralogical and petro-

graphic characterization of the Evate apatite deposit in northern Mozambique, and (2) an evaluation of practical and economical viability of apatite and/or other mineral exploitation for agriculture and industry and many other applications.

Apatite is the most important source of phosphorus used in fertilizers as well as in a large number of other applications. It occurs usually in association with magnetite, monazite, and different rare earth minerals in igneous rocks, pegmatites and gneisses. A project named "Evate apatite" under the responsibility of the National Geological Institute of Mozambique, aimed at studying the possibility of semi-artesian exploitation of this mineral is ongoing since 1993. Provided that concentrations of P_2O_5 higher than 18% will be found, the apatite can just be milled and spread on the land to increase the crops in subsistence farming. Lower concentrations imply, for the poor farmers of that region, unaffordable industrial pre-treatment. On the other hand, the possible association of apatite with monazite, which is a good REE source can make their prior extraction, viable [5].

The objects of analysis were, therefore, phosphorus and rare earth elements quantification and mapping of the main magnetite elements. In many cases the concentration of REE lied far below the PIXE minimum detectable limits but they still could be detected by IL and, despite the difficulty in obtaining absolute quantification

* Corresponding author. Fax: + 258 1 475333.

with this method, some relevant information could be extracted from the spectra combining the results of both analytical techniques.

2. Experimental

All the experiments were carried out at the Lund Nuclear Microprobe. The main features of this facility were described elsewhere [6] and only minor changes have been introduced since then. The analysis were performed in two different runs: in the first one both PIXE and IL detection systems were mounted and in the second, two X-ray detectors for PIXE analysis. The main reasons for this approach are (1) the necessity of accurate quantification of both a light element like phosphorus and heavy REE simultaneously, (2) the space available in the specimen chamber, and (3) some specificities of the data acquisition system.

Eleven thin polished sections of apatite grains in calcite matrix were bombarded by a 3 nA proton microbeam of about $10 \times 10 \mu\text{m}^2$ size. In the first run the typical blue-pinkish light activated by REE [7], was collimated to the entrance slit of a monochromator with good spectral response to both UV and visible region. The slit width was set to 800 μm , which correspond to a resolution of 16 Å, the grating scanning speed to 5 Å/s, and the initial wavelength to 3500 Å, in order to match with the transmission range of the optical lenses used to collimate the light. The upper limit of the detected wavelength is set by the response of the HamamatsuTM R943-02 photomultiplier tube (PMT) connected to the monochromator exit. Pressurized air blown through a liquid nitrogen dewar was used to cool the PMT down to -30°C in order to keep a very low dark current (less than 80 cps). The signal from the PMT was discriminated, amplified and fed into a MCS connected to a Nuclear Data acquisition system with a $\mu\text{VAX-II}$ host computer.

In the second run two Si(Li) X-ray detectors were used: the first one, with a 50 mm^2 area, viewed the sample at a good solid angle suitable for REE L-lines quantification. It was used with a 780 μm Mylar absorber to suppress the very strong peaks of P and Ca and the second one, with an area of 30 mm^2 , was used for major elements quantification, with a 77 μm Mylar absorber to stop back scattered protons. Careful energy and mass calibrations were made just before the second run and all the measurements were performed against a WilberforceTM fluorapatite standard. All the PIXE spectra were analyzed using GEOPIXE [8] software.

3. The Evate apatite deposit

The samples were collected during different geological prospective works in the eastern part of the northern province of Nampula, Mozambique. Maps with scale

1:50.000 were elaborated in earlier geological and geophysical studies by different foreign companies, which enabled the discovery of the apatite deposit during the early 1980s. It was reported to consist of fluorapatite with irregular distribution of magnetite and monazite.

The Evate formation consists of biotite gnaisses and marbles crossed by granite, pegmatite, and quartz veins [5] and different raw materials from the neighborhood like pegmatites, graphites and marbles have been exploited. The apatite occurrence in marbles is still being investigated for its optimal exploitation and use, mainly in agriculture.

The apatite mineralization is much dense in the central part of deposit, which has an area of $3 \times 1 \text{ km}^2$, and does not reach the surface. In general, the P_2O_5 concentration in the mineral increases with the depth. Both apatite and magnetite are intrusions, the magnetite mineralization being the most recent. Therefore, the presence of magnetite in the rock implies exclusion of apatites and limits of exploitability of the last can be inferred by measuring the concentration of either P_2O_5 or Fe_2O_3 .

A detailed mineralogical and petrographic characterization of the Evate apatite deposit is given by Tembe [5]. The base rock is marble and the main intrusions found are apatite, magnetite, and forsterite (Mg_2SiO_4), which aggregate in grains of up to 30 mm in size.

4. Results and discussion

4.1. PIXE

Table 1 summarizes the results of element concentrations determination in the eleven apatite samples. The sampling was made randomly using drill cores from different parts and depths of the deposit. The amount of phosphorus and iron are in perfect agreement with the standard apatite and, since phosphorus is very abundant (concentration higher than 18%) it can be used as a cheap fertilizer in the Evate neighborhood.

High strontium contents indicate the existence of mixed isotypous phosphate species. Indeed in "normal" apatite, which is usually a mixture of fluorapatite, chloroapatite, and hydroxylapatite ($\text{Ca}_5(\text{PO}_4)_3(\text{F}, \text{Cl}, \text{OH})$), the Ca^{2+} ions on a 3-fold axis are bonded to oxygen neighbors of adjacent PO_4 tetrahedra to form Ca-PO_4 chains parallel to the C-axis and the remaining ones surround channels parallel to C-axis in low symmetry positions. It turns out that the Ca ions can be replaced by Sr, Mn, Mg, or Fe and the group (PO_4) by (AsO_4) . From the results it is possible to notice the mixture (Sr, Ca)₃ which is known as strontiapatite and a much smaller amount of morelandite ((Ba, Ca, Pb)₃[(AsO₄)(PO₄)₂Cl]).

These conclusions are in good agreement with some aspects of the mineralogical and petrographic description of the deposit [5].

Table 1
Major and trace element concentrations (in ppm unless otherwise specified) of the 11 apatite samples. Void spaces mean that the concentration is lower than the MDL

	#1	#2	#3	#4	#5	#6	#7	#8	#9	#10	#11
P (wt%)	22.1 ± 0.3	19.0 ± 0.3	19.8 ± 0.3	19.6 ± 0.3	20.1 ± 0.3	18.0 ± 0.3	20.7 ± 0.3	20.3 ± 0.3	20.4 ± 0.3	20.0 ± 0.3	19.9 ± 0.3
Ca (wt%)	38.9 ± 0.9	31.4 ± 0.8	32.4 ± 0.8	32.3 ± 0.8	32.6 ± 0.8	29.5 ± 0.9	33.3 ± 0.8	32.9 ± 0.8	33.2 ± 0.8	32.9 ± 0.8	32.8 ± 0.8
Mn	—	—	—	—	—	—	—	153 ± 2	—	—	50.0 ± 0.6
Fe	259.0 ± 15	380 ± 63	391 ± 60	335 ± 77	277 ± 77	279 ± 12	195 ± 10	125 ± 12	307 ± 12	397 ± 10	140 ± 10
Cu	—	90 ± 1	—	—	—	—	82 ± 7	—	—	—	—
Sr (wt%)	0.7 ± 0.02	0.5 ± 0.01	0.5 ± 0.01	0.5 ± 0.02	0.5 ± 0.01	0.5 ± 0.1	0.6 ± 0.02	0.5 ± 0.01	0.3 ± 0.01	0.4 ± 0.01	0.16 ± 0.02
As	60 ± 2	11 ± 2	16 ± 1	16 ± 1	18 ± 2	18 ± 1	16 ± 1	15 ± 1	15 ± 1	116 ± 9	16 ± 2
Y	511 ± 17	322 ± 21	301 ± 20	168 ± 16	191 ± 15	163 ± 21	163 ± 18	153 ± 12	132 ± 10	175 ± 12	163 ± 10
La	468 ± 10	189 ± 8	59 ± 3	48 ± 3	97 ± 5	60 ± 3	—	—	—	—	—
Ce	1650 ± 140	1360 ± 112	758 ± 59	722 ± 72	867 ± 59	559 ± 54	660 ± 56	542 ± 56	442 ± 46	754 ± 76	560 ± 48
Nd	1060 ± 97	1500 ± 51	1390 ± 60	985 ± 55	1090 ± 102	1010 ± 89	970 ± 78	885 ± 55	813 ± 53	635 ± 31	998 ± 50
Sm	254 ± 9	265 ± 10	255 ± 9	172 ± 9	232 ± 10	197 ± 8	160 ± 8	150 ± 8	145 ± 8	147 ± 9	157 ± 9
Dy	70 ± 9	75 ± 8	65 ± 8	45 ± 6	51 ± 5	46 ± 6	50 ± 5	40 ± 7	25 ± 5	30 ± 6	75 ± 7
Th	40 ± 4	—	—	20 ± 3	—	10 ± 5	11 ± 1	13 ± 2	—	10 ± 1	14 ± 2

4.2. Ion luminescence

Fig. 1 presents the typical shape of apatite and calcite IL spectra. In calcite, the peak at 6200 Å corresponds to Mn^{2+} activated luminescence and in apatite luminescence peaks ranging from the near IR are present and are related to REE activated luminescence [4, 7, 10]. By comparing Fig. 1 and, further, Fig. 2 with Table 1, we see that it is possible to identify peaks of REE which are not quantifiable by PIXE. Indeed small amounts of activators are sufficient to induce the luminescence effect, which makes it very sensitive. The identification of peaks is performed using data available from cathodoluminescence studies in apatites [4, 7, 10] since the mechanisms of light generation do not depend on the form of excitation.

At the Lund Microprobe the IL method is being used intensively [3] in geological applications giving good qualitative results specially for trace elements. However, quantification using IL is not straightforward. The signal depends on much more parameters than just the concentration. Different chemical environments influence the intensity of light significantly. In Fig. 2 we can see four IL spectra of apatite samples with very different absolute peak intensities, though the concentrations of the activating elements do not vary too much. However, since the

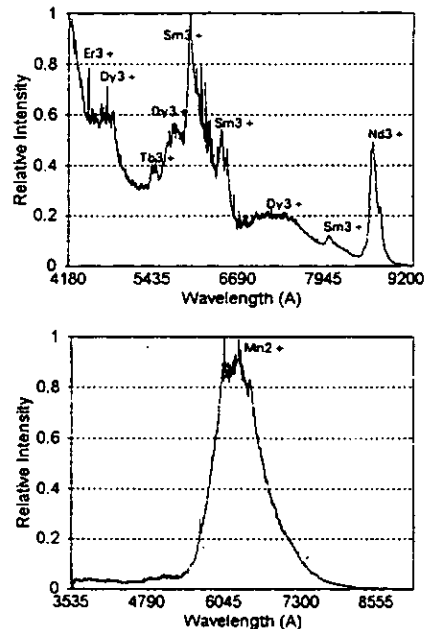


Fig. 1. Typical IL spectra of apatite (top) and calcite (bottom). In calcite spectrum the dominant peak corresponds to manganese (Mn^{2+}) activated luminescence at 6200 Å.

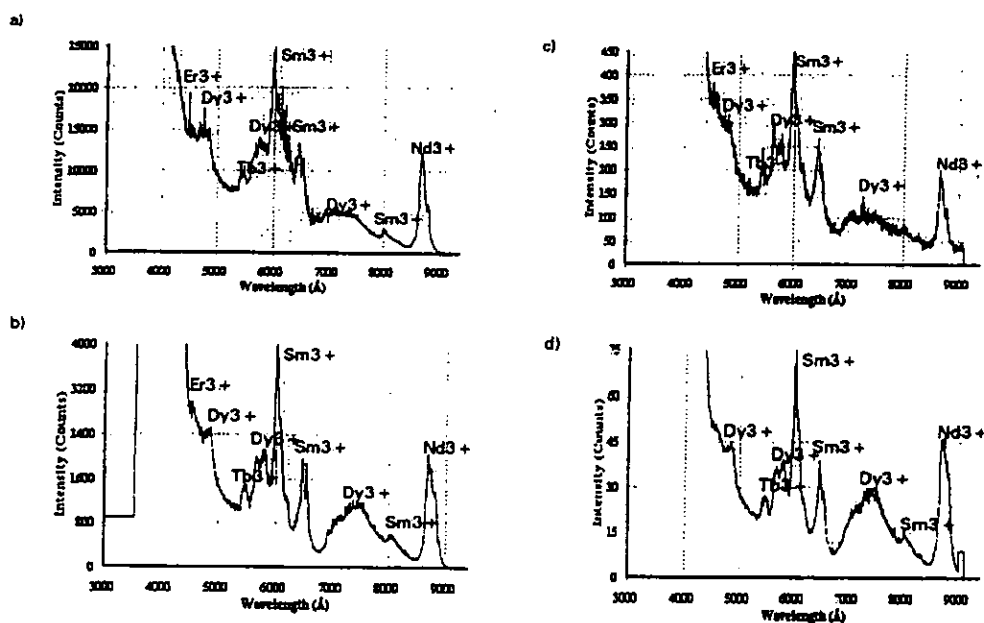


Fig. 2. IL spectra of four different apatite samples. (a), (b), (c), and (d) correspond to sample #4, #8, #11, and #9, respectively. It is noticeable the high sensitivity of the method: nonquantifiable by PIXE Rare Earth Elements are present in the spectra (see Table 1).

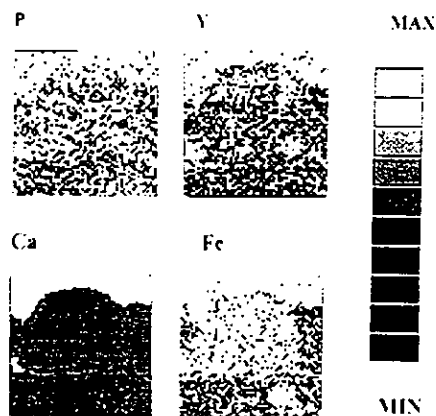


Fig. 3. Elemental map of an apatite grain (sample #11). The segregation of phosphorus by the iron is noticeable. It is due to the fact that, in the Evate deposit, the magnetite mineralization was formed later in comparison with the apatite one.

relative peak intensities are constant, then this fact can be connected to some different experimental conditions, like current fluctuations, for example.

Different approaches exist to attempt to extract as much information as possible from IL spectra like, for example, the use of multivariate statistical analysis [11], but the most promising is to associate them with some chemical background knowledge about the sample.

4.3. PIXE elemental mapping

The elements of major interest (P, Ca, and Fe) were mapped using μ PIXE with a beam of $10 \times 10 \mu\text{m}^2$ size. Fig. 3 shows the distribution of these elements on an apatite grain. No correlation between iron and phosphorus can be noticed which confirms the segregation of iron by phosphorus inside the grain, as described in [5].

5. Conclusions

The results of the nuclear microprobe analysis of eleven randomly chosen apatite samples from the Evate deposit, northern Mozambique, are in good agreement with some available geological information about the tectonic composition of the Nampula geological province and show the possibility of beginning a semi-artesian

exploitation of apatite to use the phosphate as fertilizer with very little treatment.

In the characterization of the apatite samples, PIXE and ion luminescence were used. This last is a very powerful technique, for detecting REE when combined with other IBA methods.

Acknowledgements

The authors would like to acknowledge the full support given by SAREC, Swedish Agency for Research Cooperation with Developing Countries.

References

- [1] C.G. Ryan and W.L. Griffin, Nucl. Instr. and Meth. B 77 (1993) 381.
- [2] S.A.E. Johansson and J.L. Campbell, PIXE a Novel Technique for Elemental Analysis (Wiley, New York, 1988).
- [3] C. Yang, N.P.-O. Larsson, E. Swietlicki, K.G. Malmqvist, D.N. Jamieson and C.G. Ryan, Nucl. Instr. and Meth. B 77 (1993) 188.
- [4] A.M. Morozov, L.G. Morozova, A.K. Trofimov and P.P. Feofilov, Optica i Spectroscopiya, XXIX, Vol. 6 (1970) 1107.
- [5] S.S. Tembe, Project proposal, unpublished.
- [6] K.G. Malmqvist, G. Hyllén, M. Hult, K. Håkansson, J.M. Knox, N.P.-O. Larsson, C. Nilsson, J. Pallon, R. Schofield, E. Swietlicki, U.A.S. Tapper and C. Yang, Nucl. Instr. and Meth. B 77 (1993) 3.
- [7] D.J. Marshall and A.N. Mariano, Cathodoluminescence of Geological Minerals (Unwin Hyman, London, 1988).
- [8] C.G. Ryan, D.R. Cousens, C.A. Heinrich, W.L. Griffin, S.H. Sie and T.P. Mernagh, Nucl. Instr. and Meth. B 54 (1991) 292.
- [9] W.H. Blackburn and W.H. Dennen, Principles of Mineralogy (WCB, Duberque, 1988).
- [10] P.L. Roeder, D. MacArthur, X. Ma, G.R. Palmer and A.N. Mariano, Amer. Mineralogist Vol. 72 (1987) 801.
- [11] E. Swietlicki, N.P.-O. Larsson and C. Yang, Nucl. Instr. and Meth. B 77 (1993) 195.

C. Yang, K.G. Malmqvist, J.M. Hanchar, R. J. Utui, M. Elfman, P. Kristiansson, J. Pallon and A. Sjöland "*Ionoluminescence combined with PIXE in the Nuclear Microprobe for the study of inorganic material*".(In the Proceedings of the Fourteenth International Conference on Applications of Accelerators in Research and Industry, 1996, University of North Texas, Denton, on press).

IONOLUMINESCENCE COMBINED WITH PIXE IN THE NUCLEAR MICROPROBE FOR THE STUDY OF INORGANIC MATERIALS

**C. Yang¹, K. G. Malmqvist¹, J. M. Hanchar², R. J. Utui¹, M. Elfman¹
P. Kristiansson¹, J. Pallon¹, A. Sjöland¹**

¹*Nuclear Physics Department, Lund University and Institute of Technology, Sölvegatan 14,
S-223 62, Lund, Sweden*

²*Rensselaer Polytechnic Institute, Department of Earth and Environmental, Sciences,
Troy, NY 12180-4389*

Ionoluminescence (IL) produced by MeV/amu particles interacting with materials in the nuclear microprobe and often observed as visible light, carries useful information on lattice properties and nature of luminescence centers, such as trace ion substituents and structural defects in inorganic materials. IL also allows chemical valence identification for some elements and the determination of optical/electrical properties for some materials. IL has been observed to be very sensitive to changes in lattice properties. Beam modification and damage effects using a nuclear microprobe have also been investigated. ZrSiO₄ and MgO crystals were used in the study, although this tool may also be applied to the other types of crystals. The combination of the IL technique with the well-established PIXE method in the nuclear microprobe provides a unique tool for both general luminescence studies and material analysis; it adds a new dimension to the study of the microstructure in various inorganic materials.

INTRODUCTION

Ionoluminescence (IL) is a luminescence phenomenon induced by energetic ion particles in solids. In contrast to processes leading to the production of X-rays or gamma-rays, in which the inner electron shell or the nucleus is involved, the process resulting in luminescence is usually related to the valence electrons in the outermost shell of the atom or in the sub-shell near the outermost shell. Thus, the luminescence process is chemically, optically and electronically sensitive to the chemical state of the ions and to the local conditions of chemical binding in the sample, or the conditions of the crystal lattice.

Publications concerning the investigation of ionoluminescence introduced by a beam of kinetic particles are to be found throughout the scientific literature published between the 1950's and today (1, 2, 3, 4, 5). A systematic investigation of ionoluminescence as an analytical tool for the characterization of materials was initiated by Yang et al. in Lund in 1992 in cooperation with Australian groups (6). The aim was to develop a new tool to obtain chemical/optical information for use in a nuclear microprobe and to enhance the application of traditional methods of ion beam analysis such as Particle Induced X-ray Emission (PIXE), Rutherford Back-Scattering (RBS) and Nuclear Reaction Analysis (NRA). The traditional ion beam methods are not sensitive to states of valence electrons. Introducing ionoluminescence into ion beam analysis, and in particular employing it in the nuclear microprobe, can enhance the strength of ion beam analysis considerably (7, 8, 9, 10). The simultaneous, quantitative data of multiple trace elements provided by PIXE helps interpret the IL spectroscopic and microscopic results. IL is very sensitive to the dynamic changes of the properties of the samples during ion beam analysis, making it useful as a diagnostic tool to study the processes involved in material modification by the ion beam. IL shows a great potential for the study of defects in crystals. It can reveal changes in lattice properties of a crystal that reflect the changes in geological conditions it has been subjected to during its growth. It can further identify lattice-damage induced internally over geological time scale, by radioactive-isotope impurities in some minerals. IL/PIXE studies of zircon grains provide valuable information for geochronology. The principles of the technique demonstrated in this paper on the two large-band-gap crystals $ZrSiO_4$ (zircon) and MgO can also be extended to investigations of other types of inorganic materials.

INSTRUMENTATION

The IL system employed here was partially described elsewhere (4, 5, 6). The operation range of the monochromator extends from UV to near-IR (1000 nm), with a grating of 1200 lines/mm. For spectroscopic analysis, the scan speed of the grating is usually set at a 0.5 nm/sec. Two photomultiplier tubes (PMTs) are used for IL detection. One is of the Hamamatsu R585 type with a wavelength response from 160

nm to 650 nm; the PMT has a very low dark current and it is often used as an imaging device due to its high signal-to-noise-ratio. The other PMT is of the Hamamatsu R943-02 type, with a wide response region of wavelength from 160 nm to 950 nm; it is often applied for IL spectral analysis due to this wide response range.

A photodiode-array based system for spectral analysis, Hamamatsu PMA-50, is also applied for IL spectral analysis. It makes very high-speed spectral acquisition possible, in a wavelength range from 350 nm to 900 nm. The exposure time can be set to anywhere from 20 millisecond to the order of minutes. It is especially useful for beam modification studies. By contrast, a spectral analysis system, operated with a PMT and grating-scan control, usually takes about 10 to 20 minutes to acquire a full IL spectrum. However, since the PMT offers a higher signal-to-noise ratio than a photodiode-array based system in the blue region, the PMT is very useful for IL imaging application in blue-region.

An IL image can be recorded by employing a focused beam and a PMT for light detection, where the combination of the IL imaging with μ -PIXE imaging is straight forward. An IL image can also be recorded simply with an optical microscope and a video camera (or film).

ION BEAM MODIFICATION EFFECTS IN A LARGE BAND GAP CRYSTAL

The IL method can be combined with PIXE in the Nuclear Microprobe for characterizing crystal micro-structures and for studying the effect of beam-modification of solid samples. As an example, a synthetic zircon crystal ($ZrSiO_4$) doped with holmium was tested. The PIXE result gives the following contents of trace elements: Ho 2390 ppm, Hf 180 ppm, Pb less than 30 ppm, U less than 30 ppm, Fe less than 5 ppm, Mn less than 5 ppm.

As shown in Fig. 1, the location indicated by the letter "M" in the maps was modified by using a 2.55 MeV proton beam with a fixed-beam spot (about 10 μ m beam size) and a beam dose of 6.0×10^{17} protons/cm². The intensity of the IL signal in the short wavelength region (centered at 360 nm) was quenched (shown on the lower and the left hand map), while the IL intensity in the long wavelength region (from 500 nm to 800 nm) is enhanced (shown on the lower and right hand map) due to the beam modification of the crystal.

The IL spectrum at the location probed by the static beam (indicated by letter "M" in Fig. 1) is shown in Fig. 2. The first spectral line was obtained with a fresh start for an exposure time of 0.5 sec. The beam was kept striking the same location of the sample thereafter. After an interval time of 1.0 second, the second spectrum was acquired with the same exposure time of 0.5 sec and in the same way the third spectrum was acquired. There are two broad, major distributions: one is from 300 to 470 nm, the other from 480 to 800 nm. The broad distributions are very sensitive to beam modifications. The narrow peaks superimposed on the two broad distributions,

are contributed by REE³⁺ emissions. The heights of these narrow peaks are almost unchanged if the beam current variation (a few percent) during the measurement is corrected. For the broad distributions, we observed that the continuous accumulation of the beam dose at the same location leads to a maximized level of the IL emission at the region (480 to 800 nm). A further beam dose eventually reduces the IL emission in all regions.

The IL emission intensity at the region (480 to 800 nm) was observed to be enhanced by a factor of 5 to 10 at a maximum with a certain beam dose. The modification effects caused by the beam may be applied in manufacturing a light-emission-diode (LED) made from this type of large-band-gap crystal due to the fact that electroluminescence (EL) may also show the similar color features as IL. The broad distribution of the luminescence light, in this case, from 480 nm to 800 nm, can be greatly enhanced through the optimization of beam modification of the crystal. Some narrow emission lines can also be introduced into an optical system by doping crystals with REEs. The intensities of the narrow lines can be controlled by controlling the level of the doping.

DEFECTS IN CRYSTALS

A MgO crystal was investigated by IL panchromatic imaging (wavelength range from 350 nm to 650 nm) by employing a blue-sensitive PMT (Hamamatsu R585). The result is shown in Fig. 3. The imaging range is approximately 200 μm , and a beam of 2.55 MeV protons focused down to the beam size of 2 microns was applied. The dislocation defects are clearly revealed in the IL imaging. PIXE analysis in the imaged area yields the following trace elements contents: Fe 300 ppm, Mn less than 2 ppm. Datta et al. 1980 (11) made an observation of a MgO crystal by CL method; they studied the dislocation by chromatic CL imaging and reported that the slip lines of the deformed sample yield a broad CL emission peak centered at around 466 nm.

A zircon crystal (a natural mineral) was investigated showing zonation pattern in a panchromatic IL investigation with an imaging range 300 μm , as displayed in Fig. 4. The zonation pattern can be related to the dislocation defects formed over a long period of mineral growth in different geological environments. The IL spectrum in Fig. 5, shows a strong emission with a broad distribution centered at 580 nm. PIXE analysis of the sample gives the following trace element contents: Dy 110 ppm, Er 150 ppm, Hf 9000 ppm, Fe 20 ppm, Ni 20 ppm, Cu 48 ppm. Efforts were made to look for a possible link between the IL pattern and the distribution of trace elements by the combination of the IL imaging method with μ -PIXE imaging method. There is no evidence that any luminescence activator can be related to the IL pattern. However, a correlation exists between the IL pattern and a partial distribution pattern of iron. This can be explained as the quenching effects of Fe²⁺ that is cooperated into the zircon lattice and therefore is optically activated. The partially non-optically active Fe distributed in the sample plays no role to influence

the IL pattern. We noticed that the dominant IL emission at 580 nm can be enhanced by beam modification with a certain beam dose.

The growth pattern revealed by IL can be very useful in re-constructing the information on previous geological environments, during which a crystal was formed or to which a crystal was subjected. The IL/PIXE method may also be useful in the diagnostic analysis of crystal growth characteristics in the study of crystal synthesis.

ZIRCON SAMPLE USED FOR GEOCHRONOLOGY

A zircon grain used for geological age-dating was investigated by back-scattered electron (BSE) method in the scanning electron microscope (SEM) and IL/PIXE method in the nuclear microprobe. The zircon sample, AM-86-11a, is from a fayalite-bearing leucogranite from Ausable Falls in the Adirondack Mountains, of New York State (12). Zircons from this granite have been dated with the single crystal U/Pb method (13). The data plot on a chord with an upper intercept of 1045 \pm 3 Ma. This granite is part of a group of *leucogranitic granitoids* which occur throughout the *Adirondack* region.

The zircons from these rocks commonly contain high U rims (dark in IL or CL, and bright in BSE) that when not abraded to remove these high-U regions often yield discordant U/Pb analyses. When the rims are abraded the U/Pb data from the zircons plot within error of *concordia*. The rims do not yield statistically younger ages than the inner regions of the zircons.

A BSE image of the zircon grain from AM-86-11a is displayed in Fig. 6a, and elemental and IL images obtained with the nuclear microprobe are displayed in Fig. 6b. A beam of 2.55 MeV protons focused down to about 2 or 3 micrometers was used for the IL/PIXE imaging.

The IL/PIXE study of the zircon followed an electron microprobe investigation of the same grain where a 30 keV electron beam was used. The proton beam probes a deeper excitation volume than the electron beam, therefore, the IL signal yield is still high even after the considerable beam damage made by the electron beam in a relatively shallow surface of the sample. IL is usually volume sensitive if a high energy proton beam is used in the nuclear microprobe in which a smearing of the IL image can occur due to the summation of the signals from different depths. A variation of lattice properties in zircons, such as the structure of a core and overgrowth, or an area of large lattice-damage, sometimes can not be revealed by BSE and CL methods in the SEM if the structure is not uncovered by a polishing process of sample preparation, since the 30 keV electrons can only probe a depth in the order of 1 micrometer. IL/PIXE can probe much deeper, for an example, a 2.55 MeV proton beam can reach a depth of about 10 to 40 micrometers in zircons. Therefore, it is very practical to apply the PIXE/IL method for the investigation of homogeneity of samples for selection of zircon grains used for U-Pb age-dating (4).

For the IL imaging a beam current of a few to 10 pA was applied and the IL data were collected for approximately 10 minutes. This assures that the information of interest is obtained before significant beam modification/damage takes place. The subsequent PIXE imaging was performed over the same area as the IL imaging, however, with a much higher beam current (about 100 pA).

From the IL and CL imaging patterns, it is evident that there is considerable lattice damage in the dark IL and CL regions in the zircon. These areas are enriched in trace elements including the heavy rare earth elements (HREEs), Fe, Mn, U, and Pb (as determined with micro-PIXE). Obviously, the areas of the zircon with severe lattice damage cannot contain valuable geochemical information as is possible in a normal zircon crystal. Likewise a damaged region of the zircon cannot preserve the geological age information provided by U/Pb dating technique, since the amorphous condition make it possible for various impurities to migrate and diffuse through the damaged area from/to the external environment. This could yield a considerable error in the U-Pb dating.

CONCLUSIONS

IL/PIXE can be a unique tool for the study of beam modification and damage and also for the diagnostic analysis of crystal defects. IL/PIXE can provide useful information for the study of zircons used for geochronology. The combination of the IL technique with the well-established PIXE method in the Nuclear Microprobe adds a new dimension to the study of inorganic materials.

ACKNOWLEDGEMENTS

The authors wish to thank the following Swedish foundations: The Swedish Natural Science Research Council, The Royal Physiographic Society, and C. Trygger for financial support received for the present study. One of the authors (Dr. Changyi Yang) wishes to acknowledge the support from Chinese Academy of Sciences.

REFERENCES

1. Leverenz HW (1950), *An introduction to luminescence of solids*, New York, John Wiley and sons, Inc., 1950, ch. 7, pp.399-471.
2. Derham CJ, Geake DJE and Walker G, Luminescence of Enstatite Achondrite Meteorites, *Nature*, **203**, 134-136 (1964).
3. Townsend PD (1987), Optical effects of ion implantation, *Rep. Prog. Phys.* **50**, 501-558 (1987).

4. C. Yang, N.P.-O. Homman, K.G. Malmqvist, L. Johansson, N.M. Halden, V. Barbin, Ionoluminescence: a new tool for nuclear microprobe in geology, *Scanning Microscopy*, **9-1**, 43-62 (1995).
5. Malmqvist KG, Elfman M, Remond G, and Yang C, PIXE and Ionoluminescence - a Synergetic Analytical Combination, *Nucl. Instr. and Meth.* **B109/110**, 227-233 (1996).
6. Yang C, Larsson NP-O, Swietlicki E, Malmqvist KG, Jamieson DN, Ryan CG, Imaging with Ionoluminescence (IL) in a Nuclear Microprobe, *Nucl. Instr. and Meth.* **B77**, 188-194 (1993).
7. N.P.-O. Homman, C. Yang, and K. G. Malmqvist, A highly sensitive method for rare-earth element analysis using Ionoluminescence combined with PIXE, *Nucl. Instr. and Meth.* **A353**, 610-614 (1994).
8. C. Yang, N.P.-O. Homman, L. Johansson, K.G. Malmqvist, Micro-characterising zircon mineral grain by Ionoluminescence combined with PIXE, *Nucl. Instr. and Meth.* **B85**, 808-814 (1994).
9. Bettioli AA, Jamieson DN, Praver S and Allen MG (1994), Ion beam induced luminescence from diamond and other crystals from a nuclear microprobe, *Nucl. Instr. and Meth.* **B85**, 775-779 (1994).
10. Malmqvist, K.G., Analytical techniques in nuclear microprobes, *Nucl. Instr. and Meth.* **B 104**, 138-151 (1995).
11. Datta S., Aeberli K.E., Boswarva I.M., and Holt D.B., *J. Microscopy* **118**, 367-369 (1980).
12. Chiarenzelli, J.R. and McLelland, J.M., Age and regional relationships of granitoid rocks of the Adirondack highlands, *Journal of Geology* **99**, 571-590 (1990).
13. McLelland, J.M. and McLelland, J.M., New high precision U/Pb zircon ages for Lyon Mtn. Gneiss, Adirondacks, and tectonic implications, *Geological Society of America Abstracts with Programs*, **28**, 80-88 (1996).

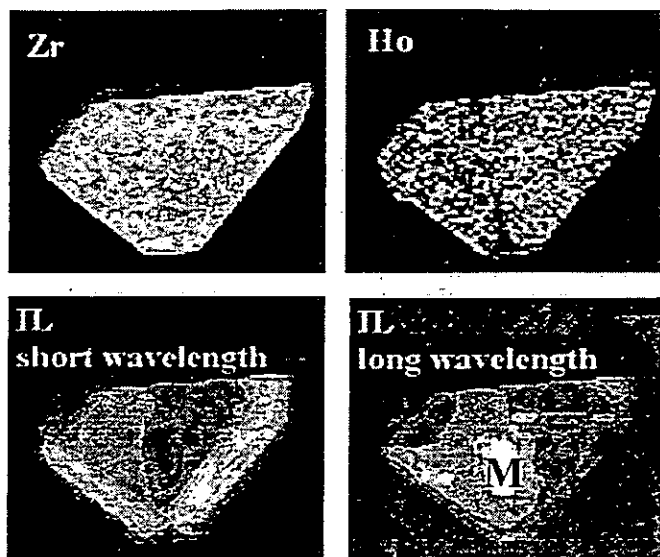


FIGURE 1. IL and PIXE imaging of a synthetic zircon (ZrSiO_4) crystal doped with Ho. The location indicated by the letter "M" was previously probed by IL/PIXE spectral analysis using a fixed-beam spot.

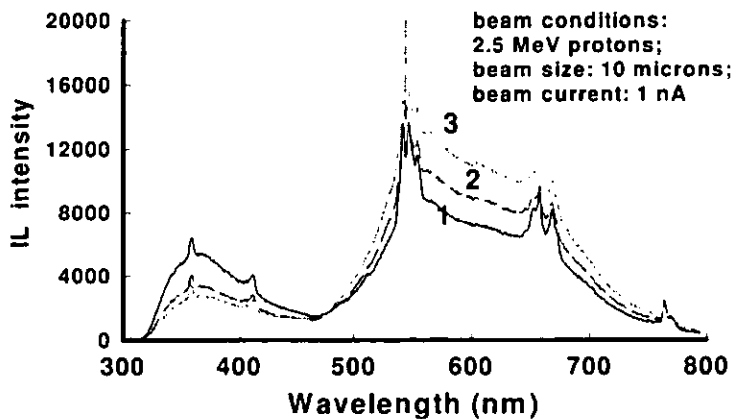


FIGURE 2. IL spectra of ZrSiO_4 (Ho doped). Exposure time 0.5 sec and interval time 1.0 sec. Beam conditions: 2.55 MeV protons, beam size 10 μm , beam current 1 nA. Exposure time 0.5 sec and interval time 1.0 sec.

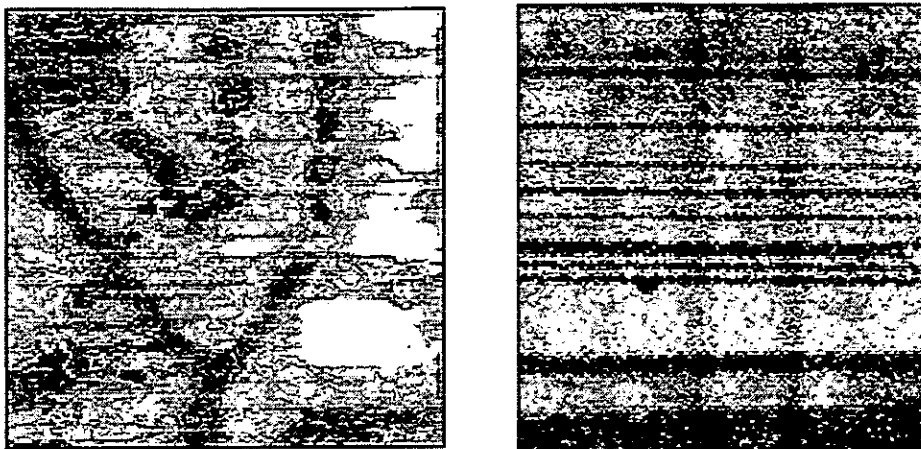


FIGURE 3. (left) The dislocation defect in a MgO crystal is revealed by the panchromatic IL image. A blue-sensitive PMT (Hamamatsu R585) was applied. Beam conditions: 2.55 MeV protons, beam size 2 μm , beam current 10 pA, accumulation time 10 min.

FIGURE 4. (right) A zonation pattern in a zircon crystal (natural mineral) under a panchromatic-IL investigation. The zonation pattern is related to the dislocation defects formed over a long period of mineral growth through different geological periods. There is a strong emission with a broad distribution centered at 580 nm. The IL spectrum is shown in the Fig. 5.

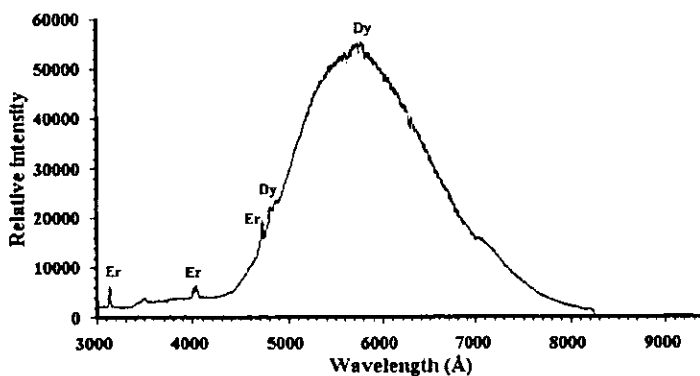


FIGURE 5. IL spectrum of the natural zircon. Trace element contents in the sample: Dy 110 ppm, Er 150 ppm, Hf 9000 ppm, Fe 20 ppm, Ni 20 ppm. Beam conditions for the spectral analysis: 2.55 MeV protons, beam size 50 μm , beam current 0.5 nA.

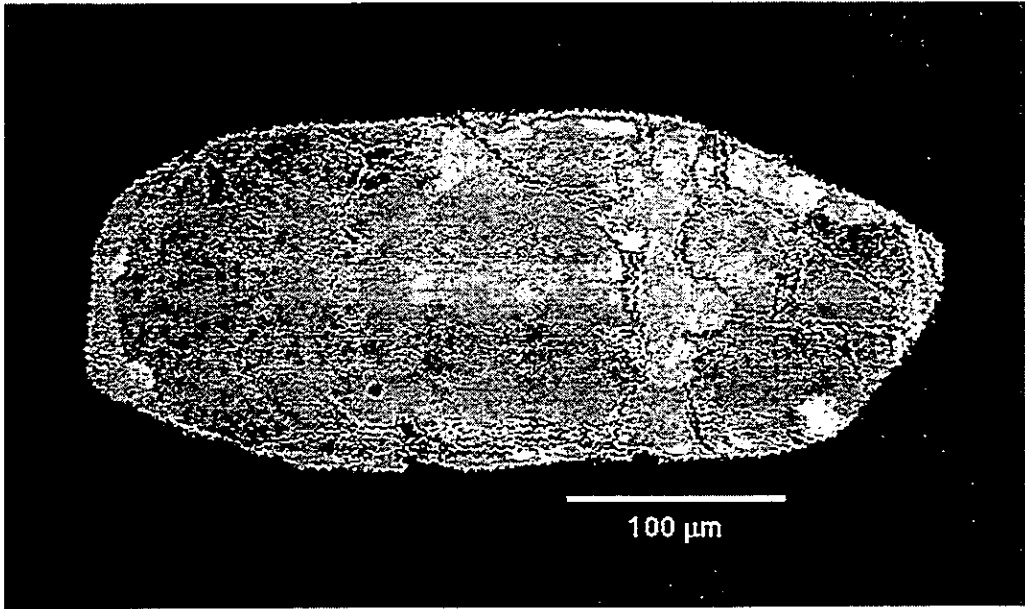



FIGURE 6a. A back-scattered electron image of zircon from sample AM-86-11a. The elemental and IL images of the same zircon are displayed in Fig. 6b.

MIN  MAX

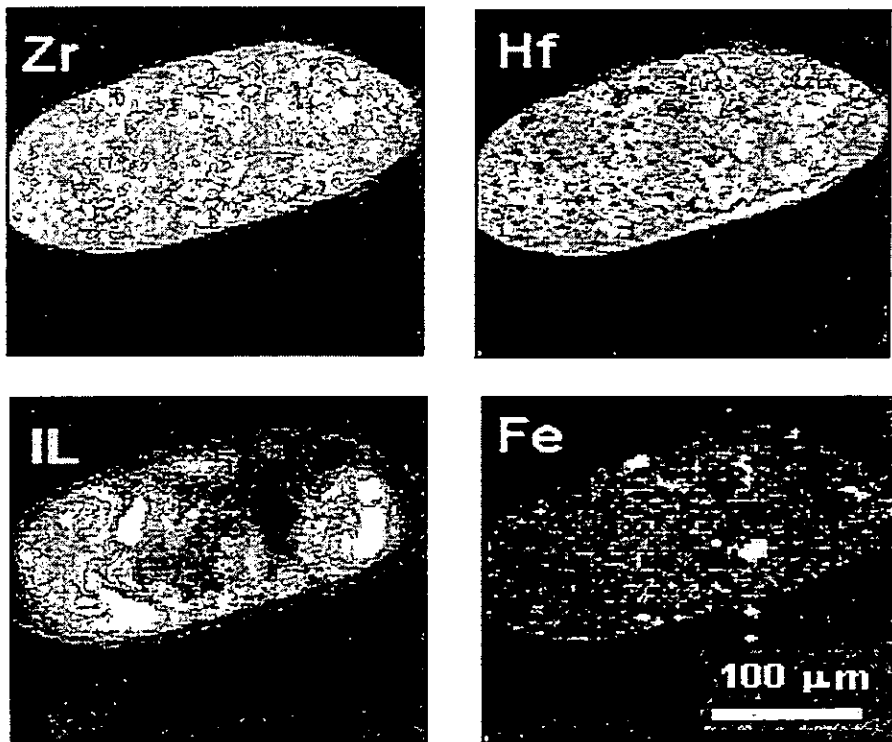


FIGURE 6b. The elemental and IL images of the zircon grain in Fig. 6a. The beam conditions for the panchromatic IL imaging: 2.55 MeV protons, beam size 2 μm , beam current 10 pA; for the PIXE imaging, the beam current was increased to approximately 100 pA.

K.Janssens, A. Aerts, L. Vincze, F. Adams, C. Yang, R. Utui, K. Malmqvist, K.W. Jones, M. Radtke, S. Garbe, F. Lechtenberg, A. Knöchel and H. Wouters "*Corrosion phenomena in electron, proton and synchrotron X-ray microprobe analysis of Roman glass from Qumran, Jordan* (Published in Nuclear Instruments and Methods B 109/110 (1996) 690-695).

With permission of Elsevier Science B.V.

IV



ELSEVIER

Corrosion phenomena in electron, proton and synchrotron X-ray microprobe analysis of Roman glass from Qumran, Jordan

K. Janssens^{a,*}, A. Aerts^a, L. Vincze^a, F. Adams^a, C. Yang^b, R. Utui^b, K. Malmqvist^b,
K.W. Jones^c, M. Radtke^d, S. Garbe^d, F. Lechtenberg^d, A. Knöchel^d, H. Wouters^c

^aDepartment of Chemistry, University of Antwerp, Antwerp, Belgium

^bDepartment of Nuclear Physics, University of Lund, Lund, Sweden

^cBrookhaven National Laboratories, Upton, NY, USA

^dDepartment of Chemistry, University of Hamburg, Hamburg, Germany

^eNational Institute for Cultural Heritage, Brussels, Belgium

Abstract

A series of 89 glass fragments of Roman glass are studied using electron, proton and synchrotron radiation induced X-ray emission from microscopic areas on the sample surface. The glass originates from Qumran, Jordan and was buried for 1900 years. The weathering layers that result from the extended contact with ground water have been studied, next to the trace composition of the original glass of these pieces. The latter information indicates that at Qumran, large quantities of glass objects were being used in Ancient times. Cross-sectional profiles of the glass show a complex migration behaviour of various groups of major and trace elements.

1. Introduction

An interesting class of archeological artifacts from ancient times consist of (fragments of) glass vials, flasks, small sculptures etc. Usually these objects have been buried for extended periods of time and show corrosion phenomena on their surface, causing the original clear glass to become covered with an opaque and flakey coating [1,2]. In some cases the corrosion layer can become so extended that the mechanical strength of the glass is severely affected. As a result, many ancient glass artifacts have become very fragile.

Information on the microscopic structure of and composition gradients inside the corrosion layer(s) is valuable for development of suitable restoration and protective conservation strategies for these objects. In this work, a series of (fragments of) 89 different glass objects, such as bottles, pearls, goblets and cups, found at Qumran, Jordan, dating from ca. 100 a.c. was studied. To investigate both the bulk composition and the microstructure of the corrosion layers of the glass fragments in a nondestructive way, different microscopic X-ray emission techniques were employed: (a) for high resolution (<1 μm) inspection of the corrosion layers, for localised major element analysis and major element mapping, EPXMA (electron probe X-ray microanalysis) was used; (b) to investigate the internal structure of the corrosion layers with respect to minor and

trace constituents in more detail, μ-PIXE (proton induced X-ray emission) was employed and (c) for obtaining fingerprinting trace element data on the various glass samples and line-scans through corrosion layers, μ-SRXRF (synchrotron radiation X-ray fluorescence) was employed. In what follows, an overview of the results of these investigations is presented; also the suitability and the degree of complementarity among of the three above-mentioned methods for analysing this type of examples is evaluated.

2. Experimental

The glass samples were taken from 89 different glass objects excavated at the Qumran ruins, Jordan in the 1950s. Most glass samples were 1–10 mm² in size and were embedded into resin blocks which were subsequently cut to expose a cross section perpendicular to the corroded glass surface and polished using diamond paste (1 μm grain size). Most measurements were done using samples prepared in this way. From the resin blocks, also relatively thin sections were cut, but in view of the brittleness of the material, the thickness of the sections could not be reduced below 100 μm.

Measurements were performed on a Jeol JSM 3300 scanning electron microscope, equipped with an energy-dispersive X-ray detector. The obtained X-ray intensities were quantified by means of a standardless ZAF scheme.

* Corresponding author.

Various NIST (National Institute of Standards and Technology) glass standards (such as SRMs 620, 1830, 1411 and 1412) were used to validate the quantitative procedure [2] and yielded deviations of the order of 5-10% between calculated and certified major compositions. SR-XRF measurements were executed at the NSLS (National Synchrotron Light Source, Brookhaven National Laboratories, Upton, NY) X26A beamline using an $8 \times 8 \mu\text{m}$ white X-ray beam and at the DORIS III (HASYLAB, Hamburg, Germany) beamline L-station; quantification was done using a Monte Carlo simulation model [3]. The μ -PIXE measurements were done at the Nuclear Microprobe facility of the University of Lund, Sweden [4], using a $5 \mu\text{m}$ proton beam of 2.55 MeV; during the image scans, a proton current of 330 pA was used.

3. Results and discussion

In many glass samples, inspection of the polish cross sections using the secondary and backscattered electron images formed in the SEM revealed three distinct regions: a central layer of original (i.e., unaffected) glass, a corrosion layer which had formed on the inside of the original glass panes and a precipitation crust on top of the original glass surface. Using EPXMA, the major element composition of these three layers was investigated: an example of typical results are shown in Table 1. The results for Na^+ can only be considered semiquantitative in view of the sample preparation procedure and the migration of Na^+ due to sample charging under electron bombardment. Nevertheless, a clear difference in the concentrations of the elements Na, Mg, K and Ca is observed; whereas Na and Ca are leached out of the original glass, K and Mg are enriched.

Table 1
Typical major element composition (wt.%) of bulk glass, corroded layer and precipitation crust in Qumran glass samples

Element	Bulk	Leached layer	Crust
Na	11.66	0.27	0.01
Mg	0.10	4.24	4.75
Al	1.33	2.17	2.39
Si	32.88	38.08	20.16
P	0.04	-	0.20
S	0.06	0.33	0.21
Cl	0.87	1.24	0.46
K	0.75	2.32	1.74
Ca	5.95	0.64	26.68
Ti	0.06	0.08	0.35
Mn	0.32	0.14	0.26
Fe	0.33	0.62	2.08
Cu	0.10	0.12	0.10
O	45.62	49.74	40.71

3.1. The original glass

As can be gathered from Table 1, the original glass of all fragments consists of *natron*-based glass (Na = major cation) as is the case for most glass which dates back from Ancient times; Medieval glass usually is Potash based, i.e., having K as major mono-valent cation. Using the major element data, as obtained by EPXMA, among the series of 89 objects, a distinction could be made between two groups: a large one, comprised of 64 objects and containing on average $8.4 \pm 0.5\%$ CaO and a smaller one (15 objects) featuring a slightly lower CaO concentration ($5.9 \pm 0.8\%$). Because of the relatively large variation in composition inside the two groups, this distinction was not very clear and in fact (see Table 2), the CaO content was the only one significantly varying among the two groups. As can be seen from Fig. 1a, from EPXMA spectra, only information on the concentration of major elements can be obtained. In order to gain a better insight into the origin of the various glass samples, μ -SRXRF was used to obtain a trace-element "finger-print" of each glass sample. Because of the high-energy components of the white synchrotron beam which was employed, it was possible to

Table 2
Average values and corresponding standard deviations for oxide concentration in the glass fragment belonging to the two groups of Qumran objects

	Group I	Group II
Major composition (wt.%) as determined by EPXMA		
Na_2O	16.5 ± 0.5	17.0 ± 0.5
MgO	0.2 ± 0.1	0.1 ± 0.1
Al_2O_3	2.5 ± 0.1	2.4 ± 0.3
SiO_2	69.6 ± 0.7	71.6 ± 0.8
P_2O_5	0.1 ± 0.04	< 0.1
SO_3	0.1 ± 0.1	0.2 ± 0.1
Cl	0.8 ± 0.1	1.1 ± 0.1
K_2O	0.8 ± 0.1	0.6 ± 0.1
CaO	8.4 ± 0.5	5.9 ± 0.8
TiO_2	0.1 ± 0.02	< 0.1
MnO	0.4 ± 0.1	0.8 ± 0.3
Fe_2O_3	0.5 ± 0.1	0.4 ± 0.1
Trace composition (ppmw) as determined by μ -SRXRF		
Cr_2O_3	22 ± 5	30 ± 20
NiO	8 ± 1	9 ± 4
CuO	143 ± 36	13 ± 9
ZnO	32 ± 21	19 ± 7
Rb_2O	12 ± 3	12 ± 2
SrO	595 ± 99	540 ± 38
Y_2O_3	9 ± 2	7 ± 2
ZrO_2	86 ± 13	71 ± 9
Mo_2O_7	3 ± 2	2 ± 2
SnO_2	117 ± 33	52 ± 29
Sb_2O_3	281 ± 127	17 ± 26
BaO	165 ± 56	129 ± 56
Ta_2O_5	18 ± 3	3 ± 3
PbO	128 ± 26	16 ± 14

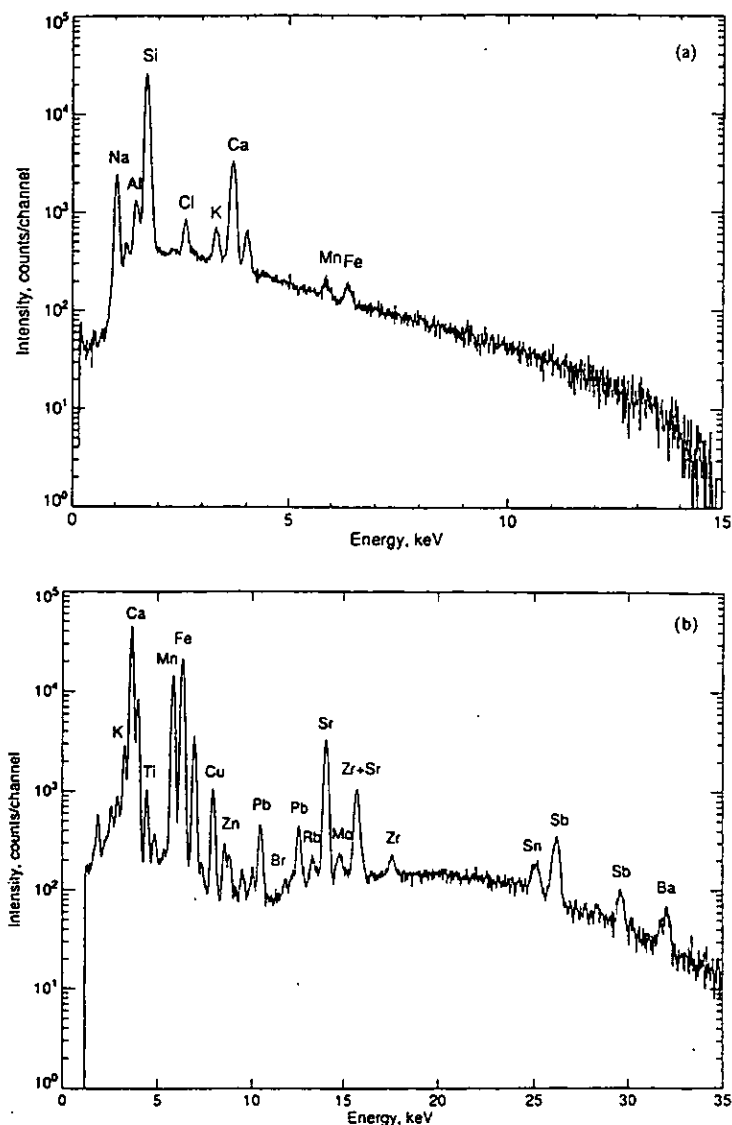


Fig. 1. Typical (a) EPXMA and (b) μ -SRXRF spectra of the unaffected region of a glass sample from Qumran.

employ the K-lines of elements such as Sn, Sb and Ba in order to avoid overlap problems of the L-lines of these elements with the K-lines of major elements such as K, Ca, Ti etc. (see Fig. 1b). The quantitative results of this investigation are summarised in Table 2 for the two above-mentioned groups of samples. Although also in the trace-element composition, inside each group, some variation persists, when considering the CuO , PbO , SnO_2 and Sb_2O_3

abundances, quite significant differences can now be observed. In addition, the fact that the large group of excavated objects have the same composition and trace element fingerprint indicates that large quantities of (valuable) glass receptacles were being used in Qumran; this is unusual since glass objects in Ancient times were hard to make and thus fairly rare. The presence of a large collection of glass objects with very similar composition

appears to indicate that either these artifacts were made on site or were purchased in large quantities elsewhere. In any case, this appears to support the view that Qumran was a center of the perfume industry in the Middle East during Ancient times [5], the glass vials, bottles etc. being used as receptacles for perfume, ointments etc.

3.2. The corrosion layer

Whereas usually a depletion of K is observed both in Ancient and Medieval glasses, in the Qumran samples, K is enriched in the corroded layers; this has been observed in all samples using both EPXMA, μ -PIXE and μ -SRXRF. The corrosion layer usually is 100–200 μm thick, which is in accordance with the corrosion rates of about 0.1 $\mu\text{m}/\text{year}$ found for other natron-based glass. The leached layer itself in many instances features a complex morphology which is responsible for the flaky and fragile outlook of corroded glass. In cases where the corrosion of the glass occurred gradually and moisture could not enter the glass through cracks or air bubbles, stacks of thin parallel sublayers ($<1 \mu\text{m}$ in thickness) have developed (see Fig. 2a). The origin of the regularly spaced sublayers is not very clear. The μ -SRXRF line scans (for an example: see Fig. 3) collected perpendicularly through such a stack show that the composition of corroded layer may be quite uniform. Also, 3 groups of elements showing similar behaviour can be discerned in Fig. 3: K, Ti, Cr, Fe and Br being enriched in the leached layer, while Ca, Mn, Pb and Mo are clearly depleted in concentration; the elements Zr, Sn and Sb appear not to be affected by the corrosion process. The reason for the existence of these different groups of elements may be connected with the size of the ions and/or with the way the various ions interact with the silica network in the glass and needs to be investigated further. In the case of the corrosion layer shown in Fig. 2b, probably as a result of temperature cycles, the difference in expansion coefficient between the original glass and the leached layer has caused the latter to become partially separated from the parent glass, permitting moisture to directly attack the exposed surface. This attack progresses the most rapidly at irregularities in the glass (e.g., inclusions of air or trapped dirt particles) and in many cases results in the hemi-spherical morphology shown in Fig. 2b [1,2]. Due to the cracking, also precipitation of Mn can occur in the already formed leached layer (light areas in Fig. 2b), as revealed by EPXMA X-ray mapping. (In Fig. 2b, also the precipitation crust which has formed on top of the original glass surface can be seen.) In order to obtain a better insight in the migration of various elements between the glass and the corrosion layer and the surrounding soil, also trace element distributions of such an area were recorded. Since, in view of the brittle character of the material (especially the corroded multilayers themselves), it was hard to obtain sections thinner than 100 μm , μ -PIXE was preferred over μ -SRXRF for obtaining these



Fig. 2. Electron micrographs of (a) quasi-parallel and (b) hemi-spherical morphology of the corrosion layer showing the sublayers inside the corroded region of the glass.

maps. Because of the high sampling depths (up to a few 100 to 1000 μm) when using XRF signals of high energy (as is the case for e.g., Sn-K or Ba-K), the lateral resolution in two-dimensional SR-XRF images may be significantly degraded [6]. A number of the μ -PIXE maps obtained are shown in Fig. 4. These data show a fairly complex behaviour of the various trace elements: next to a high Mn content, the precipitates also are enriched in elements such as Cr, Fe, Ni, Br and Mo but depleted in K and T, while alternate sublayers show higher concentrations in Ti, Fe, Cu and Zn. Also, broad alternate bands rich in respectively, K and Ca can be observed, the latter also showing a higher Sr content. Although these different layers reappear in most samples of similar morphology, the order and relative thickness of the different sublayers vary considerably among the different samples.

4. Conclusions

In this work, a series of 89 glass fragments of Roman glass were studied with respect to the weathering phe-

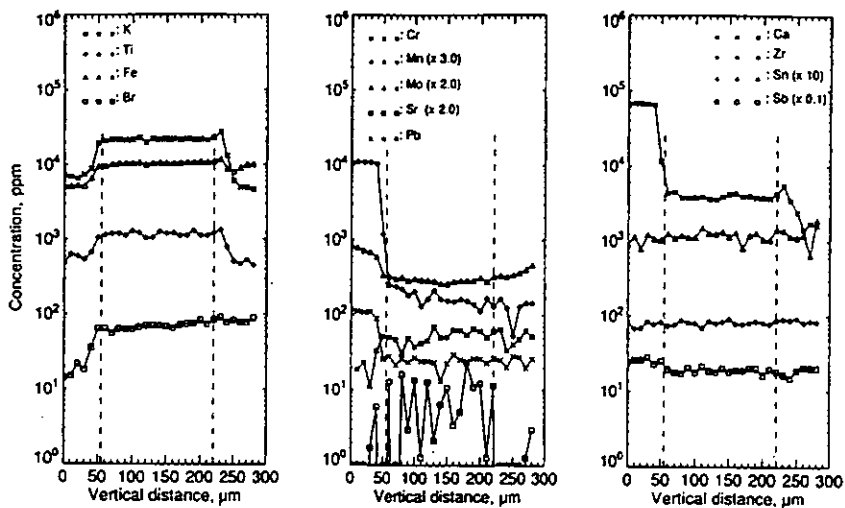


Fig. 3. Major and trace-element line-scans obtained by μ -SRXRF, collected along a line perpendicular to the glass surface, through a parallel section of the corrosion layer. 0–60 μ m: original glass; 60–220 μ m: leached layer; 220–300 μ m: crust/embedding resin.

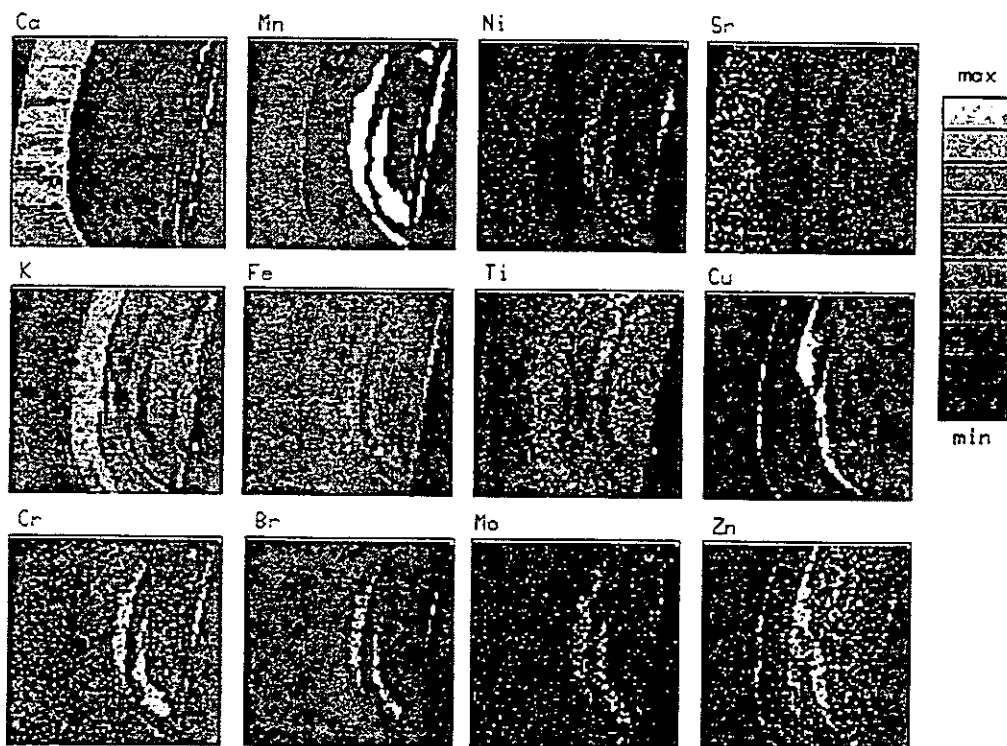


Fig. 4. μ -PIXE maps from a $1200 \times 1200 \mu\text{m}$ region of the corrosion layer on one of the glass samples; the analysed area is also visible in the center of Fig. 2b. Beam size: $5 \mu\text{m}$, beam current: 330 pA , acquisition time: 1.025 s/pixel .

nomena that have occurred as a result of contact with ground-water during a period of ca. 1900 years. Bulk analysis of the unaffected regions of the glass shows that the glass has similar properties (overall composition, durability, rate of corrosion) to that of Roman glass objects found at other sites in Europe and indicates that at Qumran large quantities of glass receptacles were being used, possibly in the Perfume industry that may have been based there.

Cross-sectional profiles of the glass fragments show a complex migration behaviour of various groups of major and trace elements and different morphologies of the corroded layers. To understand these phenomena more fully, a systematic study of the formation of the corrosion layers in controlled environments appears mandatory. It is clear, however, that the trace-element contrast obtained between the different sublayers of the affected glass is valuable in understanding the corrosion processes and their different stages taking place in the glass. The high sensitivity of μ -SRXRF for localised analysis of heavy trace elements was found to be very useful for "finger printing" type of analyses while for this particular type of

samples the combination of lateral resolution and trace level sensitivity offered by μ -PIXE allowed detailed investigation of the different sublayers in the corroded regions of the glass.

References

- [1] J. Cox and L. Ford, *J. Mater. Sci.* 28 (1993) 5637.
- [2] A. Aerts, K. Janssens, F. Adams and H. Wouters, Microanalytical investigations of corrosion in Roman Glass from Qumran, Proc. 24th MAS, New Orleans, LA, July 31-Aug. 5, 1994.
- [3] L. Vincze, K. Janssens, F. Adams and K. Jones, *Spectrochimica Acta B* (1995) in press.
- [4] U.A.S. Tapper, R. Hellborg, M.B. Hult, N.P.-O. Larsson, N.E.G. Lövestam, K.G. Malmqvist, J. Pallon and K. Themer, *Nucl. Instr. and Meth. B* 49 (1990) 425.
- [5] P. Donceel-Voûte, *Archeologia* 98 (1994) 26.
- [6] K. Janssens, A. Aerts, I. De Raedt, L. Vincze and F. Adams, μ -SRXRF analysis of Medieval and Roman Glass, *Hasylab Berichte* 1994, Hamburg (1995) p. 989.

R.J. Utui, X. Wang, F.M. Guerreiro, M. Elfman, P. Kristiansson, K.G. Malmqvist, J. Pallon, A. Sjöland and C. Yang "*Application of Nuclear Microprobe in the study of granulite rocks from the Namama Thrust Belt*" (Submitted to Nucl. Instrum. & Methods Section B, 1996).



Application of Nuclear Microprobe in the study of granulite facies rocks from the Namama Thrust Belt.

R.J. Utui^{1*}, X. Wang², F.M. Guerreiro³, M. Elfman¹, P. Kristiansson¹,
K.G. Malmqvist¹, J. Pallon¹, A. Sjöland¹ and C. Yang¹.

¹Department of Nuclear Physics, Lund University and Institute of Technology, Box 118, S - 221 00, Lund, Sweden.

²Department of Mineralogy and Petrology, Institute of Geology, Sölvegatan 13, S - 221 00, Lund, Sweden.

³Department of Geology, Eduardo Mondlane University, P.O. Box 257, Maputo, Mozambique.

Abstract

In the present work the PIXE technique at a Nuclear Microprobe was combined with the well established electron microprobe analysis (EMPA) technique for the characterization of distinct mineral facies coexisting in a metamorphic rock from the Namama Thrust Belt (NTB), northern Mozambique.

The estimated temperature, based on the garnet-biotite geothermometer, is about 650° C for the rock from the northern part of the belt (Monapo). Extensive sampling and analysis are to follow in order to test the hypothesis of crustal thickening for the evolution of the NTB and geochemical characterization of the rocks using Nuclear Microprobe techniques.

* Corresponding author. Present address: Department of Physics, Eduardo Mondlane University, P.O.Box 257, Maputo, Mozambique, Fax: + 258 - 1 - 475333; e - mail: roger@nambu.ucm.mz

1. Introduction

Particle Induced X-ray Emission (PIXE) has evolved to become a well established technique with application in different analytical problems in virtue of its multi-elemental capability, low detection limits for a wide range of elements, non-destructiveness, and possibility for absolute quantification in relatively quick analysis [1,2]. Because of these reasons, this technique became an important part of the geological tool kit where, commonly, high sensitivity for heavy trace elements is at premium.

The possibility of using PIXE in a Nuclear Microprobe (NMP) adds another dimension in the analytical capabilities of the method, since X-ray elemental maps of the distribution of different elements in the sample can be obtained. In geological studies using a NMP the partitioning profiles of different trace elements recorded at the different mineral assemblages give information about the geological physicochemical conditions that governed the process of ore deposition [3] or posterior geological metamorphism [4].

In studying metamorphic terranes, a twofold aim is pursued: i) to pigeonhole the mineral assemblages present in different facies of particular economical importance and, ii) to unravel the complicated tectonic processes responsible for the orogenesis [5]. We have initiated a series of geological studies in attempts to improve the understanding about the birth, evolution and mineralization of the Namama and Lurio belts (Figure 1), which are part of the Mozambique belt. In the present work both NMP and EMPA techniques were applied to study granulite facies rocks from the Namama thrust belt (NTB), northern Mozambique.

The microscopic ability of EMPA and NMP enabled us to characterize garnets and biotites in the metamorphic rocks. The garnet-biotite geothermometer [6] was used in order to constrain the temperature conditions during the different events that marked the rock evolution and trace elements analysis were performed to help geochemical description of the rocks.

2. The Namama metamorphic belt (Mozambique)

The Mozambique basement has been regarded as the southernmost segment of the Mozambique belt, which is described as a large orogenic structure running from Mozambique itself, to the Sudan, the Arab Peninsula and the Horn of Africa. Inside the territory of Mozambique, and north to the Zambezi river, the structure of the basement is dominated by two large linear domains, the Lurio and the Namama belts [7]. In figure 1 it is depicted the location of these geological formations.

The Lurian chain runs WSW-ENE from southern Malawi to the Indian Ocean and it is composed of high-grade metamorphites (mainly granulites)

associated with granites. Recently it was possible to reveal the presence of a second chain, the Namama thrust belt (NTB), which is presumably a slightly later satellite of the Lurio belt [8]. The present research work was done on this structure.

The thrust belt runs MNE from the neighbourhood of Vila de Maganja (17°30' S; 37°45' E) for over 100 km along a slightly arched course [7]. Its vergence is to the East and is made of a pile of basement and cover thrust sheets. The tectonic development of the NTB seems to have taken place shortly after that of Lurio belt, according to structural and radiometric evidences [9]. Unfortunately, very little information about the NTB and other related structures is available.

Studies must be done in order to unravel the metamorphic history of the belts for better understanding of the tectonic events that were involved in the Mozambiquian orogeny. Moreover, geochemical data will help to decipher the chemical nature of the parent geological material, whilst mineralogical studies will help to systematize the elements present in the rocks. Basic rocks in the NTB and Lurio belt, are enriched with Cr, Pt, V and Ti; pegmatites are associated with Li, Nb, Ta, Be, U and Th and carbonatites in granulites are rich in phosphates (for example [10]). Small scale mining of gemstones is widespread throughout the region.

The study area, Monapo, is situated elsewhere in the northeast of the NTB. This area is poorly studied. Petrographic studies and field investigations suggested that it consists mainly of metabasites, metapelitic rocks and variably deformed granitic gneisses.

3. Experimental Procedure and Results

Rock samples were collected from different zones of the Namama thrust belt. The outcrops cover the areas of Monapo (in the northern part), Muiane (in the southern part) and Naipa (in the hanging wall of the belt). Thin sections were prepared from these samples and the different mineral facies identified using petrographic microscopy.

A granitic gneiss rock, chosen for NMP analysis and EMPA was reddish grey and showed a foliated texture, consisting mainly of quartz, plagioclase, K-feldspar, biotite and small amount of garnet and hornblend.

The major elements were determined by electron microprobe analysis (EMPA) and some of them, like Mn and Fe, were corroborated by NMP analysis. Trace elements in both garnet and biotite were determined by PIXE technique at the Lund Nuclear Microprobe. A detailed description of this apparatus is given elsewhere [14]. Significant improvements to this system were made recently. These include the development of a new, more versatile data acquisition system [15].

PIXE spectra were fitted using the GEOPIXE package [16]. Garnet-biotite thermometry was evaluated by the program GEOTHERMOMETER [5].

The EMPA and NMP results of the analysed minerals are presented in Table 1. These results refer to samples collected at Monapo, in the northeast of the NTB (fig. 1). Anhedral garnets have the following composition: Alm.- 0.816, Pyp. - 0.079, Grs - 0.066, Sps - 0.037; K-feldspar: Ort. - 0.93, Ab.- 0.07; plagioclases are predominantly anorthitic (An - 0.76); and biotite composition varies from 0.60 to 0.65. The mineralogical characterization was made by EMPA in different samples.

5. Discussion and Conclusions

Geothermometry

This granitic rock is far from ideal for Pressure-Temperature determination based on element partitioning between coexisting minerals. We applied, nevertheless, the garnet-biotite geothermometer calibrated by Hodges and Spear [12] which gave temperatures of $640^{\circ}\text{C} \pm 14^{\circ}\text{C}$ and $660^{\circ}\text{C} \pm 15^{\circ}\text{C}$, for an assumed pressure of 6 - 10 kbar.

Unfortunately no suitable mineral assemblages were found in the samples, that could allow more appropriated geothermobarometric studies. The main idea is to continue a systematic sampling and analysis of the terranes of the NTB in order to determine isotherms across the belt or PTt paths of the region for better understanding of the tectonic events involved in the orogenesis of the Namama and the Lurio belts.

To our knowledge no previous work of this kind has been reported. Cadoppi *et al.* [7] have proposed, based in simple observations, a model of crustal thickening. Geothermobarometric studies using combined EMPA and NMP could quantitatively describe the two belts as part of a more vast formation: the Mozambican belt.

Geochemistry

In zoned minerals, the variation of the concentration of certain elements in relation to others as we move from the core to the rim of the mineral grains, can be used to characterize the changes in composition of the ore-forming fluids as the crystals grew. This aspect is important for geological prospecting works. One of these indicators can be the Zr/Y ratio [17].

Despite the fact that the analysed garnets didn't display visible zoning at backscattered electrons image (fig.1), some relative enrichment in Y/Zr was observed as we moved from the center to the borders (from #1 to #4 in Table1)

of the analysed grain. This fact can be regarded as evidence of posterior overgrowth of the garnets. In future works we intend to focus our attention also in this key issue in order to bring about a more detailed characterization of the geological history and mineralization conditions of the Namama and Lurio belts.

Acknowledgements

The authors wish to thank the support granted by the Swedish Authority for Research Cooperation with Developing Countries (SAREC - SIDA) and Mr. Rikard Ånehus for preparing the thin sections.

References

- [1] S.A.E. Johansson and J.L. Campbell, PIXE a Novel Technique for Elemental Analysis, (Wiley, New York, 1988).
- [2] S.A.E. Johansson, J.L. Campbell and K.G. Malmqvist, ed., Particle-Induced X-ray Emission Spectrometry (PIXE), (Wiley, New York, 1995).
- [3] S.H. Sie, C.G. Ryan, D.R. Cousens and W.L. Griffin, Nucl. Instr. and Meth. B 40/41 (1989) 690.
- [4] C.G. Ryan and W.L. Griffin, Nucl. Instr. and Meth. B77 (1993) 381.
- [5] F.S. Spear and S.M. Peacock, Metamorphic Pressure-Temperature-Time paths, in Short Course of Geology: vol. 7, (Washington DC, Am. Geophys. Union, 1989).
- [6] A.B. Thompson, American Journal of Science 276 (1976) 425.
- [7] P. Cadoppi, M. Costa and R. Sacchi, Journal of African Earth Sciences 6 A (1986) 493.
- [8] R. Sacchi, J. Marques, M. Costa and C. Casati, Precambrian Research 25 (1984) 141.
- [9] G. Ferrara, R. Sacchi, S. Tonarini and B. Zanettin, Proceedings of the 27th Internat. Geol. Congr., Moscow (1984).
- [10] R.J. Utui, N.P.-O. Homman, C. Yang, K.G. Malmqvist and S.S. Tembe, Nucl. Instr. and Meth. B 104 (1995) 432.
- [11] J.M. Ferry and F.S. Spear, Contrib. Mineral. and Petrol. 66 (1978) 113.
- [12] K.V. Hodges and F.S. Spear, American Mineral. 67 (1982) 1118.
- [13] A. Indares and J. Martignole, American Mineral. 70 (1985) 272.
- [14] K.G. Malmqvist, G. Hyltén, M. Hult, K. Håkansson, J.M. Knox, N.P.-O. Larsson, C. Nilsson, J. Pallon, R. Schofield, E. Swietlicki, U.A.S., Tapper and C. Yang, Nucl. Instr. and Meth. B 77 (1993) 3.
- [15] M. Elfman, P. Kristiansson, K. Malmqvist, J. Pallon, A. Sjöland, R. Utui and C. Yang, These proceedings (1996).

- [16] C.G. Ryan, D.R. Cousens, S.H. Sie and W.L. Griffin, Nucl. Instr. and Meth. B 49 (1990) 271.
- [17] J.A. Pearce and J.R. Cann, Earth Planet. Sci. Lett. 19 (1973) 290.

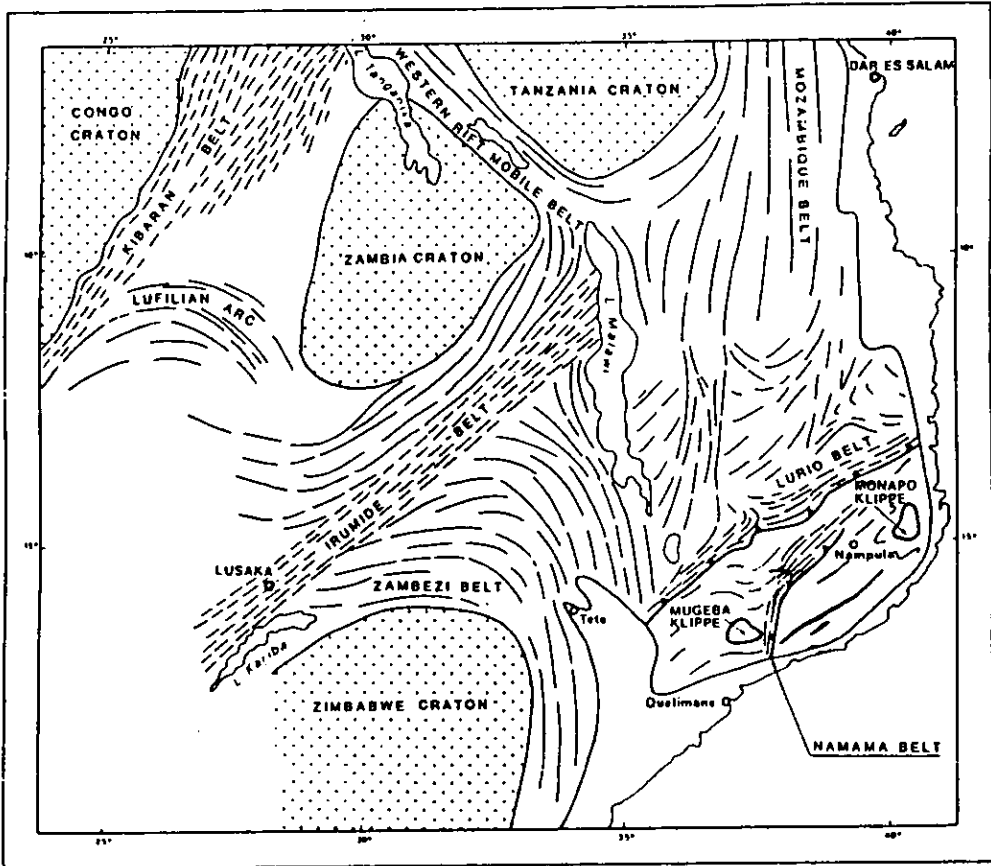
Figure captions:

Figure 1. Sketch showing the location of the Namama and Lurio thrust belts in the northern part of Mozambique. They are part of the Mozambique belt, which spans until the Horn of Africa. (Adapted from Cadoppi et al, 1986).

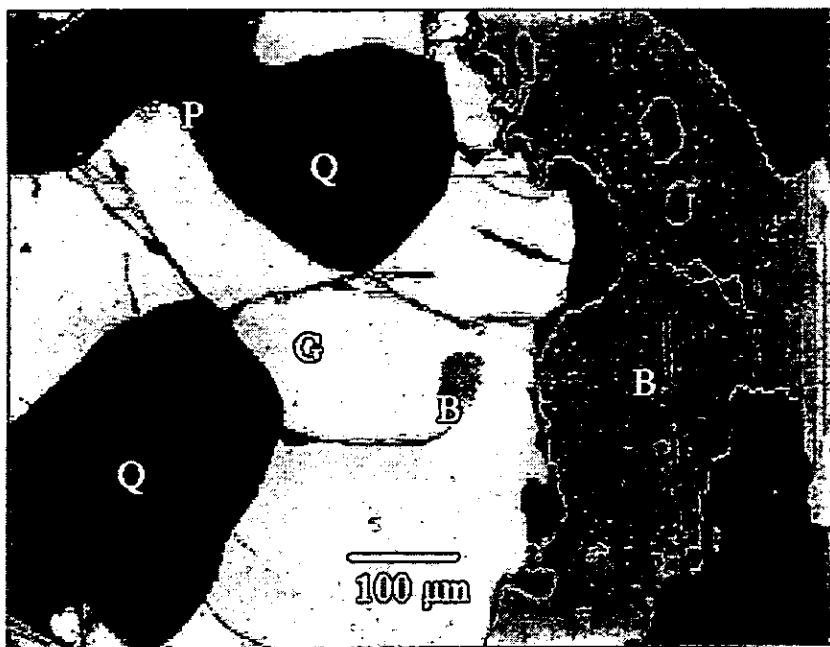
Figure 2. Backscattered electrons micrograph of the mineral assemblages used for geothermometry. Legend: B - biotite; G - garnet; P - plagioclase; Q - quartz. The closure temperature was determined from the composition of the biotite inclusion in contact with the garnet (a) and the peak temperature, from the biotite lamella away from garnet mineral (in this case, in a quartz matrix), (b).

Figure 3. Temperature values calculated using the Hodges and Spear [12] calibration of the garnet-biotite geothermometer. The samples are from Monapo, northern part of the Namama belt.

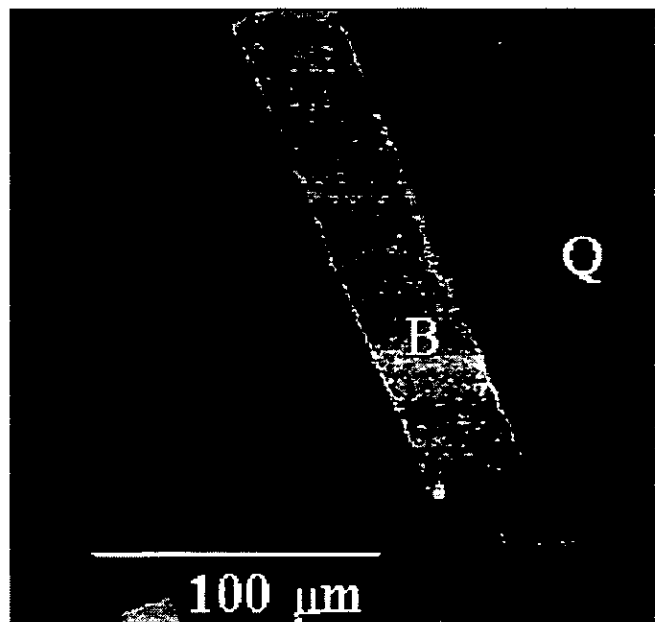
Table 1. Major and trace element data from the garnet and biotite mineral assemblages from the Namama Belt. Major elements were measured by EMPA and corroborated by NMP (Mn and Fe). Concentrations are in wt% for the major elements (oxides) and in ppm for trace elements. Typical errors are about 5 % for the EMPA data and 8 - 10% for PIXE data.

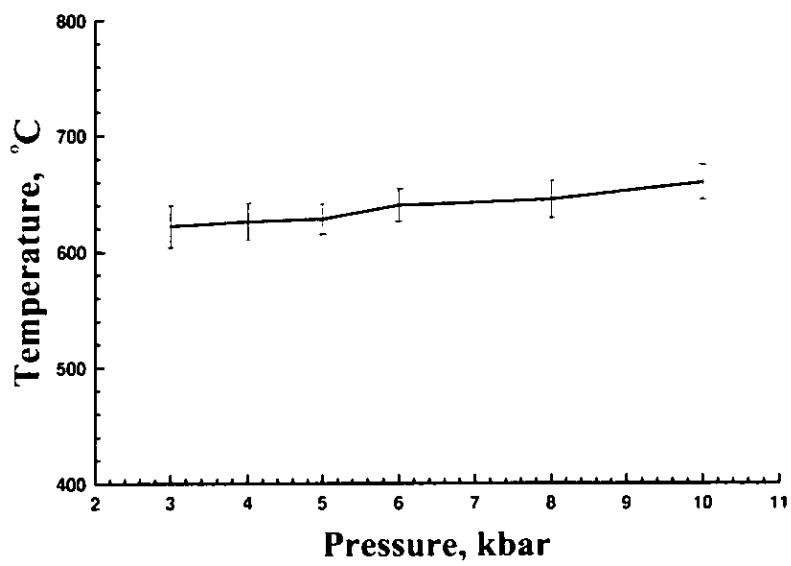


a)



b)





Garnet

Biotite #2

Biotite #1

	Biotite #1				Biotite #2				Garnet			
	#1	#2	#3	#4	#1	#2	#3	#4	#1	#2	#3	#4
MgO	8.17	6.80	6.95	7.16	7.06	7.85	7.63	8.17	2.05	2.06	2.03	1.94
Al ₂ O ₃	14.95	18.09	18.48	18.93	18.58	14.52	14.12	15.08	20.93	20.94	20.67	20.22
SiO ₂	37.63	35.15	36.03	36.38	36.13	35.07	34.34	35.69	37.46	37.52	37.11	36.79
K ₂ O	9.19	9.75	9.73	9.86	9.92	9.59	9.43	9.64	-	-	-	-
CaO	-	-	-	0.036	0.004	0.094	-	0.094	2.34	2.33	2.33	2.19
TiO ₂	6.24	1.29	1.38	1.28	1.33	5.34	5.13	5.37	-	-	-	-
MnO	0.11	0.117	0.072	0.03	0.032	0.087	0.027	-	1.72	1.69	1.76	1.64
FeO	22.65	24.60	24.62	24.61	24.52	21.95	21.34	22.10	37.65	37.52	36.66	36.49
Cu	4729	4650	4725	4190	4520	4490	4545	4398	-	-	-	-
Zn	875	920	950	930	689	675	650	680	112	109	115	119
Ge	-	-	-	-	-	-	-	-	11	10	9	11
As	1740	1697	1725	1680	1694	1752	1731	1600	456	437	476	468
Rb	1347	1280	1359	1390	1333	1295	1288	1322	9	8	9	10
Sr	52	45	43	55	52	57	63	54	9	9	9	10
Y	70	65	77	73	67	63	65	62	1035	1010	1120	1190
Zr	204	196	185	201	186	179	174	180	69	50	53	51
Nb	28	31	34	29	35	41	43	22	-	-	-	-